# INVESTIGATION OF NANOSCALE ETCHING AND POLING OF LITHIUM NIOBATE

by

Stacie Elizabeth Smith

A thesis submitted in partial fulfillment
of the requirements for the degree

of

Master of Science

in

Electrical Engineering

MONTANA STATE UNIVERSITY
Bozeman, Montana

April 2014

©COPYRIGHT

by

Stacie Elizabeth Smith

2014

All Rights Reserved

## ACKNOWLEDGEMENTS

This project relied heavily on the assistance, support, and encouragement from numerous groups and people. First, I would like to acknowledge AdvR, Inc., specifically Dr. Matt Bigelow, Dr. Tim Fry, and Dr. Phil Battle. Without the assistance of AdvR, this thesis would not have been able to be completed. They provided their time, patience, and expertise (and the *occasional* lithium niobate sample). Second, I would like to thank the members of the Nano-Optics Group, especially Dr. Wataru Nakagawa, Carol Baumbauer, and Ethan Keeler for assisting in the technical tasks of this project and providing me with too many cookies.

Third, the assistance from the entire Montana Microfabrication Facility group must be acknowledged: Dr. Phil Himmer, Amy Fox, Lana Hoagland, Jason Hundhausen, Jon Lane, and Sarah Mondl. Their expertise on fixing cleanroom equipment was an invaluable contribution to this project. Next, I would like to thank Dr. Rob Walker and Melissa McIntyre of the MSU Department of Chemistry and Biochemistry for assisting in poling the samples with the use of their Raman microscope. I would also like to acknowledge the Montana Space Grant Consortium (MSGC) who financially supported a good part of this project and the Imaging and Chemical Analysis Laboratory (ICAL) for always assisting me with imaging. Last, I would like to acknowledge Richard Revia, who continually supported and encouraged me throughout the process.

TABLE OF CONTENTS

1. INTRODUCTION .......... 1

1.1 Background .......... 1
1.2 Second Harmonic Generation .......... 2
1.3 Nano-Optics for SHG .......... 8
1.4 Fabrication Process .......... 11
1.5 Thesis Objective .......... 16

2. LITERATURE SURVEY .......... 19

2.1 Introduction .......... 19
2.2 Wet Etching .......... 21
2.2.1 Ion Implantation Assisted Wet Etching .......... 23
2.3 Electric Field Poling .......... 24
2.3.1 Conventional Poling .......... 25
2.3.2 Backswitching .......... 25
2.3.3 Surface Poling / Overpoling .......... 26
2.4 Optical Poling .......... 28
2.4.1 Light Assisted Poling .......... 29
2.4.2 All Optical Poling .......... 33
2.5 Dry Etching .......... 37
2.5.1 ICP-RIE / RIE Etches .......... 37
2.5.2 Focused Ion Beam Milling .......... 40
2.6 Analysis and Feasibility .......... 40
2.6.1 Etching .......... 40
2.6.2 Poling .......... 42
2.7 Conclusion .......... 43

3. FABRICATION PROCESS PART 1: PATTERNING CHROMIUM ETCH MASKS .......... 46

3.1 Introduction .......... 46
3.2 Fabrication Process .......... 46
3.3 Lithography Patterns .......... 52
3.4 Resist .......... 52
3.4.1 Resist Development .......... 52
3.4.2 Resist Exposure .......... 54
3.5 Mask Analysis .......... 60
3.6 Fill Factor Optimization .......... 63
3.7 Conclusion .......... 65

TABLE OF CONTENTS – CONTINUED

4. FABRICATION PROCESS PART 2: ETCHING NANOSTRUCTURES IN LITHIUM NIOBATE ........ 67

4.1 Introduction ........ 67
4.2 Etch Rate Analysis ........ 69
4.3 Proton Exchange Etch Analysis ........ 73
4.4 Sidewall Analysis ........ 76
4.5 Etch Optimization ........ 80
4.6 Aspect Ratios ........ 84
4.7 Future Trials ........ 86
4.8 Conclusion ........ 89

5. ALL OPTICAL POLING / WET ETCH ........ 91

5.1 Introduction ........ 91
5.2 Procedure ........ 91
5.3 Results ........ 93
5.4 Domain Inversion Patterns ........ 98
5.5 Sidewall Analysis ........ 101
5.6 Conclusion ........ 103

6. CONCLUSION ........ 104

6.1 Summary ........ 104
6.2 Recommendations for Future Trials ........ 105
6.2.1 ICP-RIE ........ 105
6.2.2 All Optical Poling / Wet Etch ........ 107
6.3 Impact ........ 108

REFERENCES ........ 111

APPENDIX A: Detailed Fabrication Process ........ 118

# LIST OF TABLES

Table Page

2.1. Ion Implantation Assisted Wet Etching Parameters....................................24

2.2. LAP Lasers and Wavelengths......................................................................31

2.3. AOP Lasers and Wavelengths ......................................................................35

2.4. ICP-RIE Etching Trials with Varied Parameters [61].................................39

3.1. Values for 50/50 Fill Factors ........................................................................65

4.1. Parameter Values for ICP-RIE......................................................................70

4.2. Standard Deviation of Etch Rates and Selectivity ......................................73

4.3. Changes in ICP-RIE Parameters for Different Etch Trials...........................81

4.4. Average Sidewall Angles and Standard Deviation for Different Etch Trials..........................................................................................82

# LIST OF FIGURES

Figure Page

1.1. A diagram illustrating domain inversion due to periodic poling. The top image shows the original, unpoled LN, and the bottom image shows the LN after periodic poling............................5

1.2. The effect of phase matching on the intensity of the second harmonic signal generated using periodic poling. The three curves correspond to (a) exact-phase matching, (b) quasi-phase matching, and (c) no phase matching (i.e., no periodic poling). $l_c$ represents the coherence length, and the arrows denote the polarization orientations [8].......................................................5

1.3. An illustration depicting a potential nanoscale grating etched into a lithium niobate substrate to obtain exact-phase matching .................11

1.4. Outline of the lithography process required to etch nanostructures onto the surface of LN .......................................................12

1.5. Illustration of the photolithography process ..............................................13

1.6. Schematic detailing the process of lift-off .................................................15

1.7. A second scenario detailing the process of patterning a metal layer onto a substrate surface.....................................................................16

2.1. Illustration depiction underpoling (a), conventional poling (b), and overpoling (c) [1]...............................................................28

2.2. A representative apparatus commonly used for LAP [53] ...........................30

2.3. Calculated skin depths for LN, based off Palik's values [58] ......................34

3.1. Diagram illustrating the patterning of the chromium mask .........................49

3.2. Diagram illustrating fabrication process for Method B...............................50

3.3. Left- metal mask created through Method A; Right- metal mask created through Method B ............................................................................51

LIST OF FIGURES - CONTINUED

Figure Page

3.4. Basic diagram depicting the patterned gratings after lithography; periods are labeled on the right (not drawn to scale) ....53

3.5. 6, 8, and 10 µm periodic gratings in developed resist that are severely overdeveloped ....54

3.6. 6, 8, and 10 µm gratings in developed resist that are appropriately developed....54

3.7. Image showing common deformities seen in the PMMA layer on certain LN samples (a-c), and an ideal resist layer (d) ....55

3.8. Samples with scribe marks on the bottom of the sample (depicted by the dark line across the sample in a and a 'v' shape in b) shows a correlation between the scribe marks and deformities found in the PMMA layer....56

3.9. Deformities seen to be arranged in linear patterns across the sample....56

3.10. Severely deformed PMMA layer ....58

3.11. Images showing an ideal PMMA layer spun onto a sample. Hardly any deformities were seen on the LN after the sample had been cleaned with solvents and re-spun....59

3.12. Left: 600 nm period grating made using Method A; right: 600 nm period grating made using Method B ....61

3.13. Left: 2 µm period grating made using Method A; Right: 2 µm period grating made using Method B ....62

3.14. 300 nm periodic grating made using Method A ....62

3.15. SEM images of chromium mask on lithium niobate; top: 800 nm period grating; bottom: 10 µm period grating ....64

4.1. Fabrication process after metal mask is formed....68

4.2. Top: 600 nm period grating etched in lithium niobate. Bottom: 4 µm period grating etched in lithium niobate....69

LIST OF FIGURES - CONTINUED

Figure Page

4.3. Lithium niobate etch rates for the samples etched......71

4.4. Chromium etch rates for the samples etched......72

4.5. Etch selectivities for the samples etched......73

4.6. Graph illustrating there is no major difference in etch rates if proton exchange bath is changed, circled data points represent etch rates from the first proton exchange, and the other data points represent etch rates from the second proton exchange......75

4.7. Graph illustrating there is no major difference in etch rates if proton exchange bath is changed, circled data points represent etch rates from the first proton exchange, and the other data points represent etch rates from the second proton exchange......75

4.8. Diagrams showing the ideal case for nanostructures (a), and the reality (b)......76

4.9. Two images of a 10 µm period grating; top image showing three structures and bottom image showing one structure at higher magnification......77

4.10. Sidewall angles for the samples etched (90° is desired)......77

4.11. 800 nm period grating; note the severe sidewall angle causing structures to become trapezoidal......78

4.12. 300 nm period grating; note the structures are essentially rounded......78

4.13. Left: Chromium mask (800 nm period grating); Right: Structures with chromium mask still on after ICP-RIE......79

4.14. Lithium niobate etch rates using different etch parameters......82

4.15. Etch selectivities using different etch parameters......83

4.16. Sidewall angles using different etch parameters......83

4.17. 600 nm period grating, SEM image, side view after Cr etch......84

LIST OF FIGURES - CONTINUED

Figure Page

4.18. 400 nm period grating, SEM image after Cr etch ....................................85

4.19. 2 μm periodic grating, SEM after Cr etch ...............................................85

4.20. Two SEM images of a 1 μm period grating ............................................88

4.21. Top: top view SEM image of a 300 nm period grating;
bottom: side view SEM image of 300 nm period grating..........................89

4.22. 10 μm period grating ...............................................................................90

5.1. Optical microscope image of poled area on lithium niobate
after HF etch; image obtained using dark field setting which
illuminates edges of structures..................................................................92

5.2. 10X MO image of poled regions on sample; white spots,
particularly the linear patterns, represent poled regions on
lithium niobate revealed after an HF etch .................................................93

5.3. Four images showing lines and dots littered across the surface
of the LN samples .....................................................................................94

5.4. Two images showing one box in the grid; each box was
expected to have only on poled spot .........................................................96

5.5. Poled pattern found on a sample that had been patterned with
a chromium mask, but not intentionally poled through AOP.......................97

5.6. Image of poled cluster near scratch in lithium niobate sample.....................97

5.7. Image of poled cluster near scratch in lithium niobate surface ....................97

5.8. Three images of poled regions on an unprocessed, broken
lithium niobate sample ...............................................................................98

5.9. Optical microscope image of poling pattern seen on cleaved
triangular piece of lithium niobate, etched in HF; inset showing
image of cleaved LN chip............................................................................99

5.10. Another image of the same triangular piece of lithium niobate................100

LIST OF FIGURES - CONTINUED

Figure Page

5.11. Linear poling patterns shown on a sample perpendicular to the cleaved edge; inset showing image of cleaved LN chip with grid scribed on surface .................... 100

5.12. Left: SEM image of 400 nm period grating, magnification of 40kX; Right: SEM image of poled region, revealed during HF etch, magnification of 40kX .................... 102

5.13. Left: SEM image of grating edge, magnification of 150kX; Right: SEM image of poled region, revealed during HF etch, magnification of 150kX .................... 102

A.1. Flowchart sequencing out the steps taken for the Method A (left) and Method B (right) processes used to etch lithium niobate using an ICP-RIE etch .................... 120

# ABSTRACT

The capabilities of some nonlinear optical devices can be improved through approaches such as nano-optics. Two methods, in particular, that can enhance the wavelength conversion efficiency and versatility of current second harmonic generation (SHG) devices are creating nanoscale domain inversions (to make for efficient quasi-phase matched SHG devices at various wavelengths) and gratings in lithium niobate (to potentially achieve exact-phase matching).

This thesis explores these options, creating nanoscale domain inversions and nanostructuring lithium niobate, in order to enhance current SHG devices. First, an in-depth literature survey is provided detailing the current research regarding structuring lithium niobate. Next, a description and analysis of the inductively coupled plasma reactive ion etch (ICP-RIE) etching procedures used are provided, followed by a discussion of the poling of lithium niobate using an all optical poling technique. Suggestions for continued development are presented based on the successes and failures of the procedures used for this work.

The goal of this thesis is to show that lithium niobate can be nanostructured using ICP-RIE etching techniques and optical poling methods. This goal is a foundation towards the long-term goal of building more efficient nonlinear optical devices. Nanostructuring lithium niobate suggests that improved nonlinear optical devices can be made in the future, by means of nanoscale domain inversions for quasi-phase matching or nanoengineered gratings intended for exact-phase matching.

# CHAPTER 1

# INTRODUCTION

## 1.1 Background

Nonlinear optics is a growing field involving wavelength conversion of high intensity electromagnetic fields, which has several uses such as enabling the creation of coherent optical sources at essentially any wavelength. Another important field in the photonics community is nano-optics. Nano-optics allows optical materials to be refined, adjusted, and improved by means of nanoengineering and structuring. By nanostructuring an optical device, material properties can be changed in order to achieve previously unattainable goals. The main objective of this thesis is to combine nonlinear optics and nano-optics in order to nanostructure nonlinear optical materials in such a way that can potentially lead to improved nonlinearities within the material.

For example, second harmonic generation (SHG) is the process of frequency doubling using a nonlinear crystal such as lithium niobate. The SHG process can be improved in several different areas. For instance, one disadvantage of SHG devices is that they are not very versatile over a wide range of wavelengths; they work efficiently but only at specific wavelengths. Also, the conventional methods of creating SHG involve a process making it impossible to ever achieve 100% wavelength conversion efficiency, making these devices undesirable in low-light applications. This thesis will focus on structuring lithium niobate so second harmonic generation devices that are more efficient and adaptable to various wavelengths have the potential to be made. This

involves preliminary research into structuring lithium niobate so that it can be seen whether or not these improvements via nanoengineering are feasible and practical.

Lithium niobate ($LiNbO_3$ or LN) is a manufactured optically nonlinear crystal that has numerous intriguing properties. After its initial crystal synthesis, investigations into the materials properties of lithium niobate proved the medium to hold many appealing features such as ferroelectricity, as wells as large pyroelectric, piezoelectric, electro-optic, and photoelastic coefficients [2, 3, 4]. As a result of the unique and rich physical characteristics of this crystal, it is used in a wide variety of applications; LN may be found as a common component in devices like acoustic wave transducers, optical amplitude modulators, optical phase modulators, $Q$-switches, and dielectric waveguides among others [2]. The optical nonlinearity of lithium niobate allows for its use in second harmonic wave generators. Lithium niobate will be structured in this thesis in order to determine if it is possible to improve SHG processes by means of nanoengineering.

## 1.2 Second Harmonic Generation

Second harmonic generation (SHG) refers to the frequency doubling of incident light in a nonlinear optical material; that is, SHG describes the phenomenon by which an electromagnetic (EM) wave oscillating at frequency $\omega$ interacts with some optically nonlinear material, such as LN, and gives rise to an additional EM wave oscillating at frequency $2\omega$ [3, 4, 5, 6, 7]. For instance, passing laser light through a nonlinear material capable of facilitating SHG results in two output EM waves: one oscillating at the input frequency $\omega$ and the other oscillating at $2\omega$. In the case of high wavelength conversion efficiency SHG, the second harmonic signal is relatively large, and, in effect, the input

wavelength is cut in half producing laser light a twice the original frequency. SHG is desirable for many applications. One application, for example, is low-light detection in the infrared spectrum. As there are very few inexpensive, compact detectors for infrared light, detecting IR signals with low intensity levels is a difficult feat [8]. On the other hand, visible light detectors are comparatively cheap and can detect low intensity light. Therefore, a useful application for SHG is to convert low intensity IR into visible light for easy detection.

Lithium niobate is a dispersive medium, meaning its refractive index is a function of frequency. As such, an EM wave of frequency $\omega$ propagating in LN will not travel at the same phase velocity as an EM wave oscillating at frequency $2\omega$. This means that the second harmonic signal generated in ordinary lithium niobate will gradually become out of phase with the first-harmonic wave. Such a situation leads low wavelength conversion efficiency for SHG. High-efficiency SHG is attained when the first and second harmonic electric fields are in phase with one another [3, 5]. In the case of lithium niobate, improved SHG efficiency is commonly achieved through a process called periodic poling which provides a quasi-phase matching between the fundamental and second harmonic [3, 6, 9]. Periodic poling essentially "corrects" the phase front of the second harmonic so that the first and second harmonic are phase matched again. In order to understand this process in detail, the act of poling, or domain inversion, is described.

Poling a ferroelectric material, such as lithium niobate, generates reversed polarization orientations in specific regions of a crystal. There is an inherent polarization in the crystal structure of lithium niobate on the $z$-axis, and this polarization is oriented in either the $+z$ or $-z$ directions. Under certain conditions, it is possible to switch, or flip, the

polarization from $+z$ to $-z$ (or vice versa) in controlled locations on a lithium niobate sample [7]. This act is called poling and is also frequently referred to as domain inversion. Poling is most commonly achieved by applying a strong electric field to the surface of a ferroelectric crystal. Domain inversion will only occur if the applied electric field strength is greater than the so-called coercive field strength, a physical property that is inherent to the ferroelectric (e.g., the coercive field for congruent $LiNbO_3$ is approximately 22 $^{kV}/_{mm}$ [10]).

Periodic poling inverts the local polarization directions (i.e., from $+z$ to $-z$) along the length of a crystal at evenly spaced intervals and is commonly used to increase SHG wavelength conversion efficiency. The exact periodicity of the inverted domains is chosen based on the wavelengths of interest so that just as the first and second harmonic phase fronts begin to become severely out of phase, the polarization orientation is inverted causing the two frequencies to again be phase matched [3]. A diagram of periodic poling is shown in Figure 1.1 in which the arrows represent the domain orientations. The top image depicts the original, unpoled lithium niobate where the entire crystal is of uniform polarization; the bottom image illustrates periodic poling where the domain is inverted at regularly spaced distances throughout the sample. Light propagation takes place perpendicular to the domain orientations, which is arbitrarily designated in the *x*-direction in this diagram.

The intensity of the second harmonic is shown in Figure 1.2 for three cases: no phase matching, quasi-phase matching (by means of periodic poling), and exact-phase matching. From the curves in Figure 1.2 it is seen that, in the absence of periodic poling,

the case depicted by curve (c), the fundamental and second harmonic are not phase matched leading to inefficient SHG. However, if a ferroelectric crystal is periodically poled, a quasi-phase matched situation is facilitated resulting in SHG intensity akin to that shown by curve (b) of Figure 1.2.

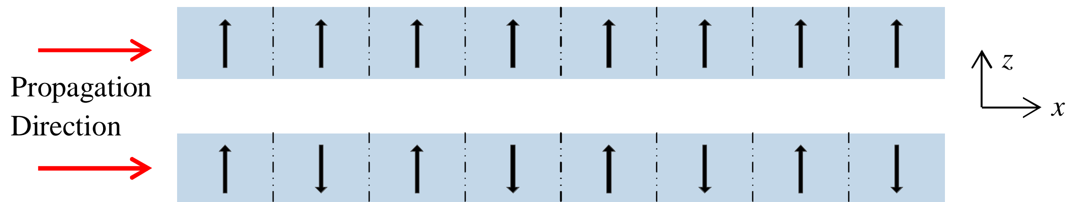


Figure 1.1. A diagram illustrating domain inversion due to periodic poling. The top image shows the original, unpoled LN, and the bottom image shows the LN after periodic poling.

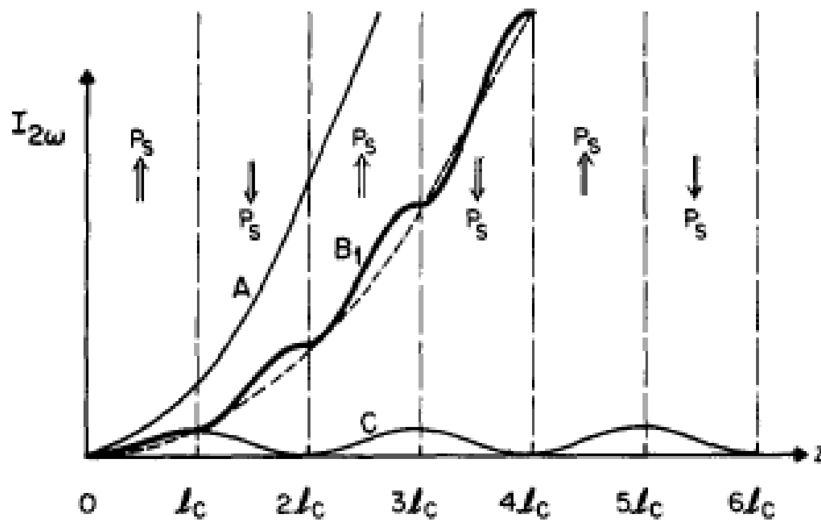


Figure 1.2. The effect of phase matching on the intensity of the second harmonic signal generated using periodic poling. The three curves correspond to (a) exact-phase matching, (b) quasi-phase matching, and (c) no phase matching (i.e., no periodic poling). $l_c$ represents the coherence length, and the arrows denote the polarization orientations [9].

The coherence length, $l_c$, represents the interaction length for which the second harmonic is efficiently generated. As the first and second harmonic frequency propagate

through the lithium niobate crystal, they will become out of phase due to dispersion. The second harmonic intensity is a function of $sinc^2(\Delta kl/2)$, where $\Delta k = k_1 - k_2$ ($k = 2\pi n/\lambda$) and $l$ is the length of the crystal [5]. Therefore, the maximum second harmonic intensity will be created when $sinc^2(\Delta kl/2)$ goes to zero, which only occurs when $\Delta k = 0$. The only solution to this condition is when $n_1 = n_2$. However, as lithium niobate is a dispersive material, this condition is not true for most frequencies.

When the two frequencies are in phase with each other, $\Delta k \approx 0$ and the second harmonic is efficiently generated. This is represented graphically from 0 to $l_c$ in Figure 1.2 on curve (c). As the two frequencies get more and more out of phase, or as $\Delta k$ increases, the second harmonic will inefficiently be generated due to destructive interference. At the point where the light has propagated $2l_c$ into the crystal, there will be no second harmonic generation. At this point, the first and second harmonic are exactly $\pi$ radians out of phase. The two frequencies periodically become in and out of phase relative to one another as they propagate through the crystal. The coherence length is defined by the distance the two frequencies will travel in the crystal in which the second harmonic is efficiently generated. Therefore, the poling period is defined by this length.

For wavelength conversions such as infrared to visible, the coherence lengths (and thereby the domain inversion periods) are on the scale of several microns. For example, using the Sellmeier equation and fitted parameters for congruent lithium niobate at room temperature [11], it can be found that the index of refraction for a Nd:YAG laser at 1064 nm is about 2.23. When frequency doubled to 532 nm, the index becomes 2.32. The phase velocities for each of these frequencies can then be calculated to be $0.448c$ for

1064 nm and 0.4304*c* for 532 nm. Based off of these phase velocities, the coherence length can be calculated to be approximately 6 µm.

If the wavelength of light desired to undergo SHG is smaller than that of infrared light, then the period of the poling must likewise be smaller in order to keep the fundamental and second harmonic quasi-phase matched. For example, in order to frequency double from blue to ultraviolet (UV) light, shorter poling periods are required [8]. To be specific, a frequency doubled argon ion laser converts light from 488 nm to 244 nm. Again, using the Sellmeier equation and parameters for congruent LN [11], the indices of refraction are approximately 2.35 and 3.06. This leads to a coherence length of about 343 nm.

Although submicron poling has been achieved by certain researchers [1, 12, 13, 14, 15], it is still regarded as a nontrivial task, and there is much room for improvement toward optimizing the creation of submicron and nanoscale domain inversions. The quasi-phase matching process achieved via periodic poling of lithium niobate has proven to be an appropriate process for SHG at *certain* wavelengths and is quite efficient at these wavelengths [16, 17, 18]; for example, SHG is commonly used for Nd:YAG lasers to convert 1064 nm to 532 nm which requires a poling period of about 6 µm. However, the process is currently not readily translatable to other, shorter wavelengths.

The main objective of this thesis is to research potential avenues of creating more efficient and versatile SHG devices. Current SHG devices are commonly made using quasi-phase matching, which can never be used to make a device with 100% wavelength conversion efficiency. The quasi-phase matching technique is also not very applicable to a wide variety of wavelengths due to the difficulty of creating submicron and nanoscale

domain inversions. Therefore, there is significant room for improving the quality of SHG devices, such as increasing the wavelength conversion efficiency and making the devices more adaptable to a wide range of wavelengths.

This thesis will consider various methods of improving said efficiency. First, it will consider creating nanostructures on LN with the purpose of eventually creating a SHG device that will convert wavelengths with exact-phase matching as opposed to quasi-phase matching. This can potentially lead to 100% wavelength conversion efficiency. Though this thesis will not actually create a functioning SHG device, the research will determine whether or not creating nanostructures on LN for that purpose is feasible. Second, the thesis will research methods for creating nanoscale domain inversions. This will allow for quasi-phase matching SHG devices to be readily translated to wavelengths that require smaller poling periods, such as visible to UV. These goals will be achieved by etching the lithium niobate using conventional micro- and nanofabrication techniques commonly used on silicon and by researching various methods of poling lithium niobate, respectively. However, before delving into the details of these goals, it is important to understand some basic concepts of nano-optics which will explain how to realize exact-phase matching in lithium niobate (discussed in Section 1.3) and fabrication processes which describe the basic procedures necessary to structure micro- and nanoscale features on lithium niobate (discussed in Section 1.4).

## 1.3 Nano-Optics for SHG

Optical materials are characterized by specific inherent properties that describe how they transmit, reflect, and absorb light (e.g., the index of refraction). However, these

material properties can be engineered to a certain degree by fabricating nanometer scale structures into optical materials [19, 20, 21, 22]. For example, the creation of a photonic bandgap device can be achieved by introducing periodic inclusions into or removing small sections from a suitable substrate at regular intervals. The photonic bandgap device will then inhibit select frequencies of light from propagating through the substrate; the range of frequencies that is rejected is determined by the precise spacing of the inclusions or defects, which for typical applications ranges from 100 nm to 1 µm [19, 20, 21]. Some materials can also be nanostructured so that the phase velocity for a specific mode at a particular frequency is changed, allowing that mode to propagate at a different phase velocity through the material [20, 22]. Nanostructuring a material can also help confine an electric field within the material to areas smaller than the diffraction limit [19, 20]. In most bulk media, the confinement of an electric field is limited by the diffraction limit due to Heisenberg's uncertainty principle [19]; however, by nanoengineering specific structures on or in optical materials, the electric field can be confined to very small areas resulting in increased light intensity.

One useful application of nanoengineering optical structures is for increasing the efficiency of optical processes such as SHG. For high efficiency wavelength conversion to occur in a nonlinear optical material, two important criteria must be met. First, the fundamental electric field needs to interact with as much crystal as possible at a high intensity [3, 5]. Therefore, it is desirable for the electric field intensity to be increased, the interaction distance to be increased, and the cross-sectional interaction area to be increased. When considering a Gaussian beam, it is impossible to meet all of these criteria due to tradeoffs. For example, a high intensity is achieved when the beam is

focused to a small spot size, which results in a highly divergent beam. This creates a large electric field at the focus but for a small interaction length and small cross-sectional area.

The second criterion is that the fundamental and second harmonic need to be exact-phase matched (or quasi-phase matched), as discussed previously [3, 5]. To ensure exact-phase matching between the fundamental and second harmonic, there should be no dispersion at these two frequencies; that is, the phase velocities of the fundamental and second harmonic should be equal.

Through nanoengineering, both of these criteria can be met in lithium niobate substrates. First, waveguides can be constructed in LN that will allow for long interaction lengths while maintaining a high intensity. Such waveguides can be constructed using conventional fabrication techniques that will be discussed in Section 1.4. Second, said waveguides can be engineered in such a way that allows for phase matching between the two frequencies. The size and shape of these waveguides can be designed so that they only allow for the propagation of a specific mode at a particular phase velocity. It has been proven using rigorous coupled-wave analysis (RWCA) that lithium niobate can be nanostructured in such a way that the first mode of the fundamental and the second mode of the second harmonic frequency travel at the same phase velocity, both at about $0.63c$ [23]. This achieves exact-phase matching, which results in 100% efficient wavelength conversion.

The final structure, referred to as a grating, will consist of several differently sized waveguides that will meet both criteria. By nanostructuring a grating similar to the illustration shown in Figure 1.3, light will be confined to small areas and the effective

indices of refraction of the first and second harmonic will be matched, thus realizing exact-phase matching for high efficiency SHG in lithium niobate.

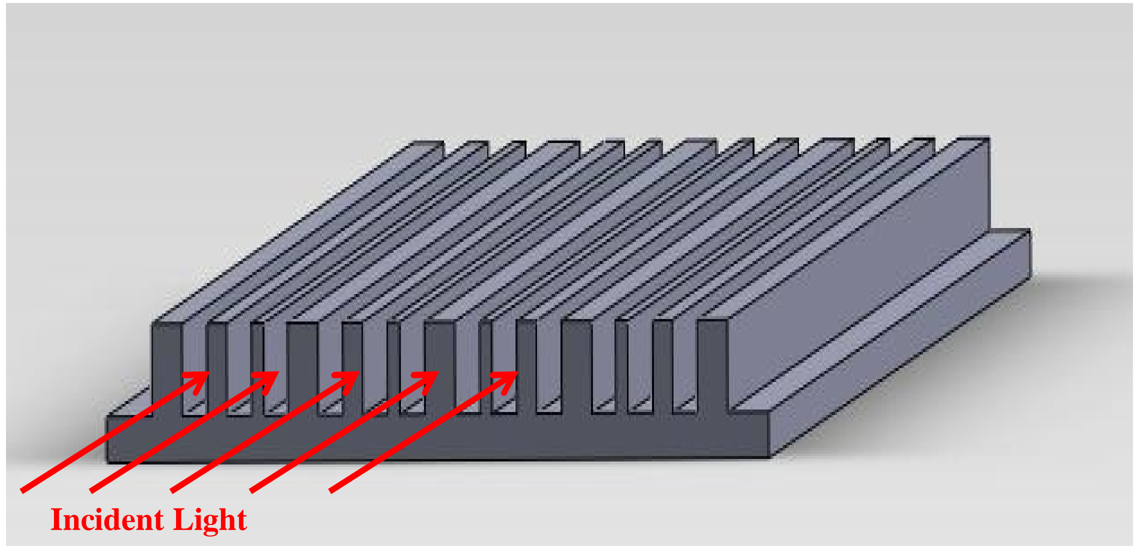


Figure 1.3. An illustration depicting a potential nanoscale grating etched into a lithium niobate substrate to obtain exact-phase matching.

## 1.4 Fabrication Process

In order to understand the fabrication processes involved in structuring lithium niobate, it is vital to grasp certain key concepts and practices that are typical of general fabrication techniques. Therefore, a rudimentary outline is provided for standard etching fabrication steps. First, a barrier layer, or mask, is deposited onto the entire surface of the substrate to be etched. This mask acts as a shield against future processes, and it can be patterned so that it only covers the substrate in specific areas. Further etching processes will only affect the substrate where there is no mask, or barrier, to inhibit the etchant. After the patterned mask is formed on the substrate surface, the sample will be etched. A basic outline of this process, termed lithography, is shown in Figure 1.4.

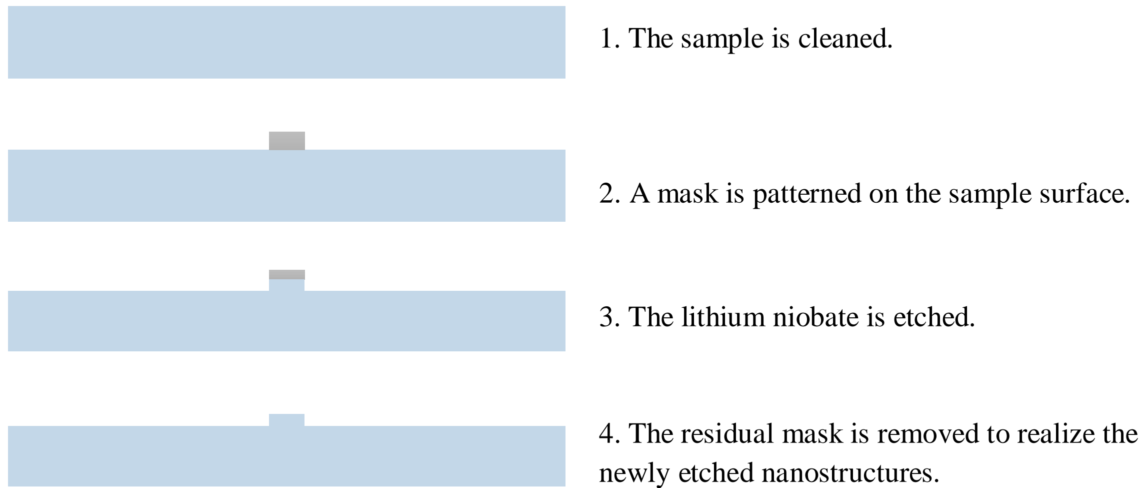


Figure 1.4. Outline of the lithography process required to etch nanostructures onto the surface of LN.

The mask can be composed of a variety of materials such as metals, oxides, and polymers. Methods of placing the mask onto the substrate vary depending on the materials used (e.g., chemical vapor deposition, sputtering, and vacuum evaporation are all different processes used to deposit masks), but a very common masking material for use in developing microelectronic devices is photoresist. Photoresist is a light-sensitive polymer that is typically applied to the surface of a substrate in liquid form through spin coating. After photoresist is spun onto a substrate surface, the substrate is baked for a short time allowing the photoresist to solidify. In order to transfer a pattern onto the photoresist masking layer, high-intensity ultraviolet light is allowed to shine through another pre-made mask containing the desired pattern and onto the photoresist layer. The mask pattern only allows UV light to expose the photoresist in specific areas. Due to the light-sensitive nature of the photoresist, exposed areas of the photoresist can be washed away in a developing solution creating windows in the photoresist that leave certain

regions of the underlying substrate uncovered. When a light source, such as UV light, is used to expose the photoresist, the term photolithography is used instead of simply lithography. Figure 1.5 demonstrates the photolithography process.

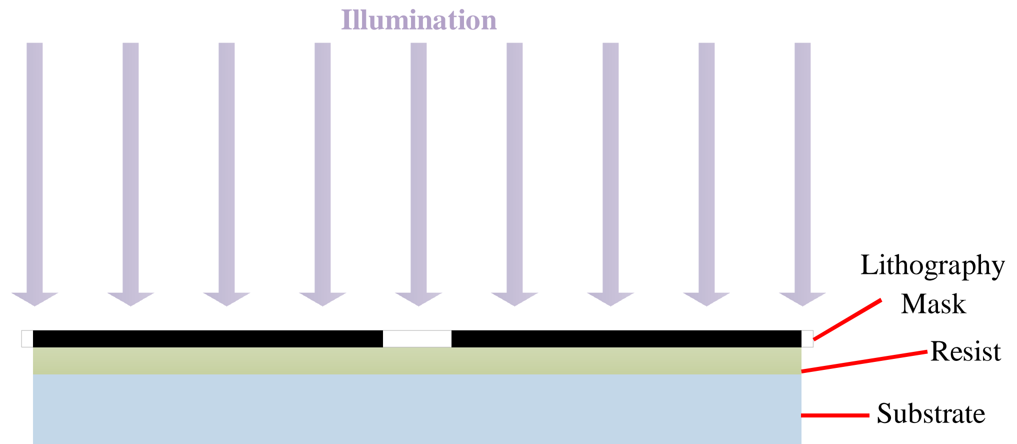


Figure 1.5. Illustration of the photolithography process.

Other types of lithography utilize alternative exposure sources other than light such as electrons in electron-beam lithography (EBL). The minimum feature size that can be patterned using optical sources in photolithography is limited by the wavelength of the light source employed [24]. Photolithography works well for achieving microscale structures, but it is difficult to use light to pattern nanoscale structures. However, EBL has the potential to pattern features on the order of tens of nanometers, and therefore, EBL is commonly used for the patterning of nanostructures. In a process analogous to photolithography, a resist is applied to the substrate surface; however, the resist used in EBL is not photon sensitive; it is electron sensitive. Then, after the sample is illuminated with an electron-beam, the developed resist will break down and be removed to form patterned windows of bare substrate.

As mentioned earlier, materials other than photoresist may be used as a mask, such as metal or oxides. When using materials other than resist as a masking layer, extra steps are sometimes required in order to transfer a pattern to the mask material. One method of creating a patterned metal mask is to first create a patterned resist layer onto the substrate surface. Then, metal may be deposited using an evaporation or sputtering process. After the metal is deposited onto the patterned resist and substrate, the resist is removed with a solvent, leaving metal on the substrate only in areas where resist was absent. Therefore, a negative image of the patterned resist will translate into a patterned metal mask layer. This method is known as lift-off. A basic outline of this process is shown in Figure 1.6.

In another scenario to form a metallic masking layer, metal is deposited directly to the sample surface, and then a layer of resist is deposited onto the metal. After the resist has been patterned and developed, there will be windows exposing select areas of metal. The sample can then be placed in an etchant which will remove any metal not covered by resist. This process is outlined in Figure 1.7.

Once the mask layer is formed, be it a metal, polymer, or oxide, the second step of the fabrication process can commence. The sample is placed in an etchant so that exposed areas of sample are removed while the areas covered by the mask material are largely unaffected. There are various methods for etching the substrate. A wet etch is a common technique which involves placing the sample in a liquid solution that will preferentially remove the substrate and not the mask via a chemical reaction. Dry etches are also used in some cases. Dry etches may refer to a chemical etch process, a physical process, or a combination of the two. Again, in a dry etch the substrate is preferentially removed while

the mask material remains mostly intact. In both wet and dry etches, the mask will be etched slightly along the substrate. The ratio of etched substrate to etched mask during a given amount of time is called the etchant selectivity. Good quality masks will have very high selectivities. After the sample is etched, the mask itself may be removed with a different etchant that only affects the mask material and not the substrate. This results in a structured substrate. By nanostructuring lithium niobate in a very specific manner using methods outlined in this section, it is possible to achieve exact-phase matching.

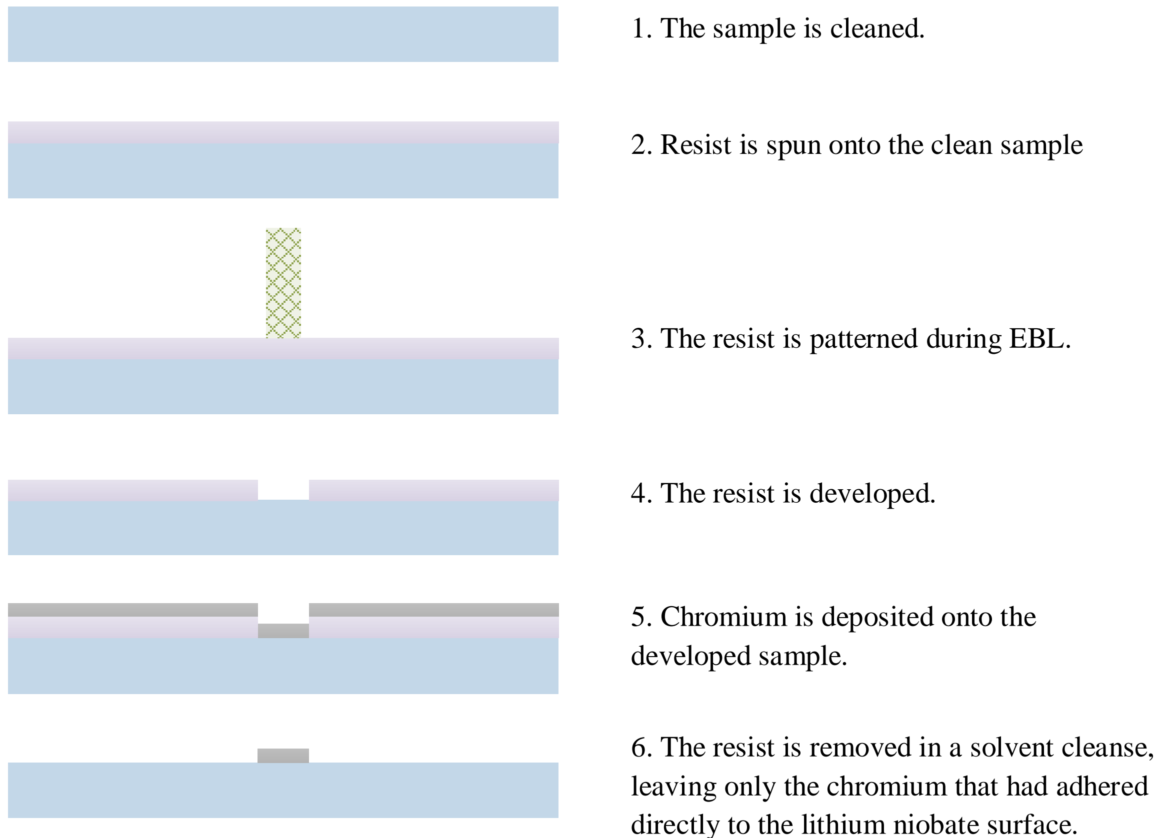


Figure 1.6. Schematic detailing the process of lift-off.

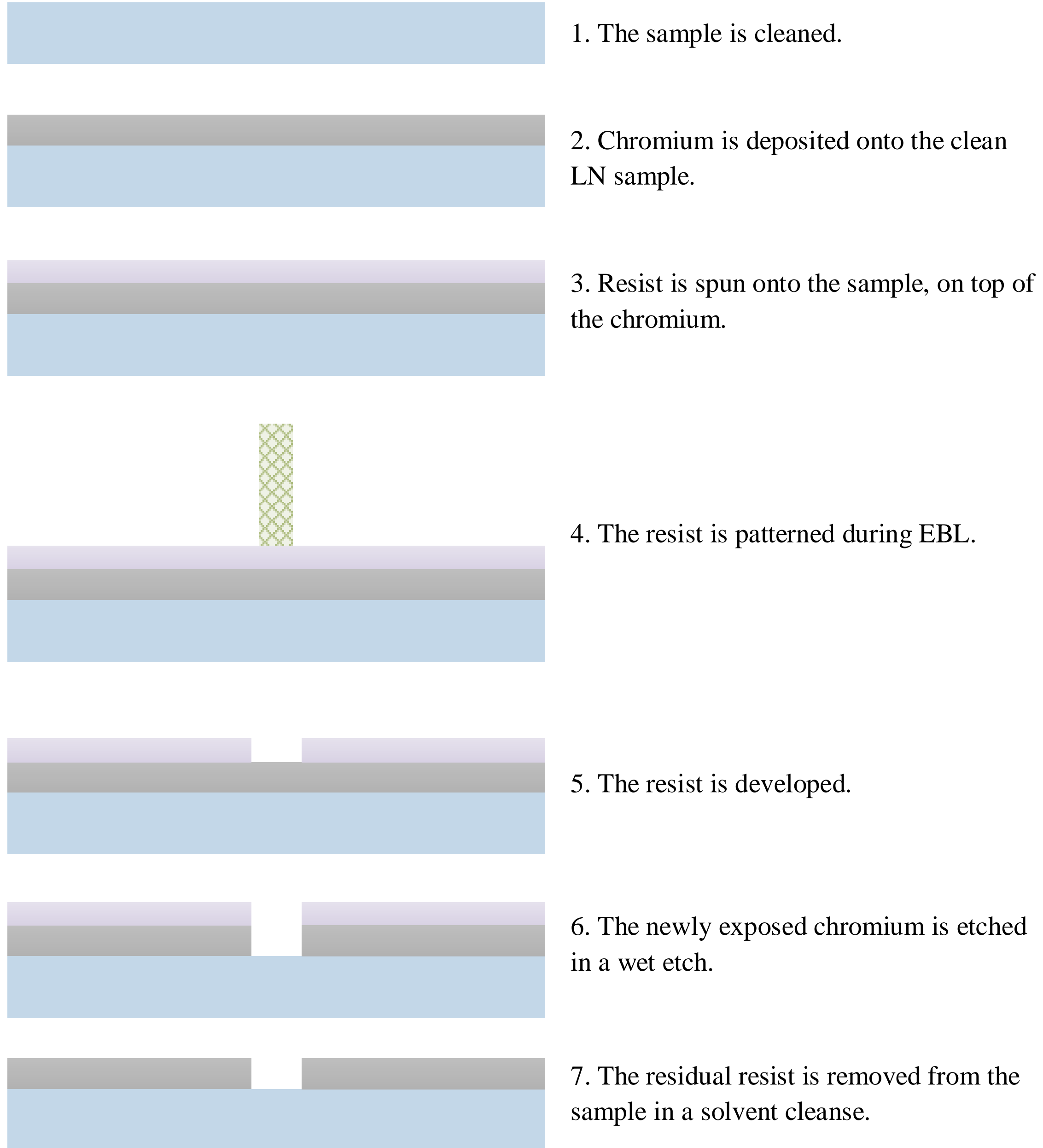


Figure 1.7. A second scenario detailing the process of patterning a metal layer onto a substrate surface.

## 1.5 Thesis Objective

The major goal of this thesis is to prove that nanoscale, submicron, and microscale features can be engineered on lithium niobate substrates to facilitate the

development of highly efficient second harmonic generation optical devices. This thesis concentrates on developing two different techniques for structuring lithium niobate; one method is the geometrical structuring of LN via etching methods and the other is domain structuring via periodic poling.

Improved second harmonic generation efficiency is important for several reasons. First, as mentioned previously, increased wavelength conversion efficiency would greatly benefit low-light applications. For example, low-light detection in the IR spectrum is difficult due to poor quality detectors and low conversion efficiency. An efficient SHG device, however, could efficiently convert low-light IR to the visible spectrum, where low-light detectors are abundant. Another application for these improved devices is versatility. Currently, quasi-phase matched SHG devices are only efficient at wavelengths which require longer coherence lengths, making the poling period on the microscale. In order to be able to make SHG devices for other wavelengths, either a device must be easily scalable to other wavelengths or nanoscale domain inversions must be realized for periodic poling. This thesis will investigate nanostructuring lithium niobate so that exact-phase matching can be achieved. This technique ensures that the devices will be scalable to a wide range of wavelengths. Nanoscale domain inversions will also be explored, so that quasi-phase matching devices can be made at a much broader range of wavelengths.

The research endeavors undertaken in this thesis work are well received by local company AdvR, Inc. This thesis will help strengthen bonds between AdvR, Inc. and Montana State University as AdvR, Inc. is very much involved with wavelength conversion using lithium niobate. AdvR, Inc. typically uses doped *z*-cut LN in their

ventures, and likewise the research described herein focuses on doped *z*-cut LN in order to comport with the research of AdvR, Inc.

This thesis will examine three methods of improving SHG efficiency using lithium niobate. The first method concerns the creation of nanoscale gratings on the surface of LN. Such gratings potentially allow for exact-phase matching resulting in 100% wavelength conversion efficiency in SHG devices. The second method involves microscale structures resembling optical waveguides. Currently, AdvR, Inc. typically uses larger waveguides with widths of several microns. If waveguides could be manufactured so that the waveguide widths are closer to 1-3 μm, AdvR., Inc. would benefit from the smaller cross-sectional area which increases SHG efficiency. The last method considers nanoscale domain inversions in lithium niobate. This may not necessarily improve the wavelength conversion efficiency of devices manufactured to convert IR to green light, but it would allow for the creation of devices with the ability to scale to other wavelengths since they could potentially require smaller poling periods.

These three methods will be investigated thoroughly first through a comprehensive literature survey. In order to review previous research efforts on these subjects, a literature survey is provided in Chapter 2. Inspection of successes and failures of prior enterprises will help to determine the best methods to use for etching and poling lithium niobate. Chapters 3 and 4 examine the etching of nano- and microstructures in lithium niobate, followed by a discussion of poling in Chapter 5. Finally, suggestions for future development based on the results of this research and an overall summary are provided.

# CHAPTER 2

# LITERATURE SURVEY

## 2.1 Introduction

The first task accomplished for this project was a thorough survey of the current literature regarding etching and structuring lithium niobate. As the main goal of this thesis is to improve SHG conversion efficiency via structuring, it is imperative to understand the science and research that has already been done in this field to adequately inform future endeavors. This extensive literature overview is intended to serve the purpose of determining the optimal strategies for the Nano-Optics Group to pursue toward structuring lithium niobate using the resources available at Montana State University.

Several different techniques and methods for structuring lithium niobate have been investigated by other research groups. First, wet etches are reviewed. Wet etching is the most common method of structuring lithium niobate, but it is predominantly used for creating microscale structures. Among the various wet etching methods, though, there are techniques that have been used to create nanostructures in LN. These procedures are relatively new and therefore not widely used.

Poling, the process of creating domain inversions, is also investigated. While this thesis is primarily focused on creating nanoscale domain inversions, it is also important to understand how microscale domain inversions are created. By understanding the limitations of conventional poling, other methods can be devised in order to overcome

these restrictions to achieve nanoscale domains. The many novel techniques for creating nanoscale domain inversions are also examined.

The last technique discussed is dry etching. Dry etching is a common fabrication procedure used for structuring materials such as silicon, and is typically preferred to wet etching when creating features on the nanoscale. Dry etching has been used to structure lithium niobate using various methods such as the reactive ion etch (RIE), the inductively coupled plasma reactive ion etch (ICP-RIE), and focused ion beam milling (FIB).

Before discussing the different etching techniques in detail, though, an important distinction must be made between doped and pure lithium niobate. It is common for lithium niobate to be doped with materials such as magnesium (Mg) and magnesium oxide (MgO). It was found that doped lithium niobate (with Mg or MgO) has a reduced coercive field [25, 26]. The coercive field defines how resistant a ferroelectric material is to flipping domains (from $-z$ to $+z$ or vice versa when considering lithium niobate). A high coercive field means that the material is not susceptible to domain inversions, and an extremely high external field is required in order for poling to occur. Because doped lithium niobate has a reduced coercive field compared to pure lithium niobate, the crystal is more apt to flip domains, which is important when considering poling for applications such as quasi-phase matching for SHG.

Another difference between doped and undoped lithium niobate is the change in the photorefractive effect. The photorefractive effect is the phenomenon seen in some optically nonlinear materials in which the index of refraction changes as a function of the electric field. In lithium niobate, due to its high photorefractive properties, high laser intensities will create changes in the birefringence of the crystal [27]. Doped lithium

niobate has lower photorefractive properties, so the index of refraction will not change as much as in pure lithium niobate under similar conditions [28]. This is important because photorefraction can cause optical damage. High intensities of light can alter the crystalline structure permanently in materials with high photorefractive properties. Therefore, in some scenarios doping the LN sample is necessary in order to avoid optical damage. However, doping lithium niobate will lead to the loss of some of its original properties. Depending on the application, it may be necessary to work with either pure or doped LN. While pure lithium niobate is investigated in this literature survey, only doped lithium niobate will be structured in this thesis because of the reduced coercive field for poling, the higher threshold for high intensity lasers, and the affiliations with local company AdvR, Inc., who predominantly use doped lithium niobate.

## 2.2 Wet Etching

Wet etching is a common method for etching lithium niobate. However, wet etches typically result with a large degree of surface roughness and poor sidewall smoothness. There are two etchants that are usually used for the LN wet etch. One etchant is simply hydrofluoric acid (HF), while the other is a solution made up of both HF and nitric acid ($HNO_3$). Various ratios of HF to $HNO_3$ have been tested, and the most common ratio used is 1:2 (HF:$HNO_3$). However, it has been seen that other concentrations of HF/$HNO_3$ etch lithium niobate too but at numerous etch rates resulting in various qualities [29]. For instance, some HF/$HNO_3$ concentrations etched the lithium niobate at a relatively quick etch rate but caused the surface of the lithium niobate to be extremely rough which leads to optical scattering and power loss in some applications.

Several different mask materials have been used during the wet etch. Metals such as chromium can be deposited and used as an etch mask [30]. Another method of masking is to use a proton exchange, patterned into a mask via lithography. A proton exchange replaces the lithium ions, $Li^+$, with hydrogen ions, $H^+$ [31]. This process is typically done by placing the LN sample in an acidic bath. The $HF/HNO_3$ acid will preferentially etch the proton-exchanged LN (PELN) over the original LN substrate [31, 32]. A third possibility is to use domain inversions as the etch mask. HF will etch the $-z$ face of LN (the side of the crystal that is represented by the $-z$ domain of the crystalline structure) at a rate significantly higher than the $+z$ face [13, 29, 33, 34]. Over long periods of time (hundreds of hours) it was observed that the $+z$ face of LN was not affected by the $HF/HNO_3$ acid [29, 35].

As mentioned earlier, most structures created via wet etch are microstructures, particularly waveguides. However, it was discovered that by using domain inversions as an etch mask and HF as an etchant, nanostructures could be created using a wet etch [13]. One sample was observed to have periodic structures of about 200 nm in width and 530 nm in depth (period of the structures was 530 nm). This indicates an aspect ratio of 2.65. The structures also appeared to be of good quality with relatively smooth and vertical sidewalls (exact angles of the sidewalls were not given). However, it was found that this process results in a small lateral etch which leads to mask undercut [36]. For example, a long etch can cause cylindrical features to turn conical. Although most of the wet etches only realize microstructures, the nanoscale features realized by the domain inversions would help realize two goals of the thesis. First, it could potentially lead to structured

lithium niobate in order to achieve exact-phase matching as described in Chapter 1, and second, it could lead to a method of nanoscale domain inversions.

### 2.2.1 Ion Implantation Assisted Wet Etching

Another wet etching method is called ion implantation assisted wet etching. For this wet etching technique, lithium niobate is masked on one face of the sample using conventional lithography procedures. Then, that face of the sample is implanted with ions so that only the unmasked areas of the lithium niobate substrate are bombarded and affected by the ion implantation. This effectively damages the crystalline structure of lithium niobate in those exposed, unmasked areas, which increases the wet etch rate of the lithium niobate drastically. After ion implantation, the sample is placed into a wet etchant (most commonly an HF solution), where the ion-implanted regions are etched extremely quickly, compared to the undamaged areas. This technique was used on the $+z$ face of lithium niobate, where $O_2$ and Si served as the bombardment ions at an energy of 1.5 MeV and a fluence of $1x10^{15}$ ions/cm$^2$ [37]. Several other heavy ions were used in this technique, but on different faces of lithium niobate. Table 2.1 shows all of these etching trials. Masks for the ion implantation varied from micron thick layers of photoresist to gold. Note that the most interest, for this thesis, lies in structuring the $z$ face of the lithium niobate because of collaborations with AdvR, Inc. This method, which results in extremely smooth sidewalls, could either be used for nano- or microstructuring lithium niobate, and could aid in realizing the thesis objective of creating both nano- and microscale features on LN.

Table 2.1. Ion Implantation Assisted Wet Etching Parameters

| Reference | Ion | Energy | Fluence | Face of LN |
|---|---|---|---|---|
| **Wang 2006** [37] | $O^+$ | 1.5 MeV | $1x10^{15}$ ions/$cm^2$ | +*z* |
| **Wang 2006** [37] | $Si^+$ | 1.5 MeV | $1x10^{15}$ ions/$cm^2$ | +*z* |
| **Gischkat 2008** [38] | $Si^+$ | 5 MeV | $7x10^{12}$ - $1x10^{14}$ $cm^{-2}$ | *x* |
| **Nicola 2013** [39] | $Cu^+$ | 5 MeV | $1x10^{15}$ $cm^{-2}$ | *x* |
| **Schrempel 2006** [40] | $He^+$ | 350 keV | $5x10^{12}$ to $5x10^{16}$ $cm^{-2}$ | *x* |
| **Schrempel 2006** [40] | $Ar^+$ | 350 keV | $5x10^{12}$ to $5x10^{16}$ $cm^{-2}$ | *x* |
| **Gill 2004** [41] | $O^{3+}$ | 6.8 MeV | (not given) | -*z* |

## 2.3 Electric Field Poling

Electric field poling of lithium niobate is used to create domain inversions (also referred to as poled regions or nucleation sites) along the *z*-axis of lithium niobate. Various methods are used to cause the domain to be flipped from +*z* to -*z* (or vice versa) in a localized area. One issue with electric field poling is that it is extremely hard to create domain inversions at a submicron and nanoscale level [42]. There are several different techniques for poling lithium niobate, which are detailed in the following sections. The first method, conventional poling, is used to create microscale domain inversions and therefore will not be considered as a viable option to create nanoscale domain inversions. However, it is important to understand the concepts and limitations of conventional poling in order to fully understand other poling techniques. The other techniques to be mentioned in this section (backswitching, surface poling / overpoling, and optical poling) will focus on techniques that will help realize the thesis goal of nanoscale domain inversions.

2.3.1 Conventional Poling

Currently, poling is typically achieved by lithographically patterning electrodes on the surface of lithium niobate, and then applying an external electric field to the LN sample via the patterned electrodes. This process inverts the domains where the electrodes are placed, and the areas not covered by the electrodes, which are commonly coated in an insulating polymer, remain at the same polarization orientation. The areas at the edges of the electrodes will become poled first, and then the domain inversions will spread to fill out the whole area under the electrode (with some domain inversions spreading outside the electrode covered area). The domain inversions will occur throughout the entire thickness of the sample, which is referred to as bulk poling. After poling, the external electric field is slowly ramped down to 0 V in order to help stabilize the domain inversions.

This method is the most common technique used to periodically pole lithium niobate [42]. However, because of field fringing, domain spreading effects, and nonuniform nucleation along the edges of electrodes, submicron poling is virtually impossible using this method [43]. The high coercive field (approximately 22 $^{kV}/_{mm}$ for lithium niobate) and "inherent non-uniformities and defects" in lithium niobate also hinders the process of submicron poling [1]. Conventional poling can achieve domain inversion periods of 4-5μm at the smallest for depths of about 500 μm [1].

2.3.2 Backswitching

As mentioned earlier in conventional poling, the external electric field is ramped down to help stabilize the domain inversions. If the electric field is suddenly brought

back to 0 V with no ramp down, the poled areas are liable to backswitch, or flip back to their original domains [43]. In poling via backswitching, this facet plays a major role. In this technique, the LN samples are patterned with metal electrodes, and an external electric field is applied in order to pole the regions under the electrodes, as in conventional poling. However, after the regions have been poled, the electric field is then rapidly lowered so that spontaneous backswitching occurs. When done under proper conditions, this poling via backswitching will create domain inversions that are only under the edges of the electrode [12]. This method has been used to create periodic nanoscale domain inversions as small as 100 nm [44].

### 2.3.3 Surface Poling / Overpoling

Another method of creating submicron domain inversions is to only pole the surface of the sample, as opposed to bulk poling. Typically, a lithium niobate wafer is around 300-500 μm thick. When bulk poling lithium niobate, as in conventional poling, the domain inversions occur all the way through the wafer. However, a newer technique demonstrates that domain inversions can be created so that they are only several microns deep, which allows for smaller domain sizes [1, 45, 46, 47, 48]. Instead of the typical metal electrodes, gel electrodes are patterned onto the lithium niobate, and the electric field is applied through liquid electrolytes. Gel electrodes are used instead of metal because charge accumulation is needed for this process, which is not possible while using metal electrodes.

In order to achieve surface poling, one of the $z$ faces of lithium niobate is covered with about 1 μm of photoresist (PR) [1]. Then, both $z$ faces are patterned with conductive

gel electrodes. A high-voltage pulse is then applied via electrodes. A technique called "overpoling" is used in order to realize submicron features [1]. The image shown in Figure 2.1 shows three different scenarios: (a) "underpoling", (b) conventional/ideal poling, and (c) overpoling (the black space on top of the sample denotes where the insulating PR is).

Next to each of the images shown in Figure 2.1, there is an acronym called EF which represents the empirical factor (EF) of the lithium niobate. The EF is used to "correct for variations in supplier dependent material stoichiometry, precise values of thickness across the sample, and specific electrical characteristics of the poling supply itself" [1]. The external electric field is applied for a specific amount of time in order to achieve the desired poling effects, and this time duration is a function of both the area of the lithium niobate to be poled and the empirical factor of the LN.

In Figure 2.1a, the EF is less than 1, which results in an irregular domain inversion pattern; not all of the areas in the LN were poled. Figure 2.1b shows the ideal case, where EF = 1, and the sample is poled perfectly in accordance with the electrode placement. However, Figure 2.1c shows the overpoling scenario. In this case, it appears that the entire sample has been domain inverted (resulting in the loss of a periodic domain inversion), but there are actually small domain-inverted structures hiding beneath the insulating photoresist that are only a few microns deep. This overpoling method is used to obtain submicron domain inversion periods in lithium niobate that are deep enough for certain applications – for most applications they essentially need to be as deep as a waveguide [1, 45, 46, 47]. This is the idea behind surface poling. One can overpole LN in order to realize submicron periodic poling.

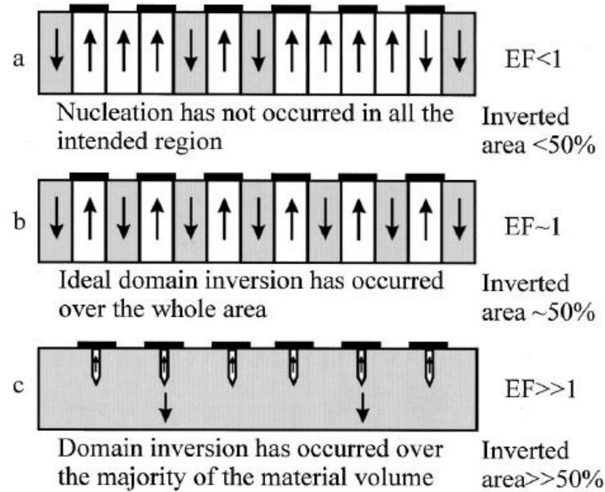


Figure 2.1. Illustration depiction underpoling (a), conventional poling (b), and overpoling (c) [1].

This overpoling method has been used for microscale periodic poling with lithium niobate [1, 45, 46, 47], but it has also been used to realize nanostructures in lithium niobate using a poling / wet etch method [13, 49]. These patterns range from 530 nm periods to 2 μm periods with the smallest feature size being 200 nm [13]. The average depth of these domain inversions is about 10 μm [49].

## 2.4 Optical Poling

It has been found that shining a laser on a lithium niobate sample can reduce the coercive field and therefore assist in the poling of the substrate [15, 25, 26, 28, 36, 50, 51, 52, 53, 54]. Applying this knowledge in conjunction with an external electric field can lead to the poling of lithium niobate. This technique is known as light assisted poling, or LAP. In addition, it has been found that at specific energies and wavelengths, the laser itself can overcome the coercive field and create domain inversions without the use of an

external electric field [14, 35, 36, 55, 56]. Poling lithium niobate using only a laser is known as all optical poling, or AOP. This section will cover both LAP and AOP, as well as discuss several key factors concerning optical poling. Optical poling is an intriguing option because it is a fairly novel concept and has been proven to achieve nanoscale domain inversions. Also, as the name suggests, the Nano-Optics Group is much more familiar working with optical setups as opposed to high power electric field configurations.

### 2.4.1 Light Assisted Poling

Light assisted poling, or LAP, has been accomplished using both UV and visible light. UV radiation can reduce the coercive field in LN, which means that the external electric field does not have to be as high as it needs to be for conventional electric field poling [26]. Visible light creates "charge distribution between electron traps" which results in the building up of electric space-charge fields [26]. A combination of space-charge fields and an external electric field results in domain inversion in lithium niobate [26]. Wavelengths of either UV or visible light can lead to domain inversion in conjunction with an external field.

In order to simultaneously illuminate lithium niobate and expose it to an external electric field, a complex setup in necessary. All of the apparati mentioned in this section are quite similar. They all involve a sealed gasket with transparent windows, and liquid electrolytes on either side of the sample. Therefore, a high-voltage electric field can be applied across an LN sample while a laser is simultaneously illuminating the sample [25,

28, 36, 50, 52, 53]. The applied electric field is typically ramped up at a set pace over a specific period of time. A representative apparatus is shown in Figure 2.2.

An important parameter for LAP is crystal orientation. When the laser is illuminating the -*z* face of lithium niobate, the polarization of the illuminated areas will be flipped to +*z*. However, when the laser illuminates the +*z* face, the laser tends to inhibit domain inversion in the presence of an electric field, while the unilluminated areas of the sample will be flipped [15, 36]. Hence, careful attention must be paid as to whether the +*z* or –*z* face is being illuminated by the laser beam.

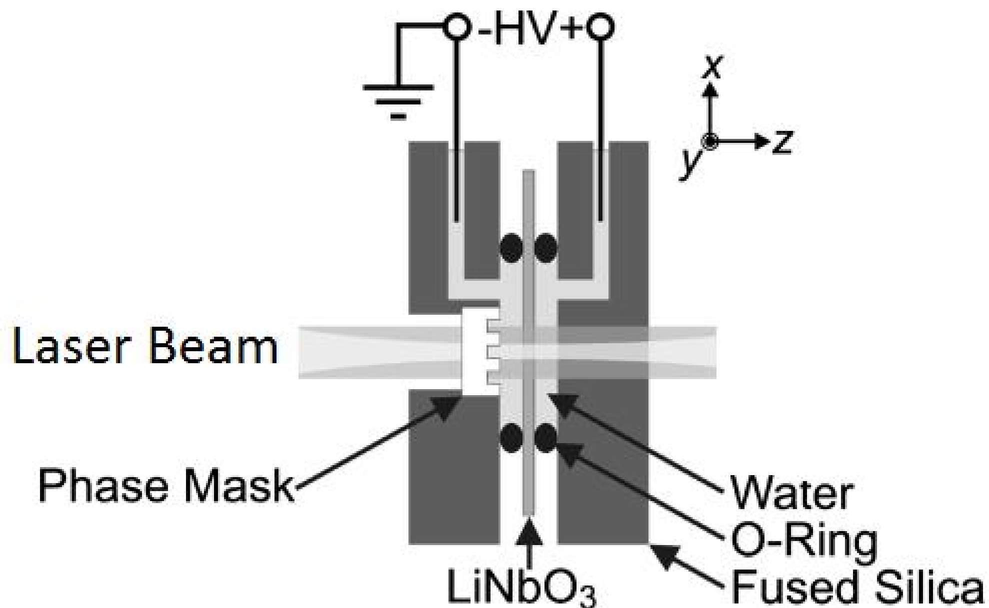


Figure 2.2. A representative apparatus commonly used for LAP [53].

There is a wide variety of wavelengths used for LAP, but most of the lasers used are argon ion lasers. Common lasers used for LAP and their associated wavelengths are listed in Table 2.2. After the sample is poled, the domains must be visualized in order to confirm poling. Unfortunately, this is no trivial task. Nanoscale domain visualization can

be done in several different ways, although some methods can be extremely complicated. Numerous techniques are listed in [42], along with a good current review of nanoscale domain visualization. However, only two methods will be discussed in this paper, electro-optic visualization and HF etching.

Table 2.2. LAP Lasers and Wavelengths

| Reference | Type of Laser | Wavelength (nm) | Pulsed vs Continuous Wave (cw) |
|---|---|---|---|
| **Sones 2008** [15] | Argon ion | 244 | (not given) |
| **Mailis 2010** [36] | (not given) | 244-305 | (not given) |
| **Wengler 2005** [28] | Argon ion | 305, 334 | (not given) |
| **Eggert 2006** [26] | Argon ion | 305, 334, 488 | (not given) |
| **Valdivia 2006** [53] | (not given) | 305, 334, 364, 383, 400, 514.5, 800 | Femtosecond pulsed |
| **Muller 2003** [52] | Argon ion | 351, 334 | (not given) |
| **Ying 2009** [50] | (not given) | 400 | Femtosecond pulsed |
| **Sones 2005** [25] | Argon ion | 457, 488, 524 | cw |
| **Dierolf 2004** [54] | Argon ion | 488 | (not given) |
| **Sandmann 2005** [51] | Argon ion | 488 | (not given) |

Several articles describe a technique in which one can monitor the domain inversion in real time using a HeNe laser, an external electric field, and a charge-coupled device (CCD) camera [28, 52, 53]. The HeNe laser and LN sample are configured in an interferometric system. When the electric field is applied and the domains are inverted, the index of refraction of the $+z$ axis will shift slightly in one direction, and the $-z$ axis will shift in the opposite direction. This will create a slight difference between the indices for the $+z$ and $-z$ axes. As the light propagates through the poled crystal, it will travel at slightly different phase velocities depending on the crystal orientation or domain.

Therefore, it will accumulate a phase difference in specific areas when the sample is poled, resulting in an interference pattern. The interference pattern can be imaged on a CCD camera, and the domain inversions can be viewed as the sample is poled. This method is very useful while performing LAP because the setup is virtually complete due to the poling apparatus; only a HeNe, CCD camera, and some optics need to be added to the system and aligned in order to visualize the domain inversions.

The second technique for domain visualization is simply etching the sample in HF after poling. Because the $+z$ face is not etched at all in HF and the $-z$ face is, the subsequent HF etch can reveal domain inversions. However, this is a physical process that destroys the sample, which may not be ideal for all applications. An advantage of this method over others, though, is that it is relatively simple and concrete. It gives necessary results without the need of a complicated optical system.

In all of the articles referenced in this section, the domain feature sizes were on the micron scale. The smallest of the features that were realized were 1-2 μm. However, no statement was made that nanofeatures *could not* be made using the LAP technique. Another important detail about domain inversions is that the domain walls followed the crystal symmetry very precisely, which means the domain inversions were not necessarily exactly where the sample was illuminated. The hexagonal crystal structures inherent in LN cause the domain inversions to follow that symmetry, which means the domain inversions will become hexagonal. If a circular pattern is illuminated on one side of the sample (and causes domain inversions), the opposite side of the sample will likely have domain inversions in the shape of a hexagon, instead of a circle.

2.4.2 All Optical Poling

Unlike light assisted poling, all optical poling or AOP - also called the direct write method - does not need an external electric field in order to invert the ferroelectric domains. The illumination itself is enough to invert the polarization of the crystals. Most AOP is done using UV irradiation [14, 35, 36, 55, 56, 57]. However, it was observed that IR illumination works for AOP as well [14]. Looking at the effects different wavelengths have on domain inversions, it was found that shorter wavelengths required lower intensities for the same reduction in the nucleation field or coercive field [53]. This means that the UV wavelengths could be at lower intensities than visible light (and much lower than IR radiation) while still creating approximately the same coercive field reduction. Therefore, higher frequencies require lower intensities in order to reduce the nucleation field by a certain magnitude.

The configuration for this technique is fairly simple. A laser illuminates a pattern on the LN sample. This pattern can be created by using optical devices such as phase or amplitude masks which create diffraction patterns on the sample; alternatively, the beam may be focused to a small spot size and then scanned over the sample. The latter method is often used with a computerized translation stage which will move the sample in front of the laser beam in order to create the desired domain inversions. In both of these methods, the laser is always illuminating the $-z$ face of the sample so that the illuminated areas will be flipped to $+z$.

One theory about all optical poling is that AOP depends on the peak temperature reached during illumination, as opposed to the LN sample staying at a specific elevated temperature [36]. Therefore, there will be a “sweet spot” in which the laser absorption is

low enough so that the light can penetrate the LN to a certain depth, but the absorption is high enough to heat the LN and cause domain inversion. Using Palik's optical constants to find skin depths (δ) for lithium niobate in UV, Figure 2.3 was created. Palik's definition is shown in Equations 2.1 and 2.2, where $\alpha$ is the absorption coefficient, $k$ is the imaginary part of the index of refraction, and $\lambda$ is the wavelength [58]. Values used for $k$ in the calculations were parallel to the $z$-axis.

$$\alpha = {4\pi k}/{\lambda} \qquad (2.1)$$

$$\delta = {1}/{\alpha} \qquad (2.2)$$

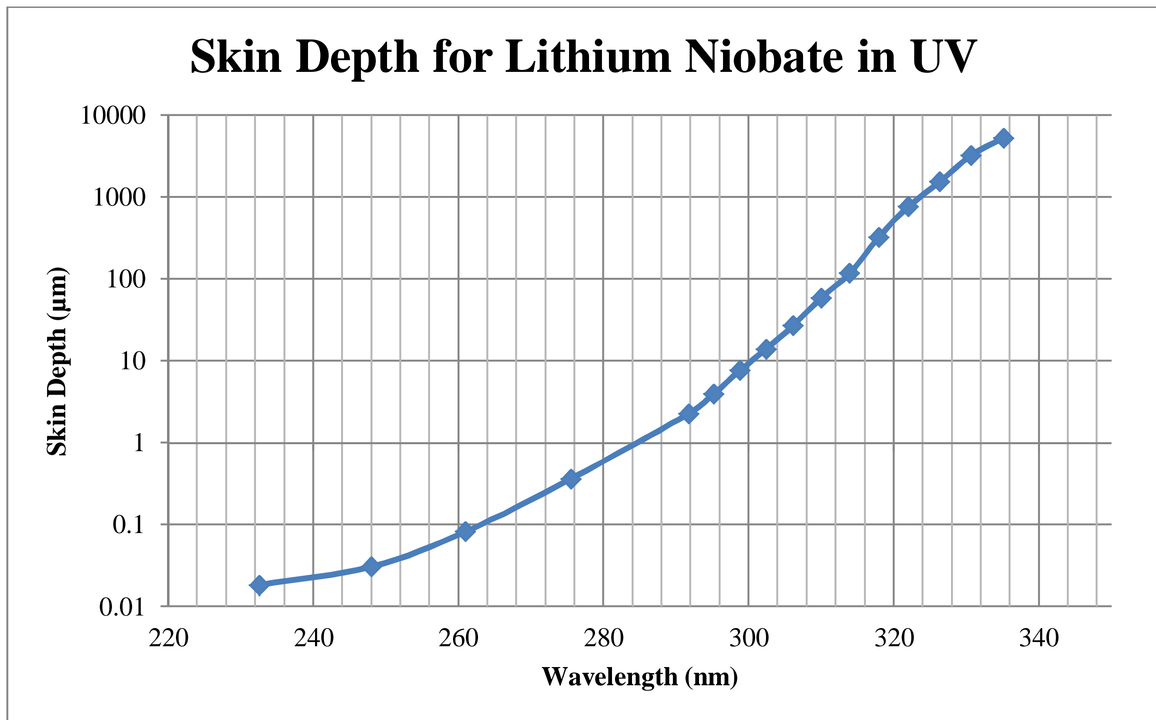


Figure 2.3. Calculated skin depths for LN, based off Palik's values [58].

This graph could be useful in order to ascertain which wavelength might work best depending on how deep the laser needs to penetrate or how deep the poling needs to be. However, it must be noted that at wavelengths with strong absorption and intensities,

lithium niobate can be damaged. In undoped lithium niobate, the absorption edge is about 350 nm [36]. From 244 to 305 nm, the light only travels a few microns or less into the LN surface, resulting in “rapid local heating” which causes surface damage or melting (for laser intensities from 300 to 400 kW/cm$^2$) [36]. Research was done on laser damage in lithium niobate due to high power femtosecond lasers [59]. At high powers, ablation, melting, and amorphization can occur in the surface of LN which can result in craters, debris, and other damage to the crystal. However, it must be noted that this testing was done using a Ti:Sapphire laser at 800 nm, and not at UV wavelengths.

For LAP, it was seen that mostly argon ion lasers are used, with a wide variety of wavelengths. For AOP, numerous types of lasers are used, but they are all relatively close in wavelength (barring the IR test [14]). This is most likely because, as mentioned earlier, shorter wavelengths will decrease the nucleation field with less power than higher wavelengths [53]. Table 2.3 lists the different lasers and wavelengths used by various groups.

Table 2.3. AOP Lasers and Wavelengths

| **Reference** | **Type of Laser** | **Wavelength (nm)** | **Pulsed vs cw** |
|---|---|---|---|
| **Muir 2008** [57] | Argon ion | 244 | cw |
| **Mailis 2010** [36] | Argon ion | 244 | cw |
| **Mailis 2005** [35] | KrF Excimer | 248 | Pulsed |
| **Valdivia 2005** [56] | KrF Excimer | 248 | Pulsed |
| **Wellington 2007** [55] | Nd:$YVO_4$ | 266 | Pulsed |
| **Wellington 2007** [55] | Dye | 298 | Pulsed |
| **Valdivia 2005** [56] | Dye | 298 | Pulsed |
| **Kuznetsov 2008** [14] | Excimer gas | 308 | Pulsed |
| **Kuznetsov 2008** [14] | $CO_2$ gas | 10.6 μm | Pulsed |

In looking at Table 2.3, mostly pulsed lasers are used; only two continuous wave (cw) lasers were used. When comparing cw and ultrashort pulsed lasers, the pulsed lasers reduce the nucleation field 5 times more than cw lasers do because of the higher peak intensities - the average intensities were about the same [53]. Also, “cw light is more likely to form hexagonal structures that will spread laterally”, while “ultrashort pulses can permit domain shapes and sizes as defined by the illumination pattern” [53]. Finally, it is mentioned that cw lasers cause more stress/damage to the crystal than ultrashort pulsed lasers cause. Therefore, it may be advantageous to use a pulsed laser as opposed to cw for AOP.

In AOP, mostly subsequent HF etching is used in order to see the domain inversions. The electro-optic visualization method is rarely used because of the complex setup; no external electric field is necessary for AOP, so to create one around the sample just to visualize the domains is impractical. Therefore, in the articles found, all of the domains were visualized after poling by etching the sample in HF.

The domain inversions created from AOP are able to get down to nanoscale features. Most of the articles found showed nanoscale domain inversions, with the smallest features being around 150 nm [56]. The nanometer domains were created using phase or amplitude masks. The two groups who used a focused spot to write patterns were only able to obtain microscale domain inversions [36, 57]. This was due to the fact that in both cases, the spot sizes were about 1.5 μm. It is possible that if the beam spot is diffraction limited, nanoscale domains could be created without the use of phase or amplitude masks. Also, the domain inversions do not tend to follow the crystal symmetry as the LAP domains do. The domain walls directly followed the shape of the beam which

results in curved domain inversions throughout the sample and no hexagonally shaped domains.

## 2.5 Dry Etching

Etching micro- and nanostructures into lithium niobate has been well researched, and several methods have been used. It is important to note that most etching done on lithium niobate is done on the micron scale in order to create structures such as waveguides. However, there has been some research (and success) in etching nanostructures into lithium niobate - mainly for photonic crystal applications. Etching lithium niobate could result in either nanoscale structures with the potential of exact-phase matching or microscale structures that could be used as low-loss ridge waveguides. Both of these realizations could assist in the thesis goal of improving current SHG devices.

### 2.5.1. ICP-RIE / RIE Etches

Two very common, and closely related, etching processes are the reactive ion etch (RIE) and inductively coupled plasma reactive ion etch (ICP-RIE) methods. The Montana Microfabrication Facility (MMF) has an Oxford Plasma Lab ICP-RIE etcher which makes this method particularly interesting to the Nano-Optics Group. The basic premise of these two etching techniques involves creating a chemical plasma which will etch the surface of the sample. A gas is pumped into the vacuum chamber of the etcher and is excited into a plasma. A DC bias is typically created with a powered electrode so that the ions from the plasma strike the surface of the sample. The gas or gas mixture to create the

plasma, referred to as the etch chemistry, is chosen based on the substrate material and the isotropy of the etch. Commonly used gases are fluorine, chlorine, and oxygen.

From the research found, all of the etch masks have been metal masks. Typically the masks are either chromium [60, 61, 62] or electroplated nickel [63, 64, 65, 66]. However, there have been other mask materials, such as a nickel-chromium alloy [66] and poly-silicon [67]. These masks have all been proven to have decent selectivities where high aspect ratios are achievable, suggesting it is beneficial to use one of these materials.

Next, the etch chemistries are investigated. All plasmas were created with a fluorine based gas. $SF_6$ is commonly used [61, 63, 64, 65, 66]. $O_2$ is used as the passive gas with $SF_6$ in all of these etch trials. Other gases used are $C_4F_8$ [60], $CHF_3$ [61, 65, 67], and $CF_4$ [62, 64]. Most of these were used with either argon or helium acting as the passive gas. Several of these papers include sections where they compare different etch chemistries and how the LN etch is affected [60, 61, 64, 66]. An excellent comparison is shown in Table 2.4 [61]. It is important to note that sidewall angles of >80° were achieved in trial number 5 using a $CHF_3$/Ar etch chemistry, while the other trials showed sidewall angles closer to 60° or 70°.

One major issue with the ICP-RIE etch for lithium niobate is the redeposition of lithium fluoride (LiF) on the sample surface. The LiF falls onto the sample during the etch and can create issues with the structures because it acts as an etch mask. This will create surface irregularities and significantly decrease the etching rate. However, the redeposition of LiF can be managed through various techniques. One method to get past this issue is to simply take the lithium niobate out of the etcher after a few minutes of

etching, clean off the sample, and then continue etching [60]. This method can be done with an "SC-1 solution" made of seven parts de-ionized water, two parts hydrogen peroxide, and one part ammonium hydroxide (7:2:1 - $H_2O$ : $H_2O_2$ : $NH_4OH$), and that helps clear off the LiF. Another way to reduce the LiF redeposition is to do a proton exchange before the etch. This can either be done before the etch mask is deposited [60, 61] or after the etch mask is patterned [67]. The proton exchange, which will be discussed in detail in Chapter 4, reduces the amount of lithium ions in the lithium niobate, thereby reducing the amount of byproduct created during the etch, lithium fluoride.

Table 2.4. ICP-RIE Etching Trials with Varied Parameters [61]

| No. | Gas and Flow Rate (sccm) | Power (W) | DC Bias (V) | Chamber Pressure (mTorr) | Sample Cooling | Average Etching Rate (nm/min) | Average Selectivity |
|---|---|---|---|---|---|---|---|
| **1** | $CF_4$ - (not given) | 300 | (not given) | 500 | None | PLN-2.62<br>PELN-8<br>Cr-2.3 | 1.12<br>3.43 |
| **2** | $SF_6$ - (not given) | 300 | (not given) | 500 | None | PLN-0<br>PELN-25.5<br>Cr-0.6 | n/a<br>46 |
| **3** | $SF_6$ - 50 | 1500 | 153 | 6 | Backside, with He | PLN-7.5<br>PELN-45.7<br>Cr-1.5 | 5<br>30 |
| **4** | $CHF_3$ - 50<br>Ar - 50 | 1500 | 122 | 6 | Backside, with He | PLN-10.8<br>PELN-48<br>Cr-1 | 10.8<br>48 |
| **5** | $CHF_3$ - 50<br>Ar - 50 | 1500 | 130 | 6 | None | (not given)<br>PELN-96<br>Cr-3 | not given<br>32 |

### 2.5.2. Focused Ion Beam Milling

Another method used is called focused ion beam milling (FIB) [60, 68, 69, 70, 71]. This "mills" into the substrate one hole at a time and can get structures as small as hundreds of nanometers. One problem with this method is that it is time consuming because there is only one beam, so the structures must essentially be milled into the substrate one at a time – as opposed to ICP-RIE, where the entire sample is etched at once. This method has been proven to work well, though it is a slow, serial process. However, this technique requires specialized equipment and machinery capable of FIB milling, which is not available at Montana State University.

## 2.6 Analysis and Feasibility

### 2.6.1 Etching

There are several different methods listed for etching lithium niobate. Taking into account the resources available at Montana State University, only a number of these processes are practical methods. Considering first the dry etches, three etches are mentioned: RIE, ICP-RIE, and FIB (note that the RIE and ICP-RIE are nearly identical processes, and do not have much discrepancy between the two when etching lithium niobate).

The FIB technique, as mentioned earlier, is considered time consuming as each structure must be made one at a time. Both the RIE and ICP-RIE techniques prove better than the FIB method regarding this issue. However, when comparing the RIE and ICP-RIE to the FIB, it must also be noted that the FIB technique is able to achieve sidewall angles of almost 90° [39, 71], while the highest seen sidewall angle for the ICP-RIE is

only about 82° [61]. Therefore, both processes have their advantages and disadvantages. However, in the Montana Microfabrication Facility (MMF), an Oxford Plasma Lab ICP-RIE etcher is available to use, and is often used by several members of the Nano-Optics Group. Neither an RIE etcher nor an FIB is available. Therefore, the ICP-RIE becomes a more viable option.

In addition to dry etching, a wet etch for lithium niobate is also considered. As mentioned in Section 2.2, there is a wide variety of possibilities for the wet etch of lithium niobate. However, most of these options are only practical when realizing microscale structures such as waveguides. This is primarily due to the fact that wet etches are commonly isotropic, which will wash out nanostructures with high aspect ratios. Because one goal is to realize nanostructures in lithium niobate, it is important to focus on etches that will allow us to succeed. Some viable options in the wet etch category are: (1) etching the sample in HF after poling the lithium niobate with nanoscale domain sizes, or (2) an ion implantation assisted wet etch.

The poling/HF etch method has been proven to have the ability to realize nanostructures in lithium niobate [13], even though it is no trivial task to create nanoscale domain inversions [42]. Ion implantation assisted wet etch has been seen to realize nanostructures as small as 500 nm [38]. As this is a fairly new technique, most researchers have only used this method to create popular features such as waveguides on lithium niobate, so there are not many results regarding nanostructuring lithium niobate in this manner. However, both of these methods seem promising in realizing nanoscale features in lithium niobate.

Both of these techniques involve unfamiliar processes. For the poling/HF etch method, the HF etch can be accomplished in the MMF, but a method for poling the nanodomains would be needed. Concerning the ion implantation assisted wet etch, no method for ion implantation is available at MSU. However, it must be noted that the steps leading up to the ion implantation can be accomplished, as they are simply lithography and mask patterning techniques already in process for silicon, and the subsequent wet etch, as already mentioned, could be accomplished in the MMF. Both of these methods would be viable options if (1) a method for poling is realized; and (2) a method for ion implantation is found.

2.6.2 Poling

There are numerous potential options that would allow for the nanoscale poling of lithium niobate. After taking each into consideration, the best option for the Nano-Optics Group is determined to be all optical poling. This method, which can be used for creating both nanoscale domain inversions and nanoscale structures (via the poling / wet etch technique), is a direct writing technique which allows for a wide variety of nanoscale shapes and patterns to be written into the lithium niobate. Electric field domain inversion techniques, however, lack this flexibility because the domain inversions typically follow the crystal structure, making it difficult to get curved domain walls. Also, two different UV lasers are available in the Department of Chemistry and Biochemistry, both of which can be used for AOP processes. The first is a Chameleon Ti:Sapphire Coherent laser, and the second is a frequency doubled argon ion laser. The Ti:Sapphire laser is a pulsed laser (100 fs pulses, 80 mHz repetition rate) that is tunable from 250 to 330 nm, and it outputs

tens of milliWatts of power. The argon ion laser is a continuous wave (cw) laser at 244 nm that is integrated into a Raman microscope.

Both of these lasers would work for AOP, as suggested by the literature survey. As mentioned earlier, pulsed lasers seem to be the preferred choice for AOP, which would make using the Ti:Sapphire laser a better option. However, it must be noted that the cw argon ion laser is configured into a Raman microscope, which means that the laser is essentially set up in a manner which would be used for AOP. The light is focused through a microscope objective (MO), and the sample sits on a translation stage, which is necessary for writing different patterns on the lithium niobate sample. The pulsed laser system is not necessarily configured in such a way for it to be immediately ready for AOP, so it may not be a convenient option. Both lasers are viable options in order to achieve AOP on lithium niobate, but the argon ion laser may be a better choice for preliminary poling trials.

## 2.7 Conclusion

Several methods were listed and analyzed in this chapter. Based off the resources available to the Nano-Optics Group, the best option is to attempt to structure lithium niobate using ICP-RIE methods. It has proven to be an adequate technique for etching lithium niobate by several credited sources, and it is a familiar process to the Nano-Optics Group as similar fabrication procedures are currently used on silicon to create polarized beam splitters. Other intriguing options are the poling/HF etch method and the ion implantation assisted wet etch. For the poling/HF etch, the lithium niobate can be poled using high powered UV lasers, available in the Department of Chemistry and

Biochemistry at MSU, and etched in the MMF. This method has the potential to help achieve two goals. First, it could lead to nanoscale domain inversions so that lithium niobate could be poled at smaller periods. Second, it could lead to nanoscale structures which would contribute to the exact-phase matching goal defined in Chapter 1. Because everything in this method can be readily done using resources available at MSU, this option is considered a technique worth trying.

The ion implantation wet assisted etch is also an intriguing method because of the ease of fabrication. In essence, the samples can easily be masked using familiar lithography and evaporation processes. Then, the samples can simply be shipped out to a vendor to be implanted with heavy ions and then shipped back to MSU for a subsequent wet etch in HF at the MMF. This technique could both create nano- and microscale structures on lithium niobate. Therefore, this technique could either be used to achieve exact-phase matching or create microscale ridge waveguides.

However, there may not necessarily be time to do all three techniques when considering the thesis deadline. Therefore, focus will be drawn to the ICP-RIE and AOP/wet etch. These two techniques will be used to create micro- and nanoscale features on lithium niobate, and the AOP/wet etch will also potentially realize nanoscale domain inversions. Between these two methods, all three goals of the thesis will be met. First, nano- and microscale features will be etched into lithium niobate for potential exact-phase matching capabilities and micron-sized ridge waveguides. Second, nanoscale domain inversions will be achieved during all optical poling, which can assist with the quasi-phase matching of visible to UV light. The remainder of the thesis will discuss in

detail the results from etching lithium niobate using ICP-RIE and the AOP/wet etch method.

# CHAPTER 3

# FABRICATION PROCESS PART 1: PATTERNING CHROMIUM ETCH MASKS

## 3.1 Introduction

In order to create etched nanostructures on lithium niobate, several fabrication steps are necessary. Researchers in the Nano-Optics Group have been processing silicon chips for several years, and most of these known and optimized processes may be simply translated over to lithium niobate fabrication. Chapter 3 discusses the first part of the fabrication process, patterning a mask on a lithium niobate substrate, where the procedure is nearly identical to patterning a mask on silicon. The steps involved in masking lithium niobate with a chromium mask should require the same steps it takes to pattern a mask on silicon. The second part of the fabrication process, in which lithium niobate is etched and structured, is detailed in Chapter 4.

## 3.2 Fabrication Process

The lithium niobate chips used are all borrowed from the local business AdvR, Inc. who specializes in using poled lithium niobate for second harmonic generation. The samples are all *z*- cut and doped with magnesium oxide (MgO). All of the samples came off of one wafer, which was coated on the –*z* face with thin films of both chromium and silicon dioxide ($SiO_2$), making it necessary to clean the samples before fabrication. This is simply done by placing the samples in a wet chromium etchant for about 10 minutes, followed by a 2 minute buffered oxide etch (BOE). The wafer is cut into several 1.4 cm x

1.4 cm die, which is slightly too large for the fabrication process. Therefore, the die are all cleaved into smaller, more manageable chips, which are roughly 0.7 cm x 0.7 cm. Then, the samples are cleaned using a three solvent cleanse involving acetone, isopropanol, and methanol. Once the lithium niobate has been ridded of the chromium and silicon dioxide, cleaved, and cleaned with the three solvents, the samples are ready to be processed. The first part of the fabrication process, patterning the chromium mask, is outlined in Figure 3.1. The sample is spun with resist, patterned via electron-beam lithography (EBL), developed, deposited with chromium, and lifted-off. A thorough, detailed description of the entire fabrication process is listed in Appendix A.

It is important to note that the resist spun onto the sample consists of a bilayer composed of two different resists: polymethyl methacrylate (PMMA) and polymethyl glutarimide (PMGI). The PMGI is spun on first and is approximately 150 nm thick. The PMMA is then spun on top of the PMGI and is about 50 nm thick. Therefore the total resist thickness is roughly 200 nm. This bilayer recipe is used in order to ensure a higher quality chromium mask after the lift-off procedure. The PMMA, which is on top, is electron-sensitive, and will be exposed by the electron-beam during EBL. The PMGI is not electron-sensitive, so it is not affected during EBL. When the PMMA is developed after EBL, patterned windows appear in the PMMA layer, which exposes some of the PMGI. When the PMGI is developed, it is dissolved where the PMMA windows are located. Therefore, developing the PMGI can essentially create wells underneath the PMMA windows.

After the resist is spun, the samples are patterned during EBL. The only anticipated difference between the fabrication process of silicon and lithium niobate is

during the electron-beam lithography. Lithium niobate is not nearly as conductive as silicon, which means that the patterns created during EBL could become marred due to charge buildup. The electrons from the electron-beam will not dissipate easily on lithium niobate, as they do with silicon, so the surface of the lithium niobate will become charged. This charge buildup will in effect steer the electron-beam away from the surface, which means that the desired pattern will most likely not be formed. Therefore, a thin film of gold is sputtered onto the lithium niobate before EBL begins. This film helps dissipate the charge on the surface of the chip, so that the electron-beam can write uninhibited.

After several chips were processed using this method that had been developed for silicon processes, a potential issue was discovered. The lift-off procedure in this technique limits the amount of chromium thickness that can be deposited, thereby limiting the amount lithium niobate that may be etched. The thickness of the chromium cannot exceed the resist thickness on the sample; otherwise the lift-off procedure fails. This issue had never come up before in the silicon etches because the metal mask for silicon does not need to be very thick. However, the etch selectivity for lithium niobate to chromium is fairly low, so thicker masks would be advantageous for creating deeper etches with higher aspect ratios. Therefore, a second method was developed. Method B, as it is known, allows for the chromium to be much thicker, which in turn allows for more lithium niobate to be etched. The second process, Method B, is outlined in Figure 3.2.

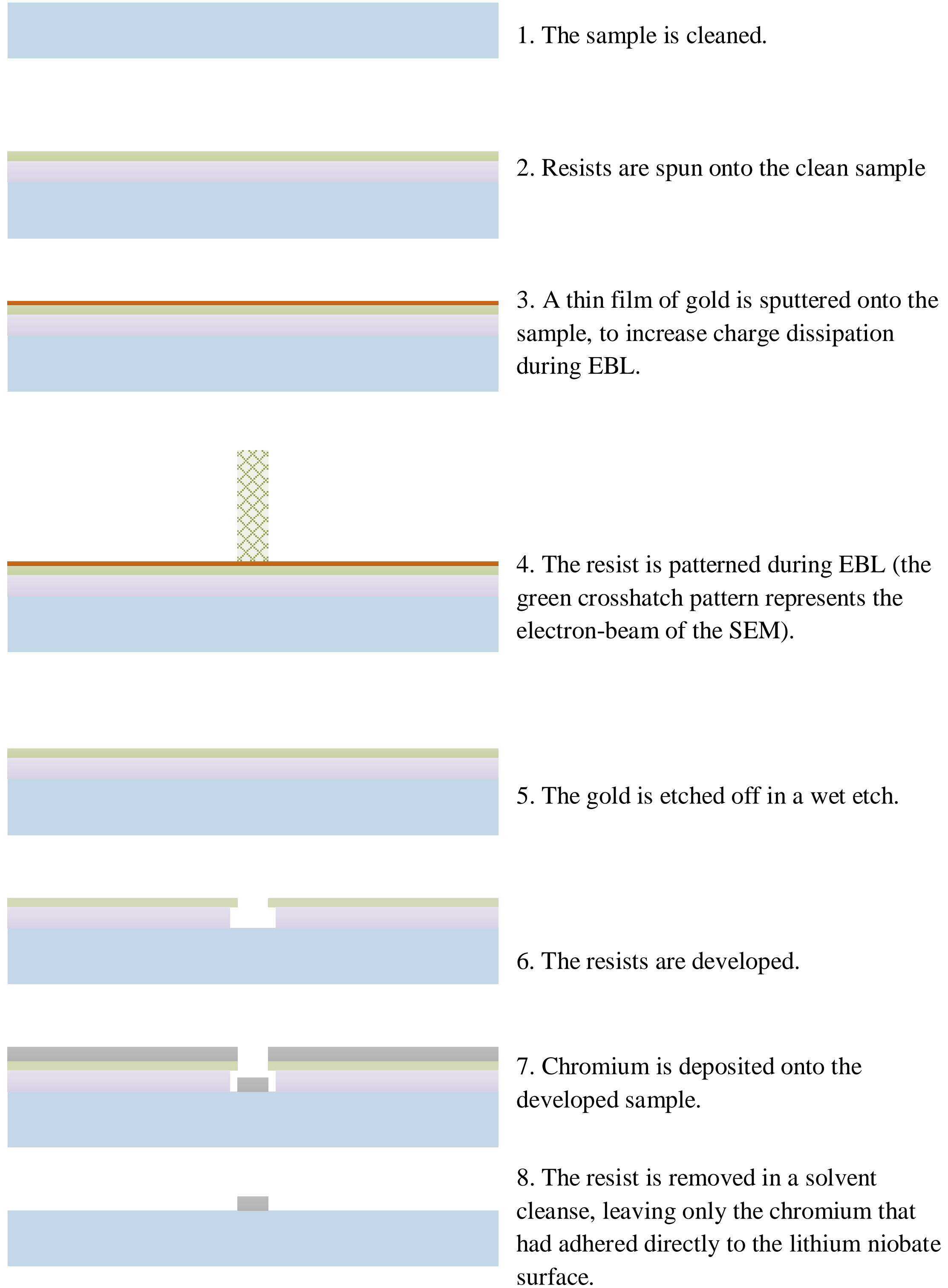


Figure 3.1. Diagram illustrating the patterning of the chromium mask.

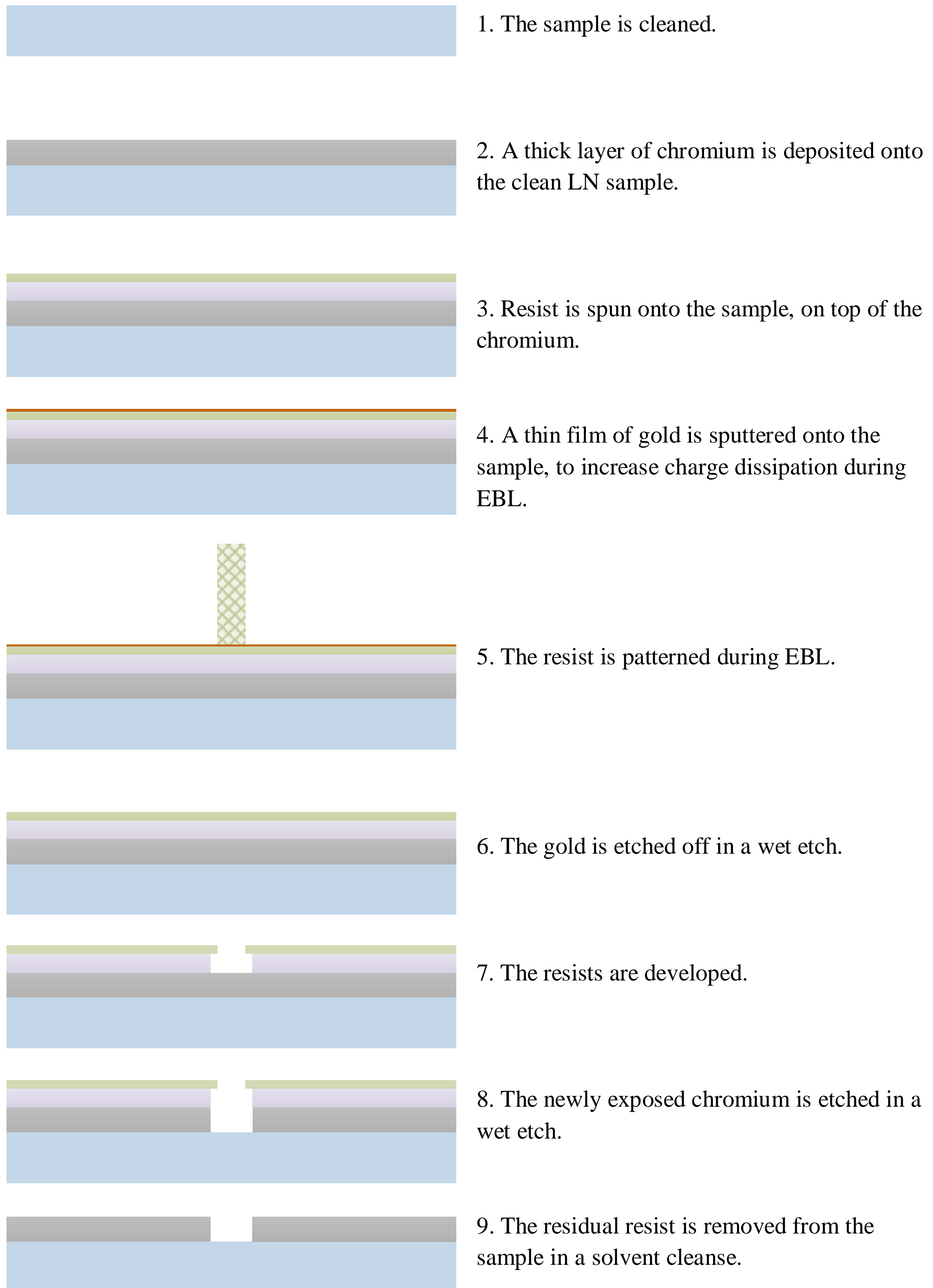


Figure 3.2. Diagram illustrating fabrication process for Method B.

One major difference between the first method, referred to as Method A, and Method B is the order of the fabrication steps. For instance, in Method A, the chromium is deposited onto the sample after the resist mask has been patterned with EBL. This is followed by a lift-off procedure where the chromium is removed from the wafer everywhere except where the patterned windows in the resist are located. However, in Method B, the chromium is deposited first, and then the sample undergoes EBL. The chromium is then etched away where the EBL created windows in the resist, resulting in an opposite, or negative, mask as seen in Method A. Figure 3.3 shows the masks created by the two different methods. One thing to note is that Method A uses a bilayer recipe in order to create a better quality mask after lift-off. Technically, this bilayer recipe is not needed for Method B. The purpose of the bilayer recipe is to improve the lift-off procedure in Method A. However, it was found that the wet chromium etchant tends to eat through the PMMA but does not affect the PMGI. Therefore, it is imperative to have the bilayer recipe, so that a proper etch mask is used during the chromium etch.

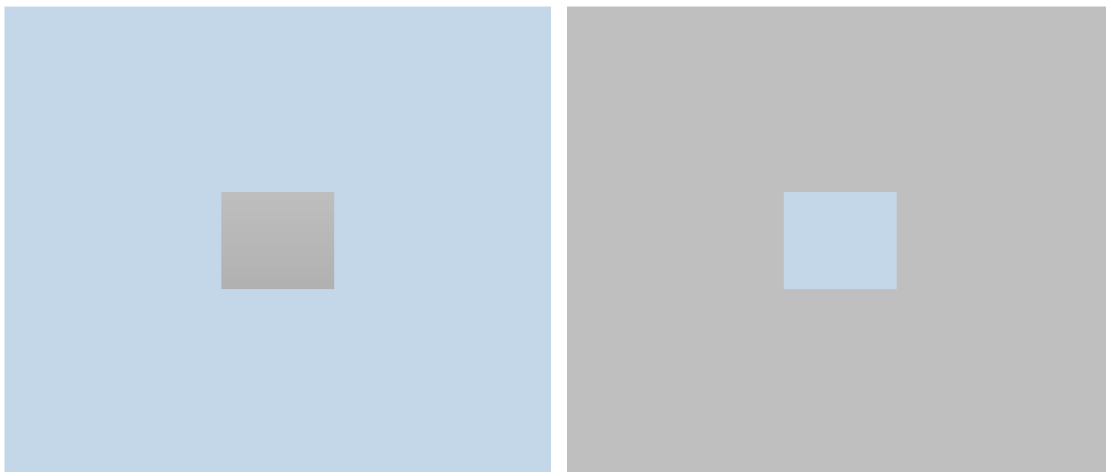

Figure 3.3. Left- metal mask created through Method A; Right- metal mask created through Method B.

## 3.3 Lithography Patterns

The lithography patterns used all entail periodic gratings, in which a wide selection of sizes are implemented, ranging from a 300 nm period to a 10 µm period, all with a 50% fill factor. This range of periodic gratings was used so that each etch trial involved both nanostructures and microstructures. The desired result is to prove that both nanoscale and microscale features can be etched into lithium niobate. The diagram shown in Figure 3.4 roughly shows how the patterned gratings look on the chips. This vertical pattern is repeated seven times on the sample – in a horizontal fashion – so that numerous electron-beam doses can be tested.

## 3.4 Resist

### 3.4.1 Resist Development

During the etching trials, it was found that a number of chips were failing at the development stage. The resists were patterned and developed, but the exposed patterns were over-developed and unusable. An example of the overdeveloped patterns developed in the resist is shown in Figure 3.5, and an example of properly developed patterns is shown in Figure 3.6. It was found that the PMGI resist was being extremely overdeveloped, to the point where a significant amount of the PMGI had been dissolved. The brown patches seen in Figure 3.5 represent areas where the PMGI had dissolved completely. Because the main goal of the PMGI is to create small wells under the developed PMMA windows, the devices were utterly useless. However, several samples had been patterned and developed before this problem was discovered, and the same

development times were being used. After some careful analysis, it seemed that the devices were failing simply because the patterned chips were being developed immediately following EBL. If the chips are developed at least 12 hours after EBL, this problem is no longer an issue. Therefore, it appears the samples need to rest, or cure, for several hours following EBL in order to be properly developed.

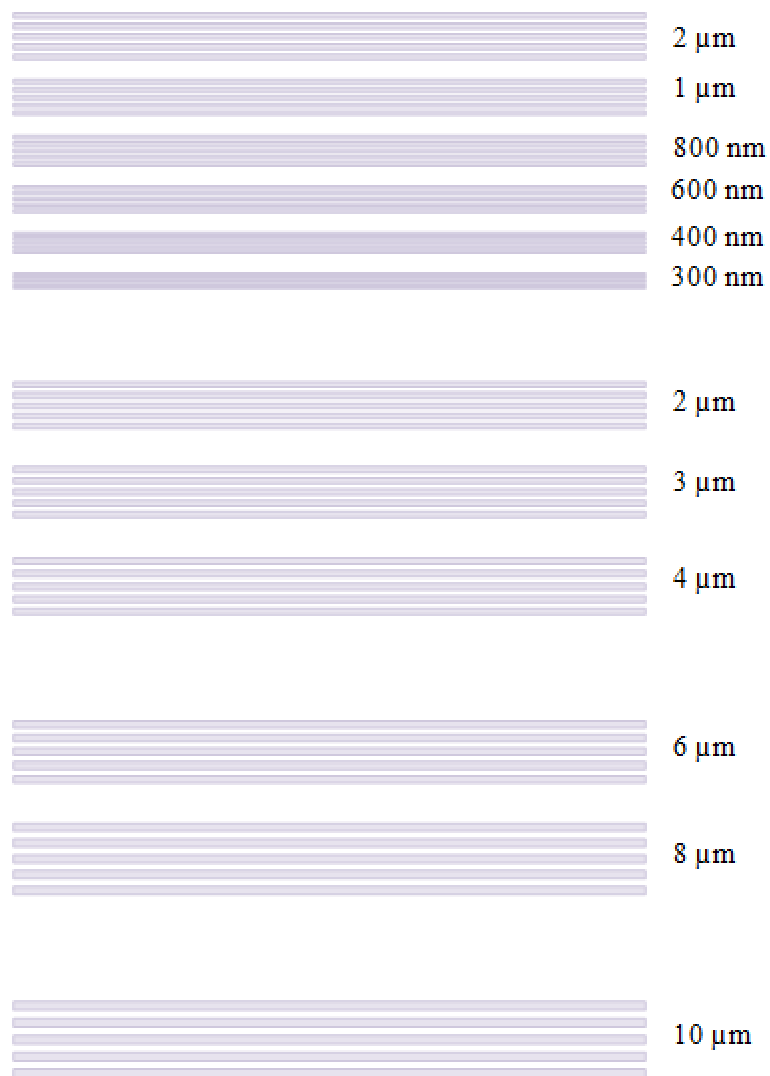


Figure 3.4. Basic diagram depicting the patterned gratings after lithography; periods are labeled on the right (not drawn to scale).

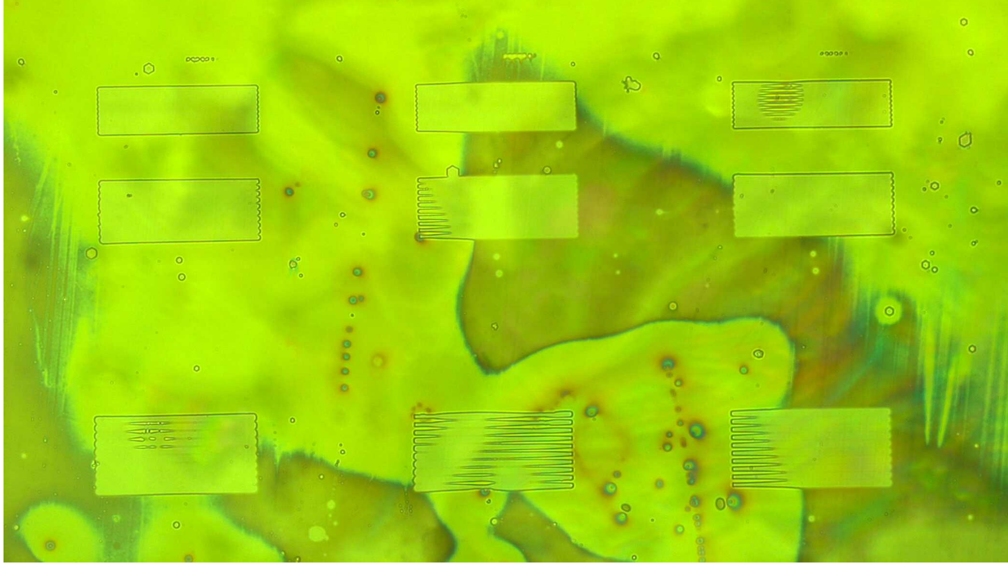

Figure 3.5. 6, 8, and 10 µm periodic gratings in developed resist that are severely overdeveloped.

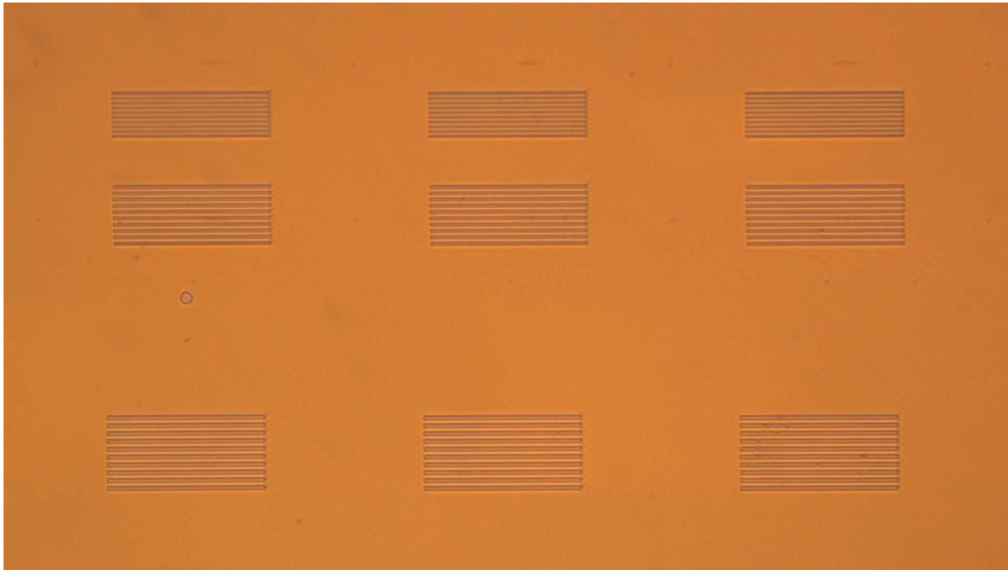

Figure 3.6. 6, 8, and 10 µm gratings in developed resist that are appropriately developed.

3.4.2 Resist Exposure

While uncovering this development issue, several chips were reused – meaning after they had been spun (and sometimes patterned and developed), they were cleaned with solvents to clean off the developed resist and spun again. It was discovered that a

large number of these chips had deformities in the PMMA layer of the resist. Further investigation proved that the PMGI layer looked fine, but the PMMA layer was extremely non-uniform and unusable. Figure 3.7(a-c) shows an example of these deformities. It can be seen that there are spots littered across the sample. The desired resist layer should be uniform in color and thickness, as seen in Figure 3.7d.

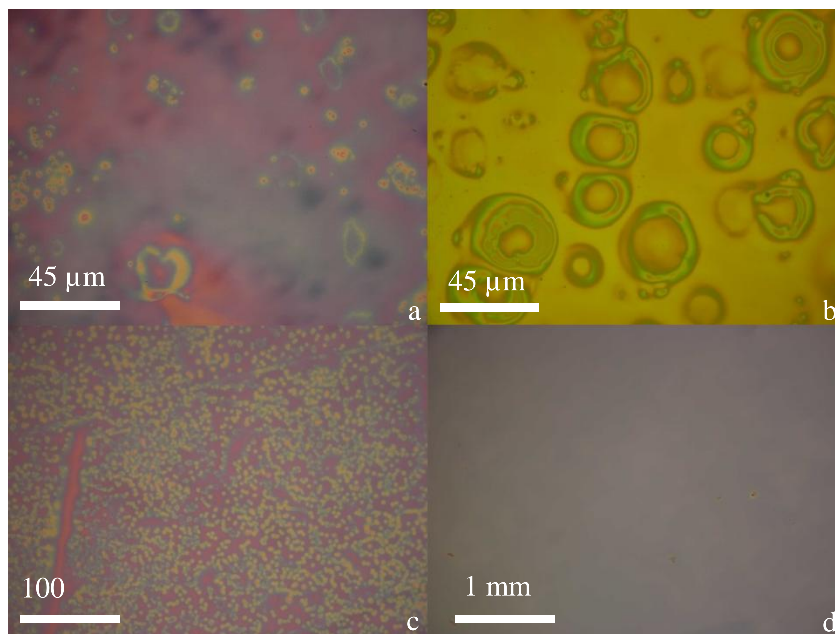


Figure 3.7. Image showing common deformities seen in the PMMA layer on certain LN samples (a-c), and an ideal resist layer (d).

After looking into this issue, it was found that not only were certain re-spun chips succumbing to this issue, but the spots or deformities tended to be affected by what was on the back of the LN samples. For instance, the spots in the PMMA layer were likely to form on areas of the chip where there was either residual resist on the back or where there were scribe marks on the back. The images shown in Figure 3.8 illustrate the deformities showing a strong affinity to a dark line, which is a scribe mark on the back of the chip.

This correlation was also seen when there was residual resist on the back of the chip from the previous PMGI spin cycle.

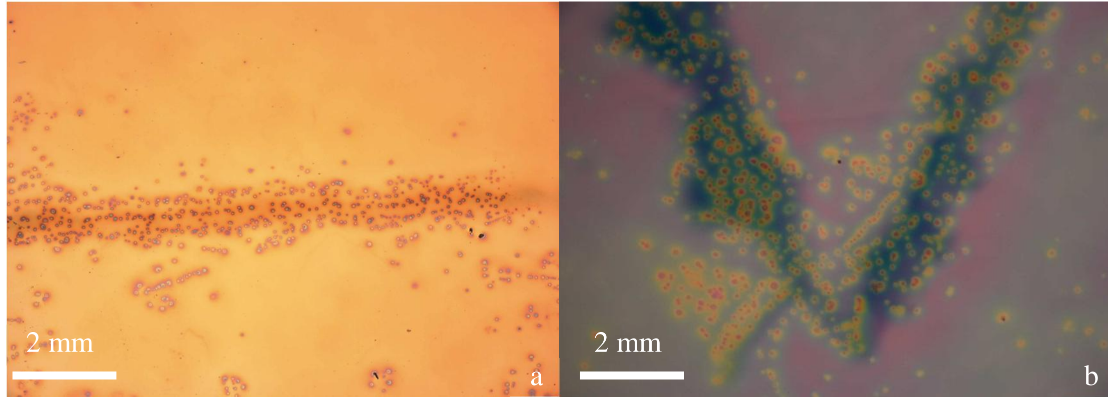


Figure 3.8. Samples with scribe marks on the bottom of the sample (depicted by the dark line across the sample in a and a ‘v’ shape in b) shows a correlation between the scribe marks and deformities found in the PMMA layer.

Another interesting facet of theses deformities is that they sometimes tend to be in distinct lines, as seen in Figure 3.9. It almost appears as though a particle has been rolled across the sample which causes the PMMA to become non-uniform in thickness.

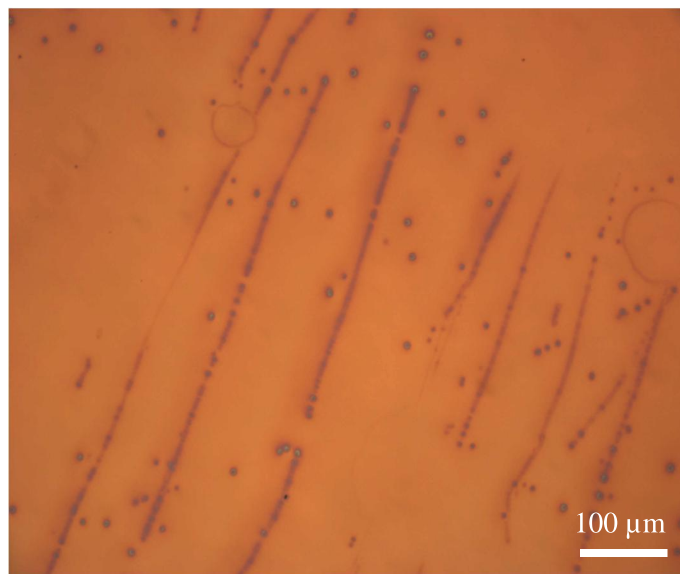


Figure 3.9. Deformities seen to be arranged in linear patterns across the sample.

The initial hypothesis for the cause of these deformities was that there is some surface contamination that affects the PMMA. This would explain why this issue is so prevalent for re-spun LN chips but not previously un-spun chips. However, this theory does not explain why the PMMA seems to be affected by the impurities on the bottom of the chip, such as scribe marks or residual resist. The second hypothesis was that the lithium niobate was becoming poled or charged in some way that affects the PMMA and not the PMGI. Being that the PMMA is electron-sensitive, the PMMA is essentially exposed when there are electric fields nearby. This reasoning would explain why the PMGI layer remains unaffected, as it is not electron-sensitive, while the PMMA becomes unusable.

Because PMGI is not affected by solvents such as acetone, isopropanol, or methanol, but PMMA is dissolved by acetone, an experiment was done. A sample was spun with PMGI and PMMA, and was found to have a severely deformed PMMA layer, as seen in Figure 3.10. Then, the sample was cleaned with the three solvents listed above (acetone, isopropanol, and methanol). This step stripped the PMMA layer off the sample, while not affecting the PMGI in any discernable way.

Then, PMMA was once again spun onto the sample. It was found after this step, that there were no more deformities, as seen in Figure 3.11. Note that the deformities are no longer seen over the scribed region, either, shown in Figure 3.11b. This procedure was repeated several times, all resulting in an ideal PMMA layer with no deformities. It seems that this intermediate step of cleaning off the PMMA and then re-spinning the PMMA solves the recurring issue of a non-uniform PMMA layer. The solvent cleanse is most likely doing one of three things to the LN sample:

It is either…

1. cleaning the sample and ridding the surface of contaminants;
2. helping the sample cool down to an appropriate temperature (a 250°C bake step occurs immediately following the PMMA spin); or
3. helping redistribute the surface charge so that it negates the charge of the lithium niobate sample.

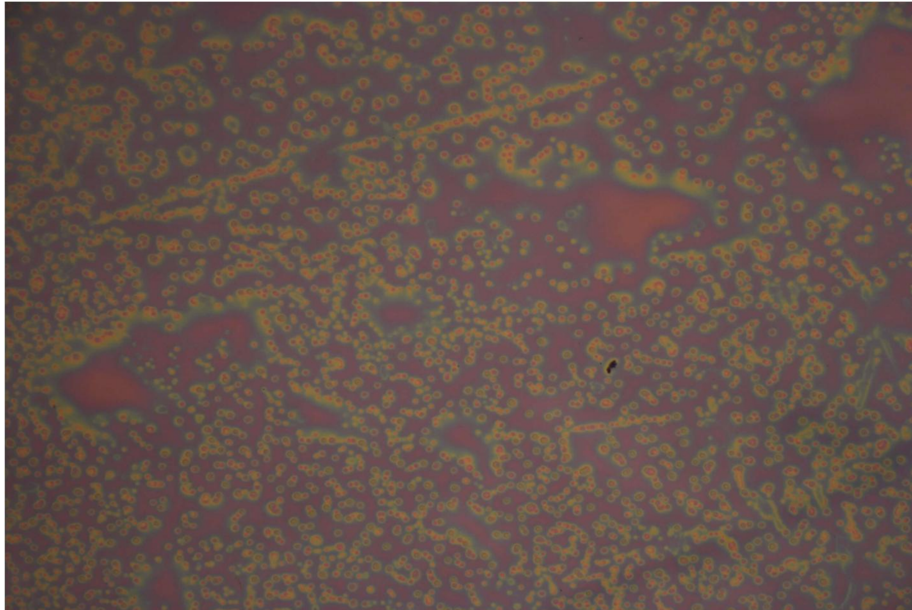

Figure 3.10. Severely deformed PMMA layer.

In order to determine which effect the solvent cleanse has on the lithium niobate, a sample, after being spun with PMGI and baked at 250 °C for ten minutes, was set out to cool for 24 hours. This prolonged time ensures that the sample is completely cooled down. After cooling down for 24 hours, PMMA was spun onto the sample. It was found that there were no deformities in the PMMA layer. Therefore, the deformities are most likely caused either by theory 2 or 3; either the solvent cleanse is thermally cooling down

the sample, or it is allowing the surface charge to be redistributed quickly. The thermal idea explains why the spots had an affinity for areas that had either scribes or residual resist on the back. Resist and scribe marks would cause the lithium niobate to cool at a slightly different rate, which means that it is possible that the areas with resist or scribe marks on the back would be warmer and not yet cooled down, even if the rest of the chip was at room temperature. Because lithium niobate is pyroelectric, electric fields can be created in certain areas if the sample is undergoing a change in temperature.

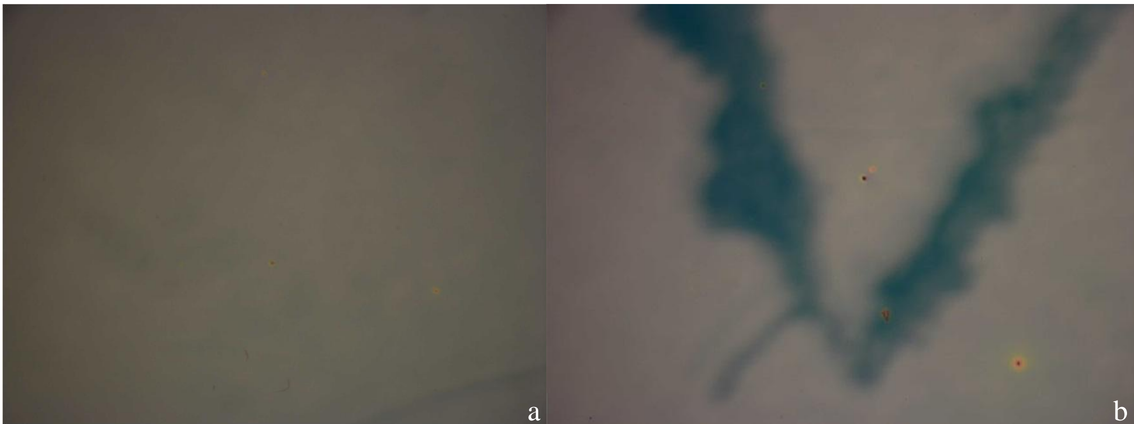


Figure 3.11. Images showing an ideal PMMA layer spun onto a sample. Hardly any deformities were seen on the LN after the sample had been cleaned with solvents and re-spun.

The charge distribution theory also could explain why the PMMA defects were often seen where there were scribe marks on the back of the samples, although it does not necessarily describe the influence of residual resist on the back of the chips. Any stress on the sample, be it thermal or physical shock, can cause poling in the sample. When there are small areas that have been poled, electric fields can be created from the interaction between $-z$ and $+z$ faces on the surface of the sample. However, the surface charge can be distributed in such a way to negate any fields coming from the lithium niobate. It is

possible that the sample needs a long period of time in order to distribute the surface charge in this fashion, and it is possible that a three solvent cleanse could act as a catalyst in this process. However, regardless of the cause of this issue, there is a procedure that will rid the sample of these deformities. When a sample becomes afflicted with a deformed PMMA layer, simply cleaning off the PMMA with acetone and re-spinning that top PMMA layer ensures that the sample can be used for further fabrication processes.

## 3.5 Mask Analysis

After all of the fabrication processes have been completed through the lift-off procedure for Method A or the chromium etch for Method B, a chromium mask is realized on the lithium niobate substrate. As mentioned before, this mask is the same pattern for both methods, but Method B will be a negative pattern of Method A. In other words, where the Method A mask has chromium, the Method B mask will have windows, and vice versa. Several differences between the two methods were detailed in Section 3.1, but some more differences were seen when comparing the quality of the masks created by the two methods. First, it was noticed that the nanoscale structures made using Method B were of a much poorer quality than those made using Method A. This difference can be seen in Figure 3.12, which is comprised of two scanning electron microscope (SEM) images of 600 nm period gratings. On the left is the mask created using the Method A fabrication process, and the right image is the mask created using the Method B process. The Method B mask clearly has extremely rough edges and is of poor quality. In contrast, the Method A mask for the same size shows smooth and uniform mask edges in comparison to the Method B masks (the roughness of the Method A mask edge is on the

scale of tens of nanometers). The quality of the mask edges is translated to the quality of the etched structures in the lithium niobate, making it necessary to have an excellent quality mask prior to etching.

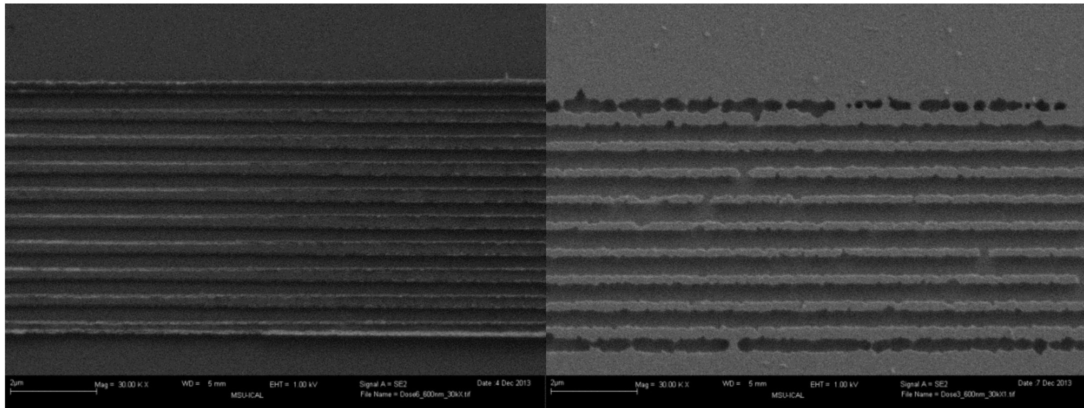

Figure 3.12. Left: 600 nm period grating made using Method A; right: 600 nm period grating made using Method B.

However, this characteristic of extremely rough mask edges from Method B is only a problem with the smaller structures. Larger scale structures have comparable mask qualities to the masks created using Method A. The images shown in Figure 3.13 show a 2 μm period grating, again with Method A on the left and Method B on the right. Here it can be easily seen that there are no major differences between the two masks. The Method B masks have adequate masks for structures larger than about 1 μm, while Method A has been seen to have adequate masks for structures as small as 150 nm, as seen in Figure 3.14. When deciding which method to use for fabrication, it is important to know what type of structure is desired. For nanoscale structures, Method A is the best option. However, for deep, microscale structures, Method B should be used because it allows for thicker chromium masks, which correlates with a deeper etch.

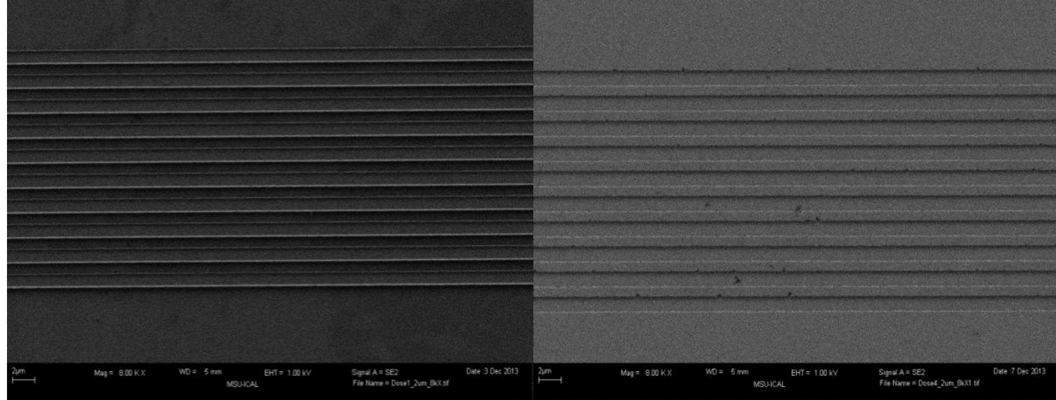

Figure 3.13. Left: 2 µm period grating made using Method A; Right: 2 µm period grating made using Method B.

Although the Method A nanoscale masks are relatively smooth, some edge roughness can be seen when examining the edges of the mask shown in Figure 3.14. This roughness is estimated to be on the scale of tens of nanometers, and is not ideal. The rough edges can translate into the etched structures, causing rough sidewalls to occur on the etched structures. These deformities in the final etched structure can lead to light scattering and loss as light propagates through the optical device. While the Method A masks on the nanoscale are adequate for this thesis project (as seen in Figure 3.14), there are some optimizations that must be made in future trials so that the mask edge is much smoother.

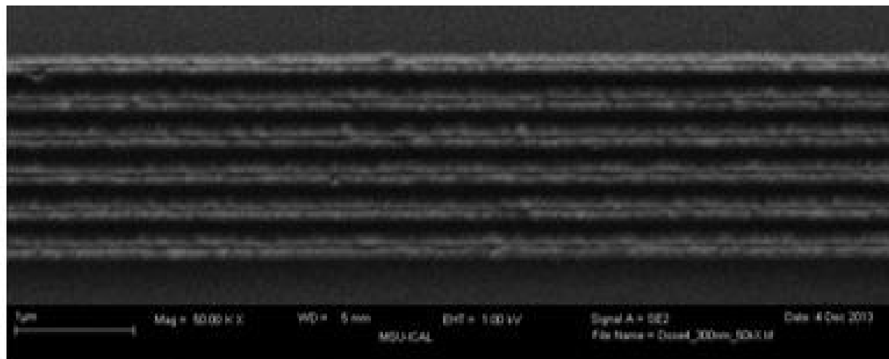

Figure 3.14. 300 nm periodic grating made using Method A.

## 3.6 Fill Factor Optimization

All of the gratings are designed to have a 50/50 fill factor, or a 50% duty cycle. Obtaining a specific fill factor is controlled by two parameters: the computer aided design (CAD) file that defines the patterns and the beam dose of the electron-beam during EBL. The CAD files are drawn out as shown earlier in Figure 3.4, and this CAD program is used to control the size and duty cycle of the gratings. This pattern is repeated seven times on each chip, so that the beam dose varies from pattern to pattern. With higher beam doses, the patterns will become overexposed and will end up with fill factors much greater than 50%. Lower doses will result in underexposed patterns with fill factors much less than 50%. If the dose is too low, the pattern will fail to appear at all after development. This suggests that for a specific material there exists an appropriate beam dose, where the sample is properly exposed by the beam.

The CAD file patterns can be altered so that the fill factor is not exactly 50%, in order to compensate for over- or underexposures caused by the beam dose. Therefore, there exists a "sweet spot" where the beam is an appropriate dose and the CAD file patterns are close to 50%. For example, a CAD file could be written to have a fill factor of only 20%, and the beam could be set to have a higher dose. This would make the 20% fill factors be overexposed resulting in a fill factor close to 50%. On the other hand, a CAD file could be designed to have gratings with 80% fill factors, and a low dose could be used to compensate the fill factor to bring it back down to 50%. However, both of these scenarios often result in poor mask quality, which is not ideal for subsequent steps in the fabrication process. Therefore, the two parameters must be optimized so that a 50%

fill factor can be obtained while maintaining a good quality mask. In optimizing these two parameters, it was found that the CAD file fill factor needs to be much less than 50% for most of the gratings, specifically the nanoscale gratings, and the doses ranged from 120 to 180 μC/cm$^2$, and this range of values will work for both Method A and Method B. The exact values are shown in Table 3.1. Chromium masks for an 800 nm and 10 μm period grating are shown in Figure 3.15.

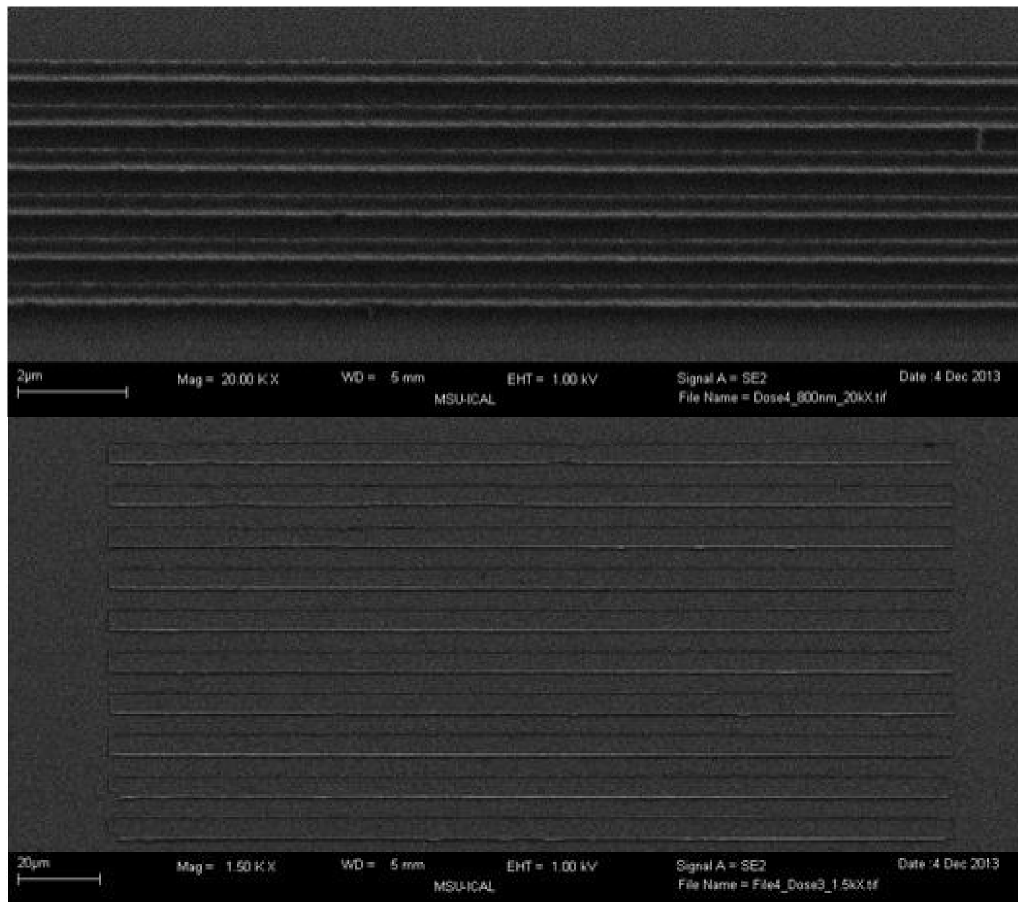


Figure 3.15. SEM images of chromium mask on lithium niobate; top: 800 nm period grating; bottom: 10 μm period grating.

Table 3.1. Values for 50/50 Fill Factors

| Grating Period | CAD File Fill Factor | | Beam Dose ($\mu C/cm^2$) |
|---|---|---|---|
| **300 nm** | 100/300 | 33.3% | 150-180 |
| **400 nm** | 112/400 | 28% | 150-180 |
| **600nm** | 185/600 | 30.8% | 150-180 |
| **800nm** | 250/800 | 31.3% | 150-180 |
| **1 µm** | .35/1 | 35% | 150-180 |
| **2 µm** | .735/2 | 36.8% | 150-180 |
| **3 µm** | 1.4/3 | 46.7% | 130-160 |
| **4 µm** | 1.85/4 | 46.3% | 130-160 |
| **6 µm** | 2.7/6 | 45% | 130-160 |
| **8 µm** | 3.7/8 | 46.3% | 130-160 |
| **10 µm** | 4.7/10 | 47% | 120-150 |

## 3.7 Conclusion

Thus far, it has been seen that lithium niobate can be patterned with a chromium mask containing both micro- and nanoscale features. As mentioned earlier, this first part of the fabrication process outlines the steps involved in masking lithium niobate with a chromium etch mask. Although lithium niobate is a significantly different material than silicon, a material the Nano-Optics Group is experienced in structuring, it was found that there is a lot of overlap in the two procedures leading up to an etch mask. Issues such as PMMA resist exposure prior to EBL were certainly unexpected, but resulted in a better understanding of lithium niobate crystals and a resolution to the issue at hand. Also, it was discovered that development subsequent to EBL should be stalled for about 12 hours following the lithography, which potentially allows the polymers to cure. Nonetheless, it was presented that both nano- and microscale chromium mask structures can be patterned on lithium niobate. After the masks have been patterned on the substrate, the samples are ready for the second half of the fabrication process, which will be discussed in Chapter 4.

Here, the samples will be etched so that structured lithium niobate is realized, thus maintaining the thesis objective of creating nano- and microstructures on the surface of lithium niobate in order to facilitate the making of efficient second harmonic generation devices.

# CHAPTER 4

# FABRICATION PROCESS PART 2:
# ETCHING NANOSTRUCTURES IN LITHIUM NIOBATE

## 4.1 Introduction

After the masks are patterned on the samples, the pattern needs to be translated into etched lithium niobate structures. This is done by etching the lithium niobate samples using the ICP-RIE. The second part of the fabrication process involves a proton exchange bath and the actual etching of lithium niobate. Note that after the chromium masks are realized on the lithium niobate samples, there is no difference in the fabrication process between Method A and Method B, so no further distinction will be made between the two techniques. For the second part of the fabrication process, only a few process steps are needed, as outlined in Figure 4.1. Although the first part of the fabrication process is a fairly well known procedure, as it is similar to silicon processes, the second part of the fabrication process had to be developed from scratch. The fabrication process was designed based off of results found in the literature survey discussed in Chapter 2.

After the metal mask is realized, the LN sample is proton exchanged in a heated bath. The proton exchange (PE) bath consists of a heated benzoic acid solution. By placing lithium niobate in benzoic acid, the lithium ions ($Li^+$) will diffuse out of the sample and will be replaced by hydrogen ions ($H^+$) from the acid [31]. This step is not completely necessary in the fabrication sequence but is included for two reasons. First, it reduces the redeposition of lithium fluoride (LiF) on the sample during the ICP-RIE process. As mentioned earlier in Chapter 2, this redeposition will cause the etch rate to

slow drastically as debris builds up, and it can also cause undesired structures to be formed on the lithium niobate samples. The second benefit of the PE is that it increases the etch rate, which in turn increases the etch selectivity between lithium niobate and the chromium mask. This suggests that deeper etches can be accomplished for the same amount of chromium. Because benzoic acid is not readily available in the Montana Microfabrication Facility, the proton exchange was performed at AdvR, Inc. with the assistance of Dr. Matt Bigelow.

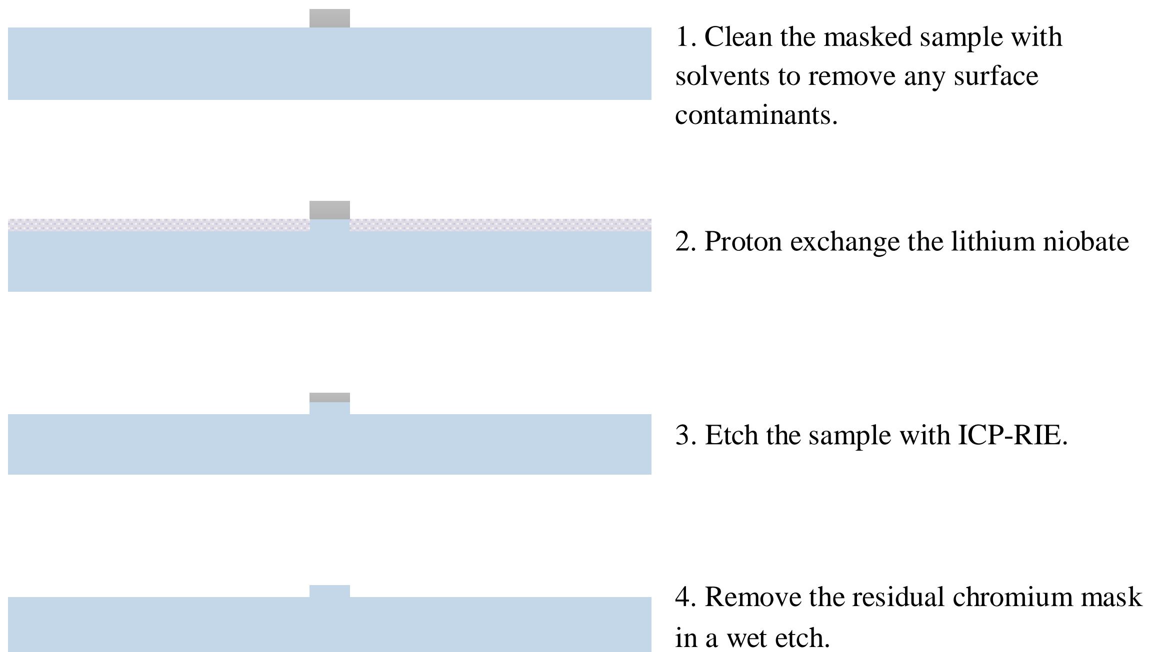


Figure 4.1. Fabrication process after metal mask is formed.

After the sample is proton exchanged, the lithium niobate is then etched using an ICP-RIE technique. This preferentially etches the proton exchanged lithium niobate (PELN) over the chromium, but will etch some of the chromium, too. After the samples are etched with the ICP-RIE, the residual chromium mask is removed in a wet chromium

etch, leaving only the structured lithium niobate. Using this technique, both micro- and nanostructures can be achieved in lithium niobate, as seen in Figure 4.2.

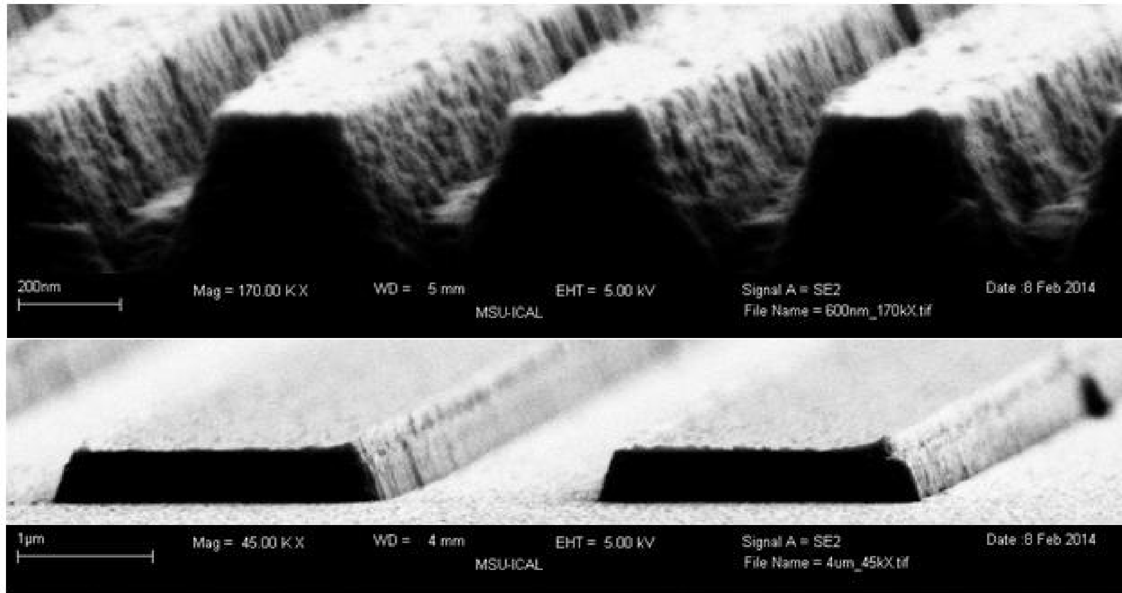


Figure 4.2. Top: 600 nm period grating etched in lithium niobate. Bottom: 4 µm period grating etched in lithium niobate.

## 4.2 Etch Rate Analysis

One of the first parameters examined after the ICP-RIE is the etch rate of the lithium niobate and the etch selectivity between the lithium niobate and chromium. Ideally, the etch rate of lithium niobate is reasonably fast so that the etch duration is an appropriate amount of time - not several hours or days long. Another desired parameter is that the chromium etch rate is relatively slow, compared to the lithium niobate etch rate. This creates a high etch selectivity between the lithium niobate and chromium and means the chromium mask should not be etched away during the lithium niobate etch, even when subjected to longer duration etches.

The etch rates and selectivities are all found using an atomic force microscope, or AFM. Each sample is imaged with an AFM at three separate points during the fabrication process: after lift-off to see how thick the chromium mask is, after the ICP-RIE to see the combined height of the residual chromium mask and the lithium niobate etch depth, and after the chromium etch to see the actual height of the lithium niobate etch depth. Using these three values, the lithium niobate etch depth as well as the chromium etch depth can be calculated. In this manner, the etch rates and etch selectivities for all the etched samples were calculated, and these values are shown in Figure 4.3, Figure 4.4, and Figure 4.5.

Several samples were etched using identical etch parameters; these parameters are listed out in Table 4.1. The first task is to determine the consistency the etch rate for lithium niobate. It has been seen in silicon etches that the etch rate can vary greatly from one etch trial to another. Therefore, several chips were etched in order to determine if this is an issue for lithium niobate as well. The lithium niobate etch rate data is shown in Figure 4.3.

Table 4.1. Parameter Values for ICP-RIE

| Parameter | Value |
| --- | --- |
| **ICP Power** | 1500 W |
| **Chamber Temperature** | 25 °C |
| **Chamber Pressure** | 6 mTorr |
| **RF Power** | 100 W |
| **DC Bias** | 218 V |
| **Etch Chemistry** | 10 sccm $CHF_3$<br>5 sccm $O_2$<br>50 sccm Ar |

Most of the etches tend to be around 50-60 nm/min, with one data point seen at about 42 nm/min and a 9 minute etch time. This outlier possibly has a much lower etch rate than the others because the etch may have gone past the proton exchanged region in that sample. For this particular chip, the proton exchange depth was expected to be close to 450 nm, but the temperature during the actual proton exchange was lower than anticipated, thus creating a proton exchange depth of less than 450 nm. This outlier was etched to a depth of approximately 380 nm, and it is possible that the proton exchange depth was less than 380 nm. Therefore, it is uncertain as to whether this low etch rate is due to a shallow proton exchange depth, or if the etch rate of PELN simply slows after 6-8 minutes. However, the lithium niobate etch rates for the other samples are relatively close in value, with the average being approximately 55 nm/min.

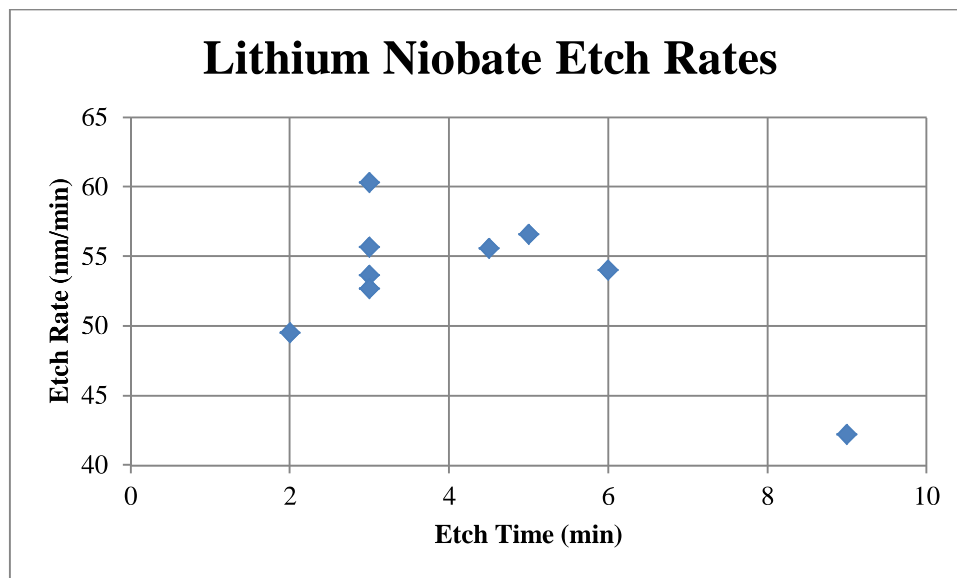


Figure 4.3. Lithium niobate etch rates for the samples etched.

Looking at the chromium etch rates, in Figure 4.4, it can be seen that there is quite a variety of rates, ranging from 6.5 to 12.3 nm/min. The selectivities also show a similar

range of values, ranging from about 4.5 to 9, shown in Figure 4.5. For comparison purposes, the standard deviation and the percent relative standard deviation (the standard deviation divided by the average) for each parameter was found, and is listed in Table 4.2. The lithium niobate etch rate is relatively constant, with only a 10% percent relative standard deviation, but the chromium etch rate and the selectivity both vary quite a bit, with approximately a 20% percent relative standard deviation. However, these values are a good base point for moving forward. Lithium niobate can be expected to etch at a rate of about 50-60 nm/min when using this etch chemistry, and it can be seen that the etch rate is fairly constant. The selectivity can also be expected not to exceed 10. This value can be used in future etch trials when determining the amount of chromium needed in order to etch a certain depth in lithium niobate.

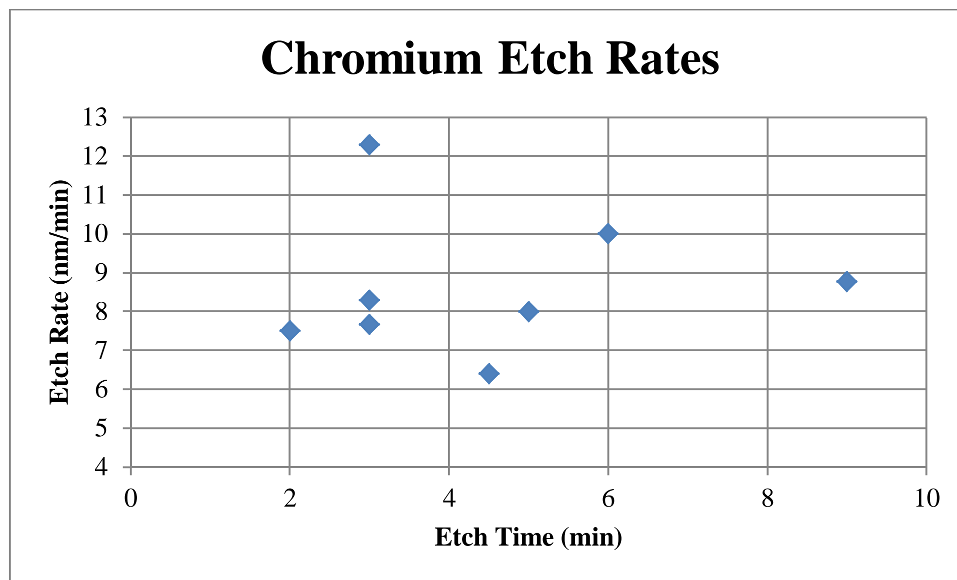


Figure 4.4. Chromium etch rates for the samples etched.

Table 4.2. Standard Deviation of Etch Rates and Selectivity

| Parameter | Average Value | Standard Deviation | Percent Relative Standard Deviation |
|---|---|---|---|
| **LN Etch Rate** | 54.75† nm/min | 5.4† | 9.6%† |
| **Cr Etch Rate** | 7.77 nm/min | 1.8 | 20.2% |
| **Selectivity** | 6.34 | 1.3 | 21.1% |

† One data point was excluded from this set (the 9 minute etch)

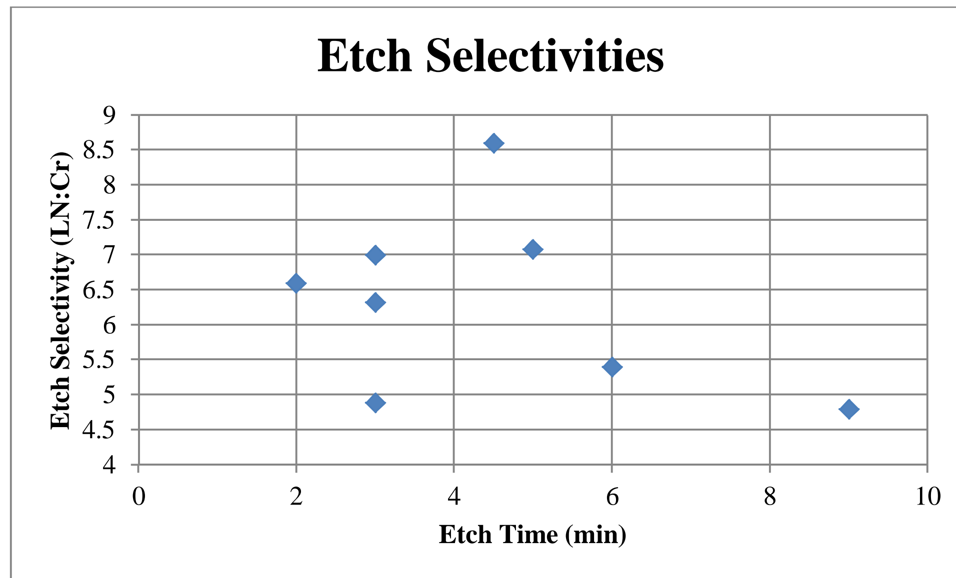


Figure 4.5. Etch selectivities for the samples etched.

## 4.3 Proton Exchange Etch Analysis

Because the proton exchange must be done at AdvR, Inc., several samples are typically taken over to be proton exchanged at the same time. This takes up less of the company's time, and requires less frequent trips out to their facilities. When regarding the samples analyzed in Section 4.1, it must be noted that two different proton exchanges were used, and the first bath was slightly different than the second. This first bath, which two samples were subjected to, was comprised of 0.1% molar weight lithium benzoate and 99.9% benzoic acid. AdvR, Inc. had done a literature survey and found that the

lithium benzoate slows down the proton exchange depth rate. A slower proton exchange rate makes the depth calculations, based off of time and temperature of the bath, much more accurate. AdvR, Inc. uses the proton exchange to make waveguides in the LN, and they also found that the lithium benzoate proton exchange baths allow for more optically stable waveguides at higher powers. The lithium benzoate proton exchange proved to be an ideal bath for AdvR, Inc.

However, it was found that over time, the lithium benzoate would evaporate out of the solution while the benzoic acid did not. This evaporation causes the concentration to change, which affects the depth calculations. If the concentration of lithium benzoate to benzoic acid is not what is expected, the proton exchange depth calculations will not be accurate. Because AdvR, Inc. depends on having very precise and accurate proton exchange depths, they decided that it was not worth the risk, and switched to a pure benzoic acid bath. Therefore, the second proton exchange was done in a pure (100%) benzoic acid bath, even though the first had been done in a lithium benzoate / benzoic acid solution. Both of the baths were done at a temperature of approximately 170 °C, and the times were both around 3 hours. The times and temperatures were calculated by Dr. Bigelow using an algorithm that determines the proton exchange depth based off those two parameters.

As two different bath solutions were used, there was concern that this would affect the lithium niobate etch rate during the ICP-RIE. However, it can be seen in Figure 4.6 that the two samples used in the first bath (circled in red) have a similar etch rate to the others. Therefore, it seems that the difference in proton exchange solutions has little to no effect on the subsequent etch of the lithium niobate. Just to be certain that the

change in proton exchange baths also has no effect on the chromium etch rates, Figure 4.7 was examined. It appears that these etch rates are not altered by the different proton exchange, either.

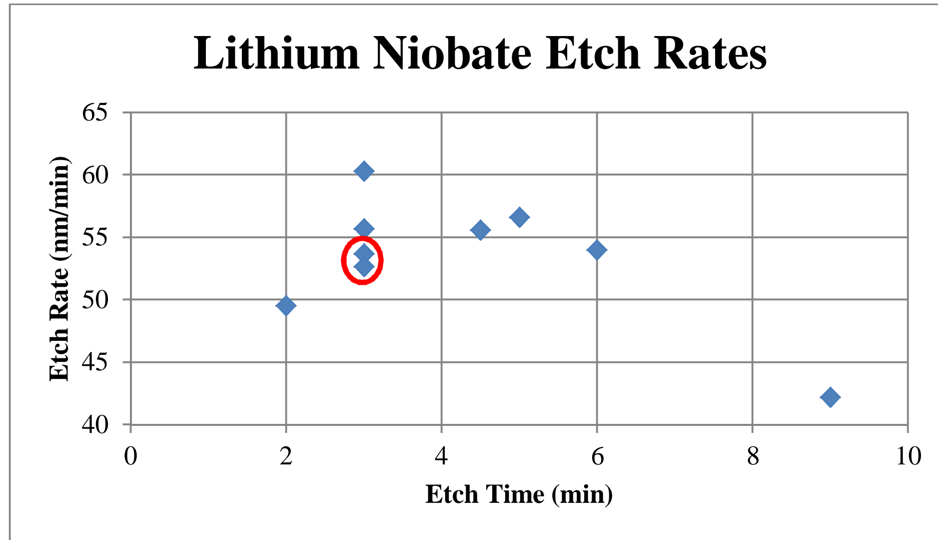


Figure 4.6. Graph illustrating there is no major difference in etch rates if proton exchange bath is changed, circled data points represent etch rates from the first proton exchange, and the other data points represent etch rates from the second proton exchange.

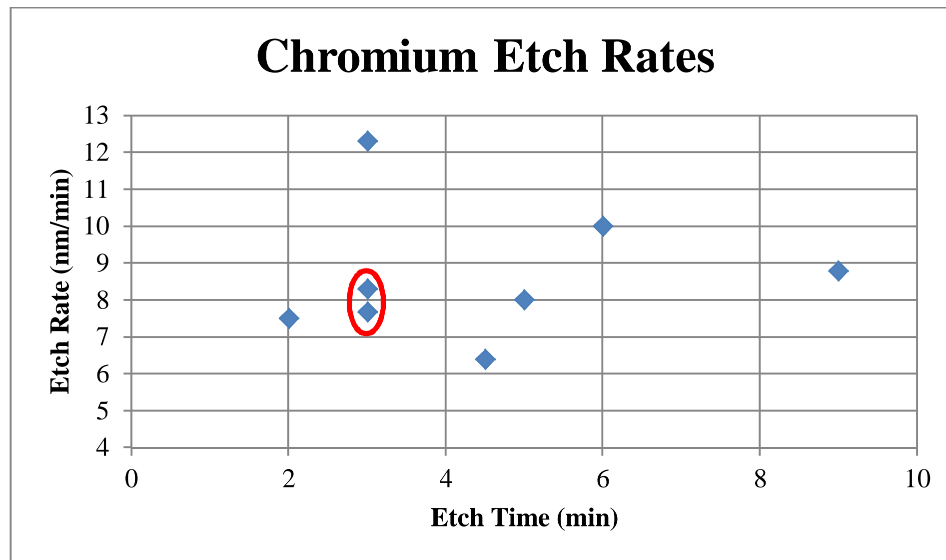


Figure 4.7. Graph illustrating there is no major difference in etch rates if proton exchange bath is changed, circled data points represent etch rates from the first proton exchange, and the other data points represent etch rates from the second proton exchange.

## 4.4 Sidewall Analysis

Another parameter analyzed is the sidewall angle of the structures. The desired outcome is that all of the nanostructures have perfectly vertical sidewalls, as depicted in Figure 4.8a. However, the typical structures will not have perfectly vertical sidewalls, but will have angled walls as seen in Figure 4.8b. If this sidewall angle is very close to 90° off the horizontal, then the structures will be good enough for all practical purposes. However, if the sidewall angle is much smaller than 90°, high aspect ratios cannot be reached, and smaller features will become triangular in profile, as opposed to rectangular. For some applications, triangular or trapezoidal structures might be perfectly acceptable. However, for all intents and purposes, a 90° sidewall angle is a desired outcome in this thesis.

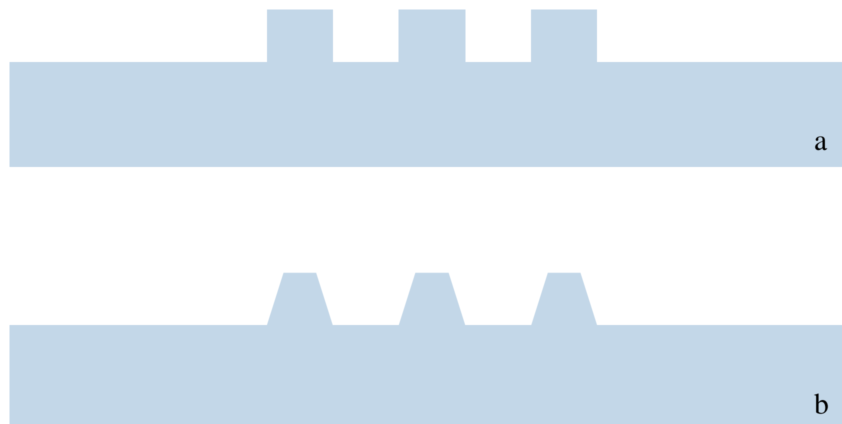


Figure 4.8. Diagrams showing the ideal case for nanostructures (a), and the reality (b).

In order to analyze the sidewalls of the lithium niobate samples after the etch, the chip is cleaved into two pieces. In doing so, the sample may be placed sideways in the SEM so that a side view image may be seen, such as seen in Figure 4.9. After imaging

several samples and measuring the sidewall angle, it was determined that the sidewalls were not quite at 90°. As can be seen in Figure 4.10, the sidewall angles are closer to 70° instead of 90°, with the average being 69.26 and a standard deviation of 5.26. While these angles are not quite ideal, there is definitely a chance to improve.

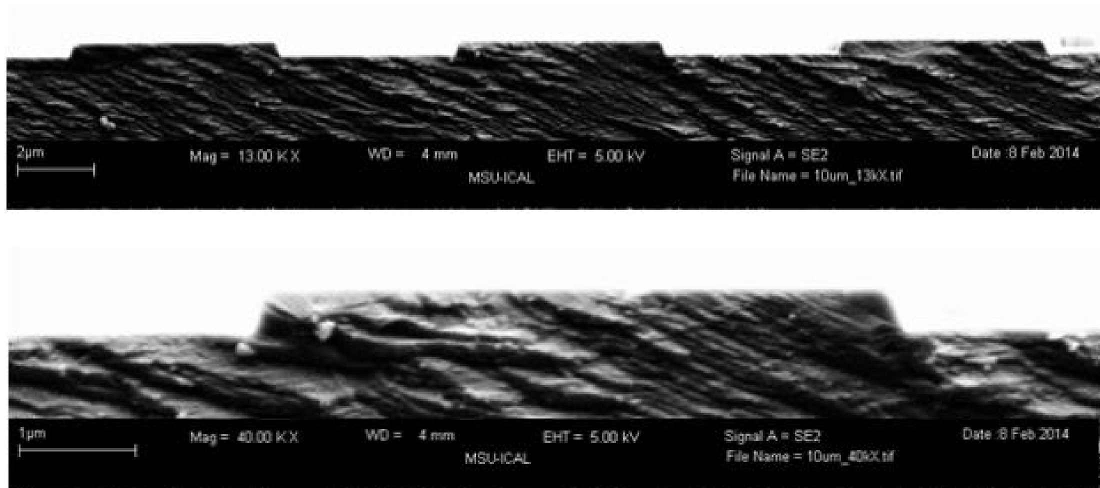


Figure 4.9. Two images of a 10 µm period grating; top image showing three structures and bottom image showing one structure at higher magnification.

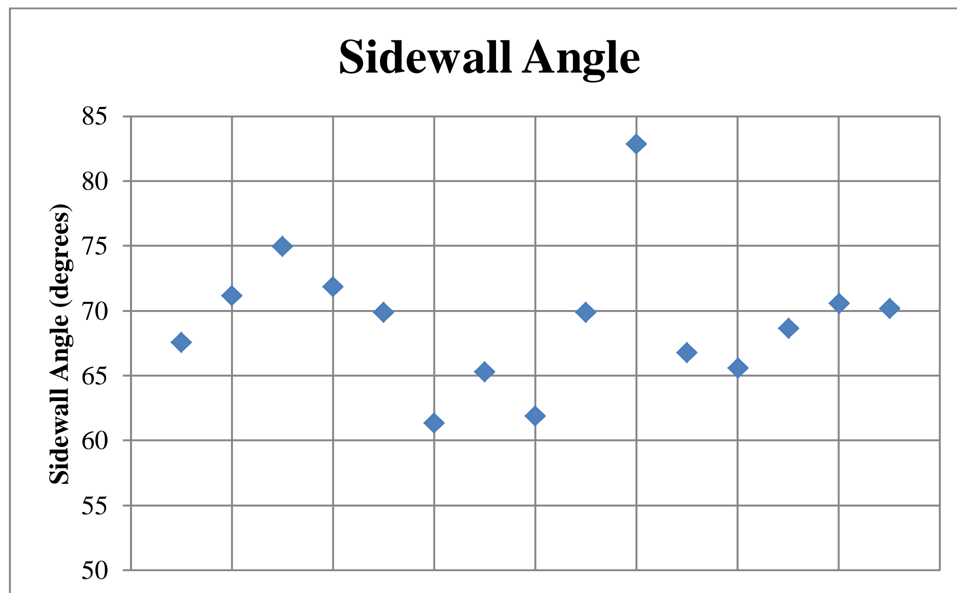


Figure 4.10. Sidewall angles for the samples etched (90° is desired).

The image shown in Figure 4.9 shows a microscale structure, with a period of 10 μm. Because of the large size of the structure, the sidewalls do not affect the basic shape of the rectangular grating. Looking at Figure 4.11, an 800 nm period grating, it can be seen that the structures are largely trapezoidal instead of rectangular. Figure 4.12, a 300 nm period grating, illustrates the structures becoming nearly triangular because of the large sidewall angle. These trapezoidal structures can be caused by different parameters such as mask erosion and isotropic etching.

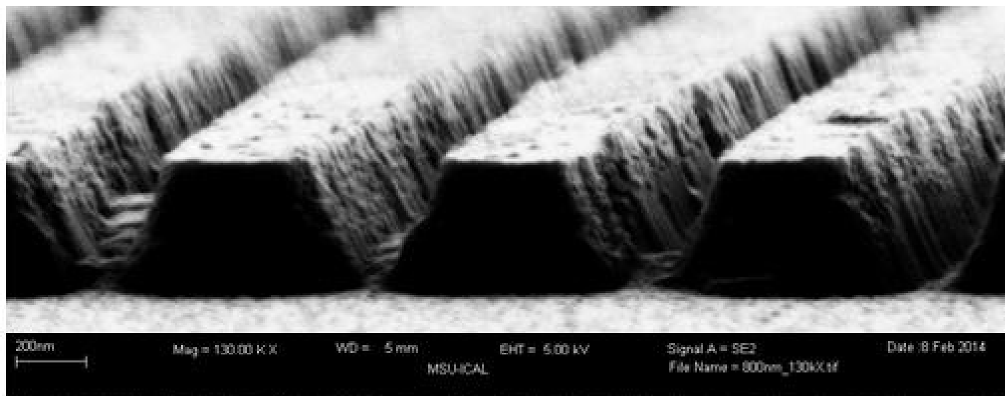


Figure 4.11. 800 nm period grating; note the severe sidewall angle causing structures to become trapezoidal.

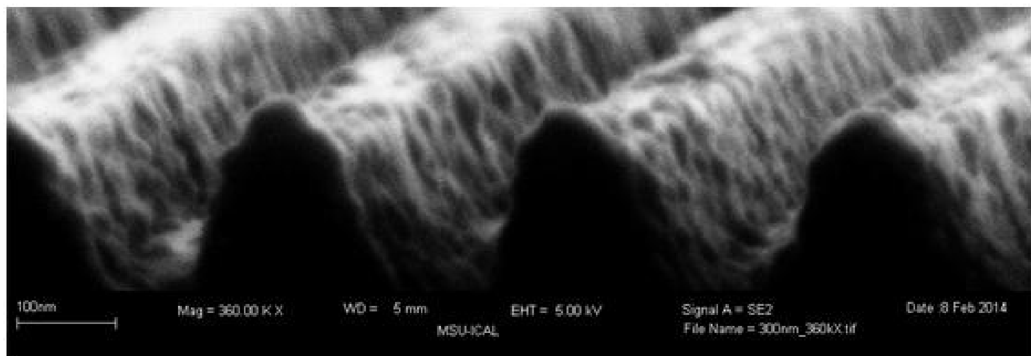


Figure 4.12. 300 nm period grating; note the structures are essentially rounded.

In investigating the cause of these deformities in the structures, it was found that most likely the ICP-RIE etch is slightly isotropic. Analyzing the width of the mask versus

the width of the final structures, it can clearly be seen that the structures are not succumbing to mask erosion. An example is shown in Figure 4.13 where an 800 nm period grating is shown as an etch mask (left) and after the ICP-RIE etch – before the residual chromium mask is etched off (right). If mask erosion was causing these structures to be trapezoidal, the etched structures (in the right image) would be significantly smaller than the mask shown on the left. The structures in the right image do appear to be slightly smaller than the structures in the left image, though, which could be caused by slight mask erosion or mask undercutting.

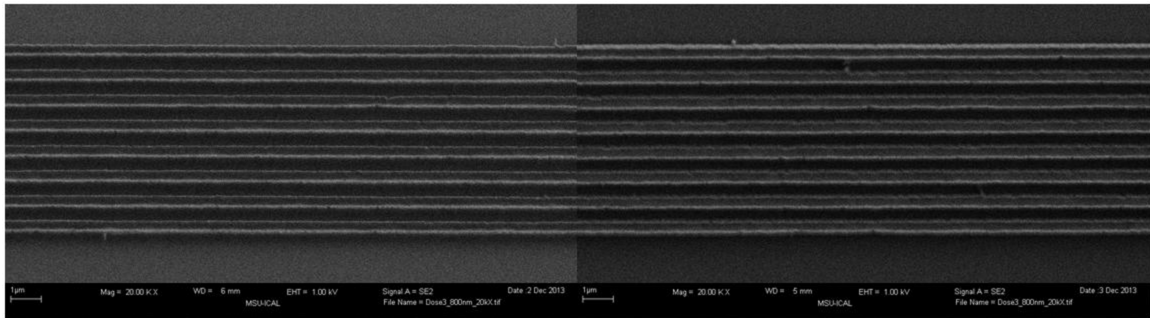

Figure 4.13. Left: Chromium mask (800 nm period grating); Right: Structures with chromium mask still on after ICP-RIE.

The severe sidewall angles, though, are most likely not caused by mask erosion. To be specific, the difference between the base width and the top width of the trapezoids in Figure 4.11 is about 250 nm. If this shape was caused by mask erosion, then the mask width before the ICP-RIE and after the ICP-RIE would vary by about 300 nm. Looking at Figure 4.13, it can be seen that the masks are virtually the same size. This makes it clear that mask erosion is not the main cause for the trapezoidal structures. Thus, it is most likely that the isotropic etching during ICP-RIE causes the severe toll on the shape of the nanostructures. Because of the strong sidewall angle, this issue must be addressed and

improved. Improvements will be made by optimizing the etch chemistry during the ICP-RIE so that a more directional etch is achieved.

## 4.5 Etch Optimization

After the first analysis is complete, different etch chemistries are tested in order to see what the differences are and to see if improvements can be made. Two major goals for improvement are to improve the etch selectivity: by increasing the lithium niobate etch rate and/or decreasing the chromium etch rate, and increasing the sidewall angle to be close to 90°. As of now, a total of three different etch trials have been attempted, all three with slightly different parameters. The three parameters that were adjusted between etching trials were the etch chemistry and the RF Power. In Table 4.3 the different parameters are listed out so that the changes made can be easily seen. Note that the table lists both RF power and DC bias. With the particular etcher in the MMF, the RF power, and not the DC bias, is defined by the user. However, they are essentially the same parameter; a certain RF power will result in a specific DC bias, and generally, the DC bias term is referred to when discussing ICP-RIE processes. Therefore, both terms are listed. All other parameters were kept constant between the different trials.

These adjusted parameters were chosen for very specific reasons. For the second etch trial, the DC Bias was increased from 218 to 286 V (the RF power was increased from 100 W to 150 W). In theory, a higher DC bias creates a more directional etch, which should improve the sidewall verticality. In the third etch trial, the RF power was returned to 100 W, but the etch chemistry was adjusted to 50 sccm $CHF_3$ and 50 sccm Ar. These values were chosen because in the literature survey, this chemistry was used and was

found to realize structures with 82° sidewall angles [61]. Therefore, with both of these etch trials, better sidewall verticality is expected, but the etch rates and selectivities are also subject to change when adjusting parameters.

Table 4.3. Changes in ICP-RIE Parameters for Different Etch Trials

| | **Etch Chemistry** | **RF Power** | **DC Bias** |
|---|---|---|---|
| **Etch 1** | 10 sccm $CHF_3$, 5 sccm $O_2$, 50 sccm Ar | 100 W | 218 V |
| **Etch 2** | 10 sccm $CHF_3$, 5 sccm $O_2$, 50 sccm Ar | 150 W | 286 V |
| **Etch 3** | 50 sccm $CHF_3$, 50 sccm Ar | 100 W | 209 V |

First, the lithium niobate etch rates and selectivities are examined. The lithium niobate etch rates, shown in Figure 4.14, from the second and third etch trial are both significantly greater than the previous etch rates. The etch rate from the second etch trial, labeled with red, is about 75 nm/min. The etch rate found in the third etch rate, shown in green, averages out to be slightly higher at 82.2 nm/min. The etch rates from both of these trials are significantly higher than the etch rates seen previously in the first etch trial. However, when looking at the selectivities shown in Figure 4.15, it can be seen that selectivity from the second etch trial is not much greater than it was before in the first etch trial. The second etch trial actually shows a significantly low selectivity. The third etch trial selectivity is slightly higher than both the first and second etch trials, with an average of about 9.3. While the third etch trial shows some improvements over the first etch trial, there is currently little data to conclusively say the etch parameters are significantly better. For example, two of the three etch selectivities found during the third etch trial are approximately the same values as seen in the first etch trial. One data point

from the third etch trial shows a significantly higher selectivity, but it is not clear as to why this value varies so much from the other two.

The second goal for improvement is to increase the sidewall angle to closer to 90°. When comparing the second etch trial results with the first, it seems that the angles are around the same, if not slightly lower than the previous results. The third etch trial, has an average sidewall angle slightly higher than both the first and second etch. However, the results are still roughly the same as the first etch trial results, and therefore do not show any significant improvement. The angles are shown in Figure 4.16, and the averages and standard deviations are shown in Table 4.4.

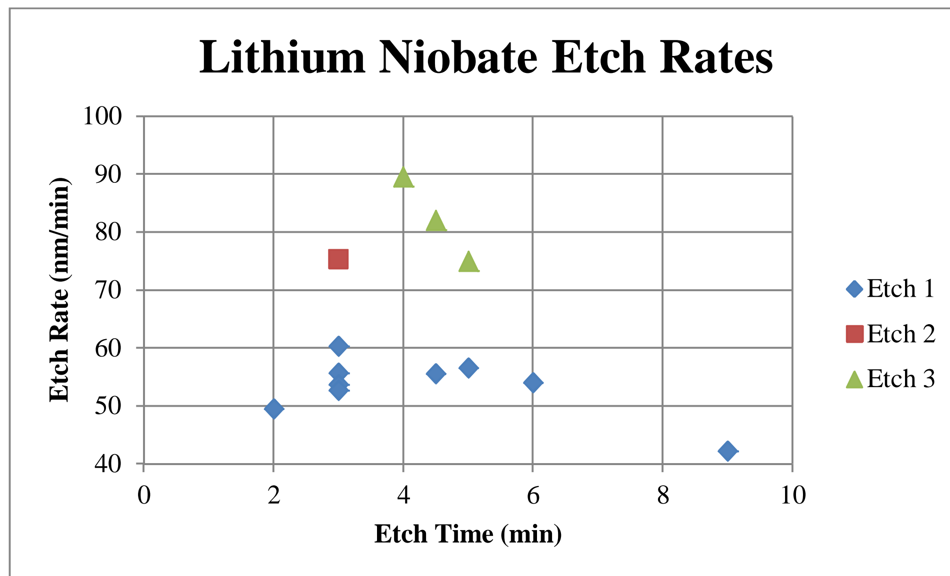


Figure 4.14. Lithium niobate etch rates using different etch parameters.

Table 4.4. Average Sidewall Angles and Standard Deviation for Different Etch Trials

| Trial | Average | Standard Deviation |
|---|---|---|
| **Etch 1** | 69.26 | 5.26 |
| **Etch 2** | 65.43 | 6.85 |
| **Etch 3** | 70.49 | 3.43 |

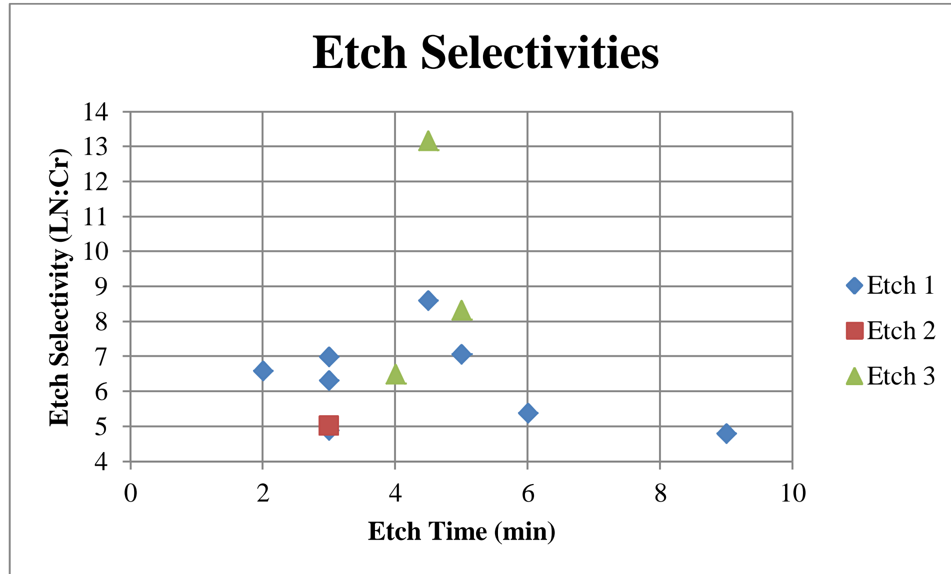


Figure 4.15. Etch selectivities using different etch parameters.

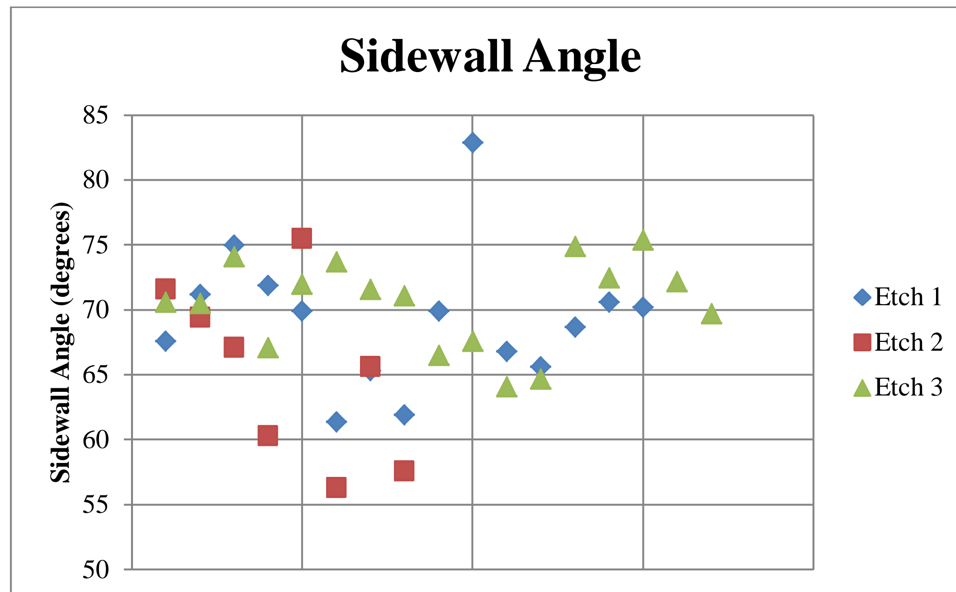


Figure 4.16. Sidewall angles using different etch parameters.

It can be seen that the second etch trial both had a low selectivity and a low sidewall angle average, in comparison to the first etch trial results. Because neither goals were realized in this etch trial, this chemistry will not undergo further testing. Based off

of these results, it is no better than the first etch trial. The third etch trial, however, showed some promise. Although neither goal was clearly met, it can be seen that the average selectivity and sidewall angle are both higher than the averages from the first etch trial.

## 4.6 Aspect Ratios

The etch trials so far have not resulted in large aspect ratios. This is due to both the mask undercut and the small etch depths. It is possible that higher aspect ratios could have been achieved if the samples were etched to larger depths. For example, the SEM image shown in Figure 4.17 is of a 600 nm period grating. Using the average width (approximately the full width at half maximum value or FWHM), the aspect ratio is calculated to be roughly 1.2, meaning the etch depth was slightly larger than the FWHM. However, it is clear by the strong sidewall angle that these devices are not ideal.

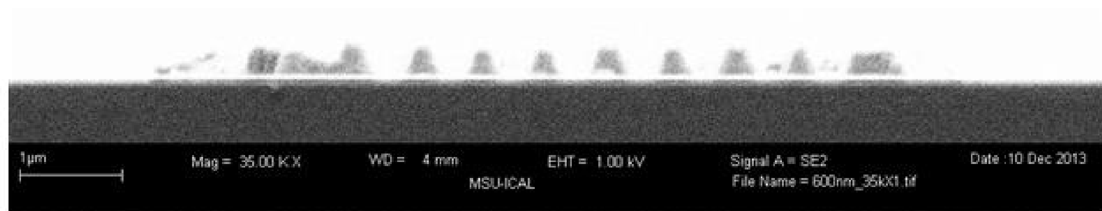


Figure 4.17. 600 nm period grating, SEM image, side view after Cr etch.

Most of the aspect ratios are less than 1, with the highest aspect ratios being just above 1 (seen in the nanostructures). A 400 nm period grating is shown in Figure 4.18. Note that the etched spaces between the gratings are at an elevated height compared to the rest of the sample. This is due to the fact that nanostructures etch at a slightly slower rate than the rest of the substrate. The gases from the ICP-RIE have a hard time

squeezing into the small gaps inherent in the nanostructure gratings, which results in a decrease of etch time. The microstructures do not have this issue, as the gaps in the gratings are much larger. Figure 4.19 demonstrates the 2 µm periodic gratings etch at the same rate as the bulk of the substrate.

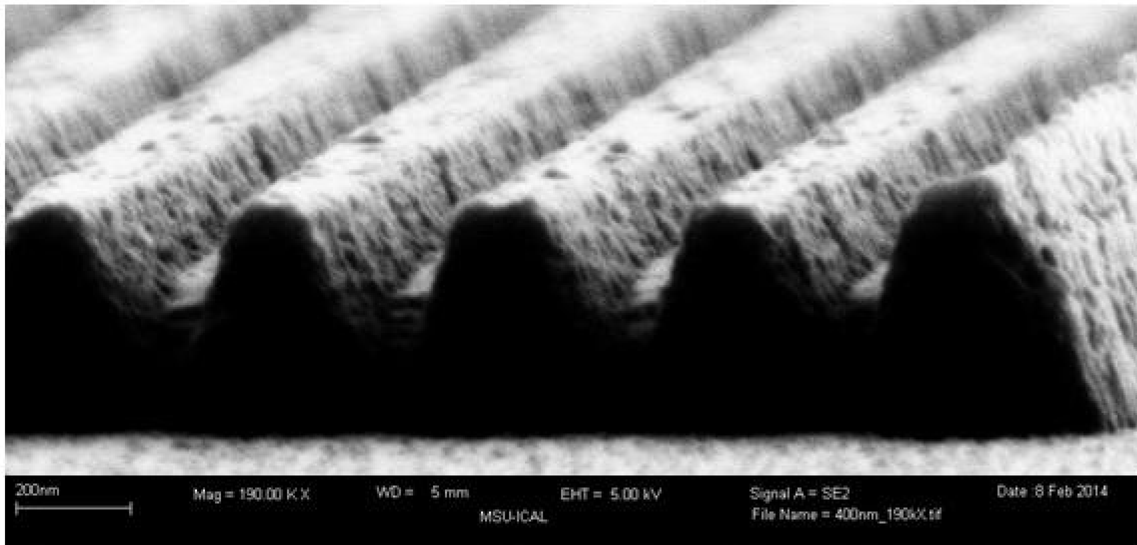


Figure 4.18. 400 nm period grating, SEM image after Cr etch.

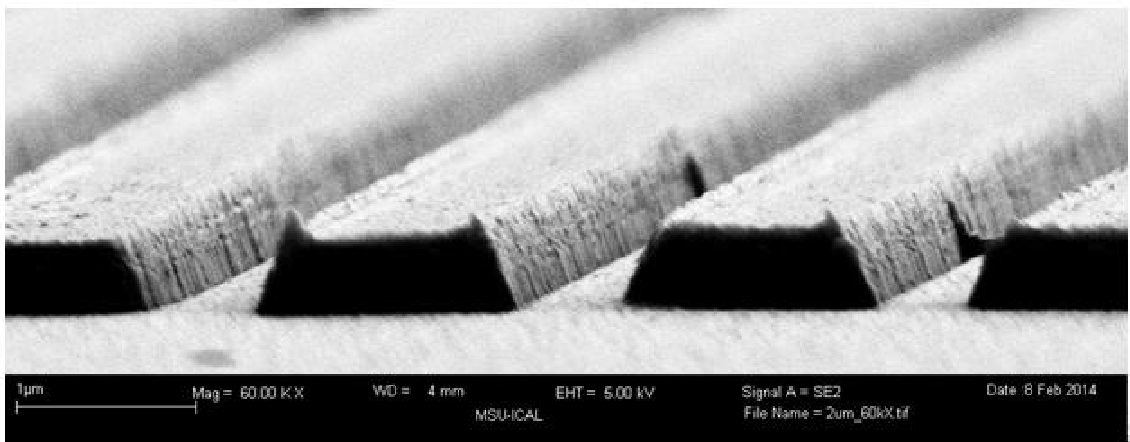


Figure 4.19. 2 µm periodic grating, SEM after Cr etch.

With the decreased etch rate in regard to nanostructures, longer etch durations are necessary in order to create higher aspect ratios. Because the etch times have not yet exceeded 10 minutes, the nanostructures have all been limited in depth. With longer etches, it is anticipated that higher aspect ratios are achievable using this process.

## 4.7 Future Trials

Currently, several samples have been etched successfully. Both nano- and microscale features were etched into lithium niobate using the ICP-RIE. However, after careful analysis of the results, there are several factors that need to be improved. First, the etch selectivity should be improved. Ideally, this value would be at least 20 so that 2 μm of lithium niobate could be etched while only losing 100 nm of mask. The etch selectivity can be improved several different ways. One method is to improve the mask so that it etches slower in the current chemistry. The mask could be improved by either changing the material of the mask (so that it is no longer a chromium mask) or by optimizing the chromium deposition process so that a denser mask is formed. The etch selectivity could also be improved by optimizing the etch chemistry in such a way that the chromium mask etches slower and lithium niobate etches much faster. Different chemicals and chemical ratios will have different etch rates, so by testing various different etch chemistries the etch selectivity could potentially be improved.

Another improvement to be made is increasing the sidewall angle. As seen in earlier sections, the sidewall angle is close to 70° which creates trapezoidal nanostructures. These angles could be improved through optimizing the etch chemistry, so that a more directional etch could be achieved. Without proper directionality, the etch

is more isotropic which leads to non-ideal structures. This is no trivial task and will be a long, iterative process.

The third improvement that needs to be addressed is the sidewall smoothness. Two images of a 1 μm period grating are shown in Figure 4.20. By looking at the sides of the grating walls, the severity of the roughness on the sidewalls can be seen. Waveguides and gratings with rough edges cause the light to scatter which results in lossy and inefficient optical devices, so it is important to improve these structures. These rough sidewalls are most likely due to roughness in the chromium mask, although it cannot be said definitively at this point. Both the roughness in the sidewalls and the roughness in the mask edge are on the range of tens of nanometers, which supports the fact that they are likely correlated. Therefore, in order to achieve smoother sidewalls, the process of patterning the chromium mask will need to be optimized so that the mask edges are as smooth as possible, which will translate into smooth sidewalls in the nanostructures. The main objective of this thesis is to create structures meant for efficient second harmonic generation devices. If the structures are lossy because of rough sidewalls, they will not be adequate for this thesis. The sidewalls could be improved by, once again, optimizing the etch chemistry.

The last major improvement necessary to make is to increase the aspect ratio. Currently, no samples have been etched deep enough in order to see if higher aspect ratios are achievable. In some applications, high aspect ratio structures will be required, and by realizing said structures, it will ensure that a wide variety of structures can be made using this etching process. Also, in order to create efficient ridge waveguides on the micron scale, it may be necessary to have aspect ratios close to 1 which requires a depth

of at least 1 μm. Therefore, another etch trial should be run for a long period of time in order to see high aspect ratios among the nanostructures and aspect ratios of about 1 among the microstructures. Assuming an etch rate of about 78.5 nm/min (based off the Etch 3 results), an etch depth of 1 μm would take about 13 minutes.

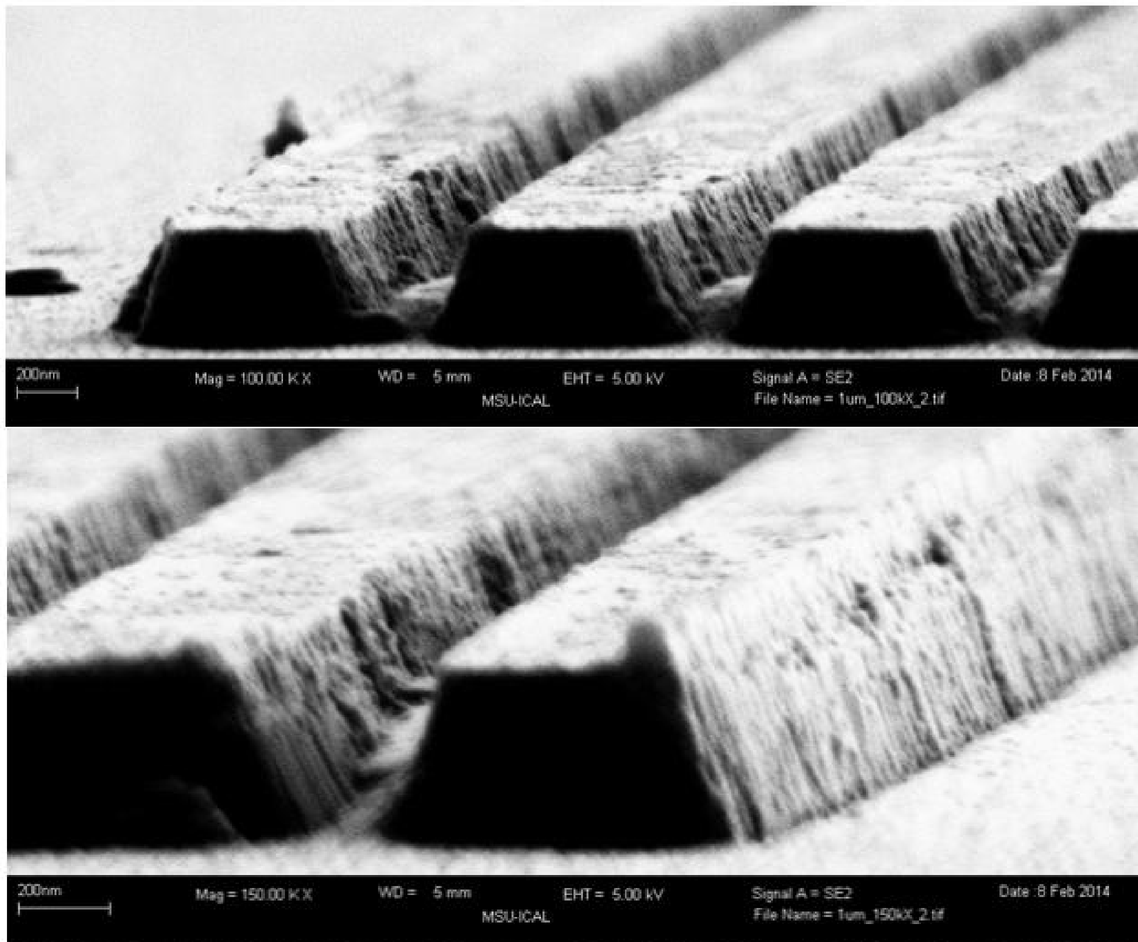


Figure 4.20. Two SEM images of a 1 μm period grating.

With all of these improvements in mind (improving the etch selectivity, the sidewall angle, the sidewall smoothness, and the aspect ratio), several future trials are in store. First, a deep etch trial is required in order to obtain higher aspect ratios. Second,

several iterative processes will be done in order to optimize the etch mask and etch chemistry. By developing these processes, an optimum etch mask and chemistry can be found so that the etched structures can efficiently propagate light.

## 4.8 Conclusion

It is important to emphasize the fact that this fabrication process is capable of realizing both nano- and microscale features. The largest structures that have been made are gratings with a period of 10 µm, as seen in Figure 4.21. The smallest nanostructures successfully made using this fabrication process, so far, are 300 nm period grating nanostructures, as seen in Figure 4.22. Because gratings with 300 nm, 400 nm, 600 nm, 800 nm, and 1 µm periods have been realized on lithium niobate, it can be said that this recipe can be used to successfully nanostructure lithium niobate. Although optimization is certainly needed to improve the sidewall angles and etch selectivity, the results thus far are promising. Once the fabrication process is fully optimized, the nanostructures can be designed in order to achieve exact-phase matching in lithium niobate. It was also seen that microstructures were made with periods of 2, 3, 4, 6, 8, and 10 µm. While structures of this size will be ineffective when considering nanoengineering the lithium niobate, these microscale structures can be designed to make excellent ridge waveguides.

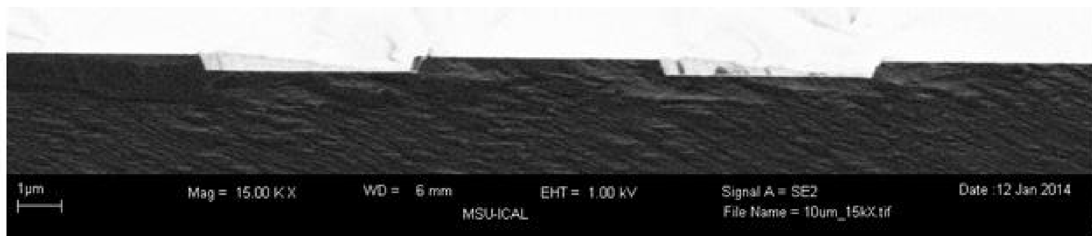


Figure 4.21. 10 µm period grating.

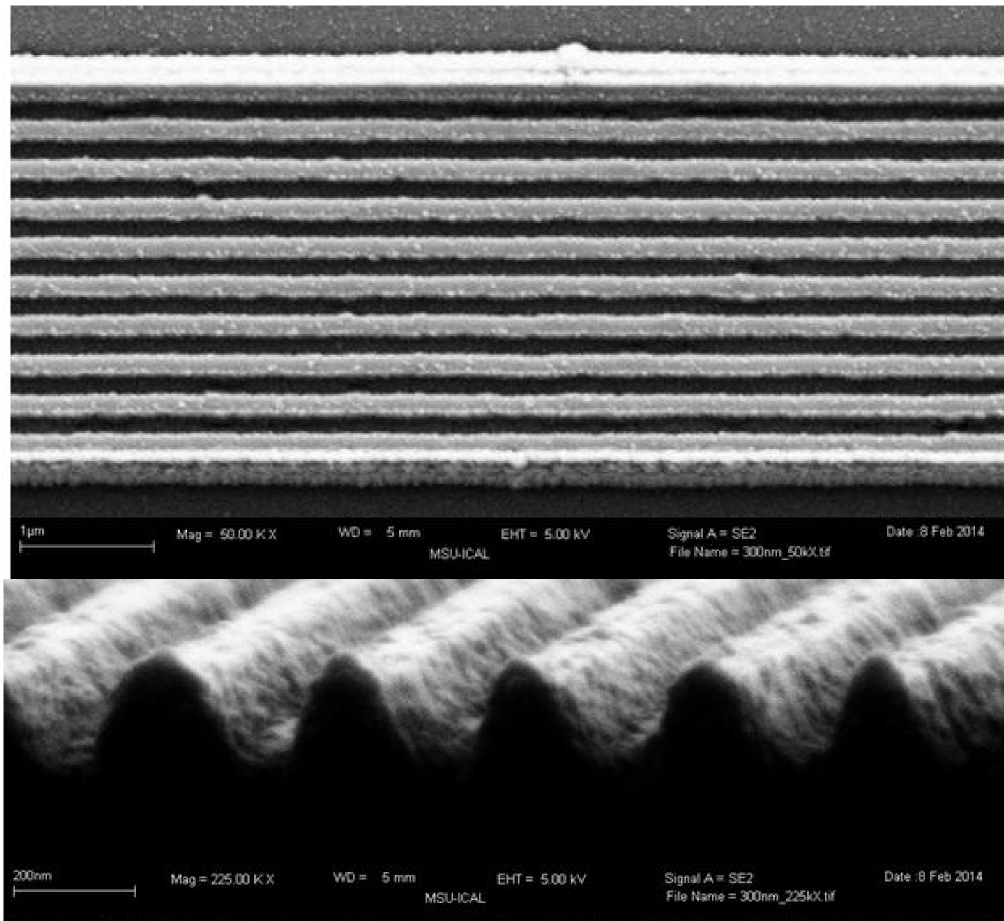


Figure 4.22. Top: top view SEM image of a 300 nm period grating; bottom: side view SEM image of 300 nm period grating.

# CHAPTER 5

# ALL OPTICAL POLING / WET ETCH

## 5.1 Introduction

The second method of structuring lithium niobate is all optical poling / wet etch. Here, a UV laser is used to pole lithium niobate, as described in Chapter 2, and then the sample is etched in HF. The HF etch both verifies that the poling has been achieved and creates nanostructures on the surface of the poled lithium niobate. The inverted $+z$ face of the lithium niobate will not be etched but the $-z$ face will [35]. Therefore, the poled structures will be physically apparent on the surface of the sample after the HF etch. This technique accomplishes two goals of the thesis. First, it potentially allows for nanoscale domain inversions (after the sample is poled and before it is etched). Nanoscale domain inversions are intended to improve the wavelength versatility for second harmonic generation quasi-phase matching in lithium niobate. Second, it potentially leads nanoscale physical structuring of the lithium niobate surface (after the HF etch). Designed nanostructures on lithium niobate can lead to exact-phase matching so that 100% wavelength conversion efficiency is attained in SHG.

## 5.2 Procedure

The LN samples are illuminated with a cw frequency doubled argon ion laser at a 244 nm wavelength. This laser is provided by Dr. Rob Walker in the Department of Chemistry and Biochemistry, and is integrated into a Raman microscope. The lithium

niobate samples are placed under the 40x microscope objective (MO) of the microscope so that the light is focused onto the surface of the substrate. Then, using the manual translation stage, the beam is steered about the sample so that numerous exposure tests are performed. The goal is to illuminate the sample with intensities of approximately 100-150 kW/cm$^2$ so that the sample will be poled [57]. However, the precise spot size of this laser is unknown, which makes it hard to predict the exact intensity of the laser at the sample. The maximum power incident on the sample is measured to be approximately 6.3 mW. After the samples are illuminated by the UV laser, they are then etched in 25% HF at AdvR, Inc. for 1 hour at room temperature. This provides a surface etch so that poled areas can be easily seen using an optical microscope. For example, a single poled area etched in HF is shown in Figure 5.1. The image is taken using a dark-field setting on an optical microscope so that the edges of structures can be viewed easily. The entire hexagonal structure is taller than the rest of the sample, but only the edges have contrast.

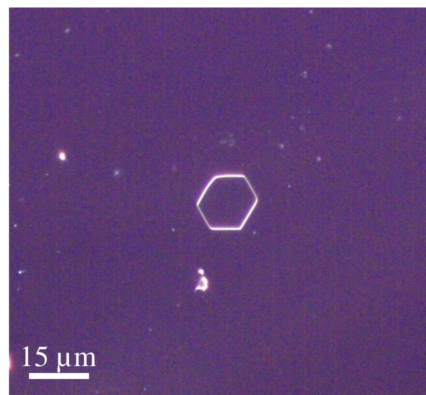


Figure 5.1. Optical microscope image of poled area on lithium niobate after HF etch; image obtained using dark field setting which illuminates edges of structures.

## 5.3 Results

A total of three samples underwent the AOP / wet etch procedure, and unfortunately it was seen that the UV illumination did not pole the sample. The first two samples resulted in a poling pattern on the sample, but the pattern had no correlation to the UV illumination pattern. Several images were taken of these two chips. Interestingly enough, both chips seemed to be covered with poled lines and dots, as seen in Figure 5.2. Poled regions seem to be spread throughout the entirety of both samples, creating hundreds of dots. This is concerning because the samples were not illuminated with the laser except in very small, confined spaces. For example, Figure 5.2 shows an area of the sample which was never illuminated by the laser. Figure 5.3 shows more images of these poled regions at a higher resolution.

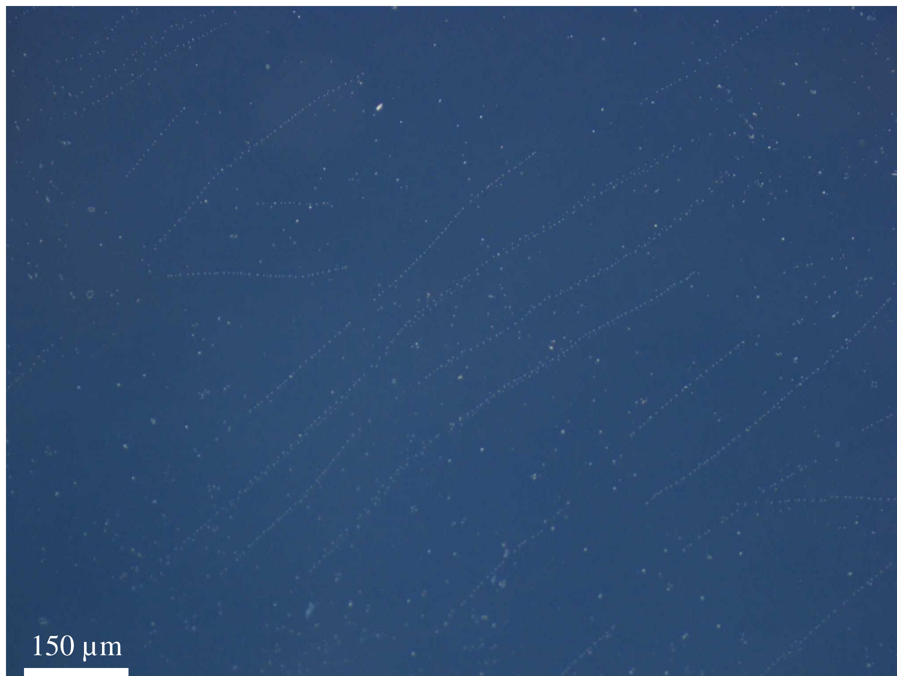


Figure 5.2. 10X MO image of poled regions on sample; white spots, particularly the linear patterns, represent poled regions on lithium niobate revealed after an HF etch.

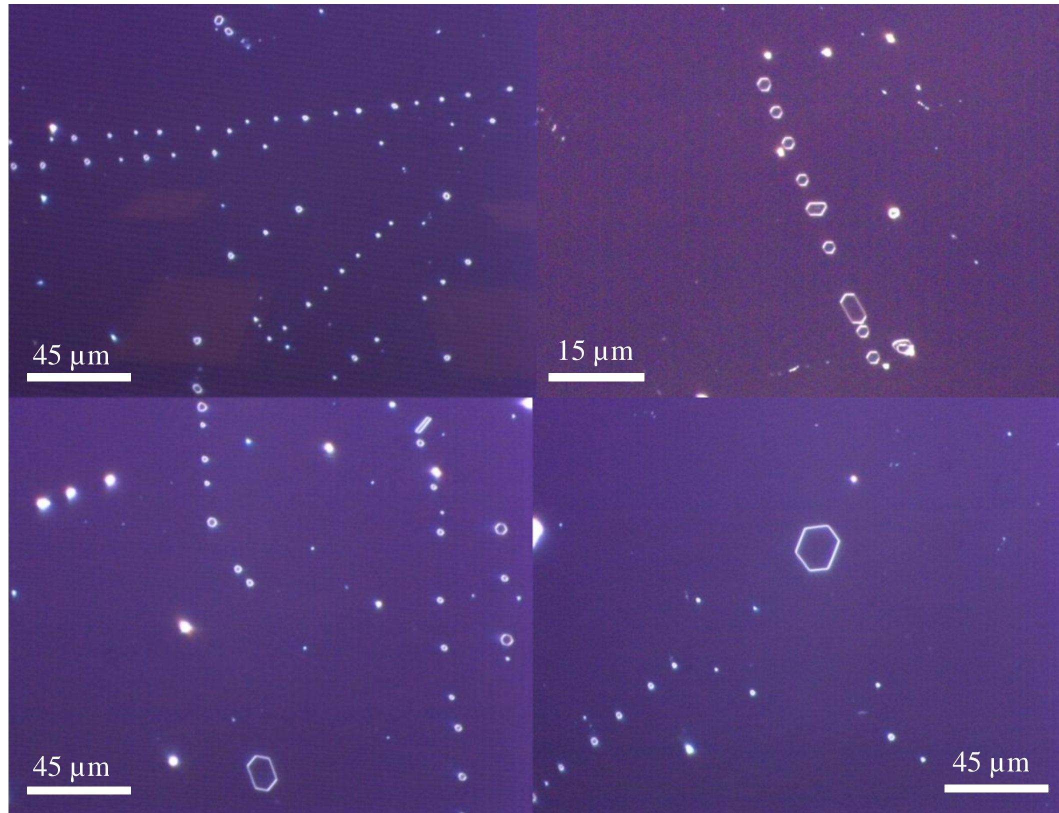


Figure 5.3. Four images showing lines and dots littered across the surface of the LN samples.

The hexagonal structures ensure that these regions are localized poled areas on the sample. Domain inversions will typically follow the crystal structure, which is hexagonal in lithium niobate; therefore, most domain inversions on LN are hexagonal in shape. Now, it can easily be seen that the samples were indeed poled, but the poling pattern on both of these chips do not quite match up with the expected pattern. Prior to UV exposure, a grid was drawn onto the samples using a diamond scribe. What was expected was one small poled region about every 1 mm (one poled region within each grid box), and two horizontal lines on one of the chips. However, both samples were littered with poled areas all over the samples. For example, the two images in Figure 5.4 each show

one box in the grid (the scribe marks seen in the image indicate the edge of each grid box). There are several, almost vertical, lines of poled regions on the sample in addition to some seemingly random poled spots. In each of these boxes, the laser illuminated a single spot; therefore, a single poled region was expected within each box. Because there are so many poled areas within the box, it is impossible to see whether or not the laser poled the sample or not.

It was decided that the samples were poled at some other time other than the AOP trial. It seems that there is something in our fabrication process that is poling the samples; however, it is unclear exactly what is doing it. A lithium niobate sample that had not been processed or intentionally poled was etched in HF, and it was found to not have any domain inversions on the sample. Another sample that had undergone fabrication procedures such as cleaving, spinning, baking, EBL, and chromium deposition was also etched in HF, and it was found to have numerous poled areas as well. For example, various poled patterns are found in a sample that had undergone mask patterning procedures (as defined in Chapter 3), even though it had never been intentionally poled. An image of poled areas on this sample is shown in Figure 5.5. Therefore, it is probable that some stress induced during standard fabrication processes is poling the sample. Most likely, the poling is caused by thermal stress from baking the samples on hotplates or mechanical stress from cleaving the samples prior to spinning.

It is possible, though, that the AOP samples were indeed poled by the laser, but because there is so much ‘background noise’, there is no way of telling whether the samples were actually poled or not by the UV laser. In order to determine whether the samples could be poled with the cw argon ion laser, the test was repeated on a different

sample. This sample had not gone through any fabrication processes, so it was uniformly poled. After poling the sample (using a maximum power so that about 6.3 mW was incident on the substrate), it was found that the poling did not work. The majority of the sample had no domain inversions on it, although there were a few small poled areas seen. Most of these poled areas were seen near scratches on the sample, as seen in Figure 5.6 and Figure 5.7.

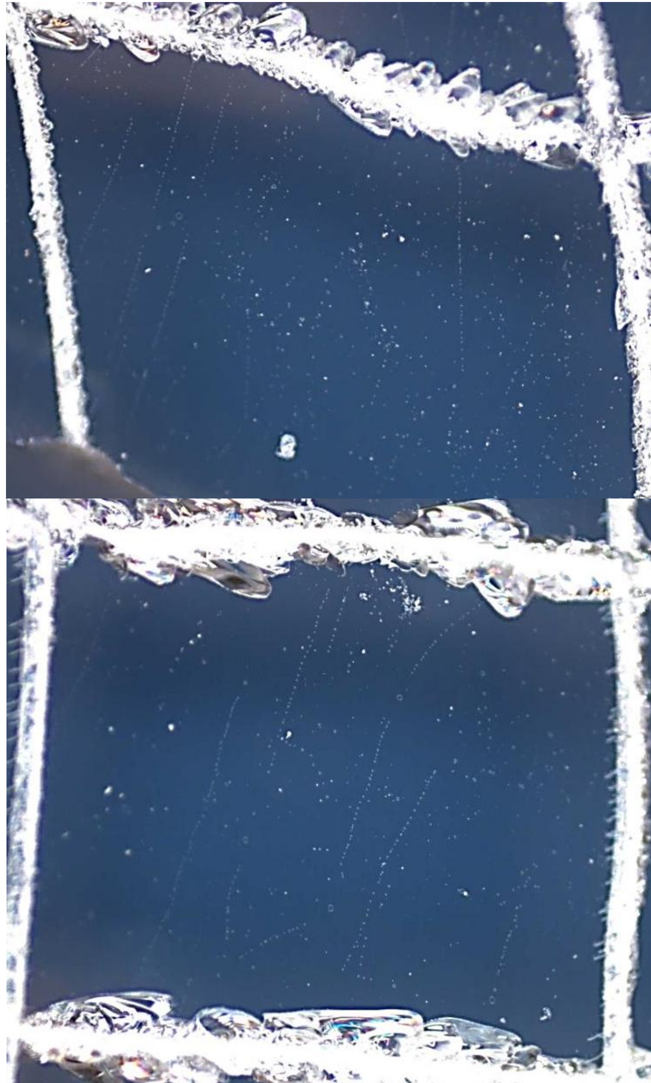

Figure 5.4. Two images showing one box in the grid; each box was expected to have only on poled spot.

Figure 5.5. Poled pattern found on a sample that had been patterned with a chromium mask, but not intentionally poled through AOP.

Figure 5.6. Image of poled cluster near scratch in lithium niobate sample.

Figure 5.7. Image of poled cluster near scratch in lithium niobate surface.

## 5.4 Domain Inversion Patterns

While it cannot be said with absolute certainty, these randomly poled areas are most likely caused by mechanical stress in the sample. As mentioned earlier, samples that had not undergone any fabrication processes such as cleaving were found to have virtually no domain inversions on the substrate, so that it was uniformly poled. Another uniformly poled sample that had not undergone any fabrication processes was accidently dropped on the floor and broke into two pieces. One of these broken pieces was etched in HF, and it was found to have a significant amount of domain inversions, likely caused by the fall. As seen in Figure 5.8, several microscope images were taken and it was seen to have recurring poling patterns throughout the sample. It is probable that these poled regions were created when the sample was broken.

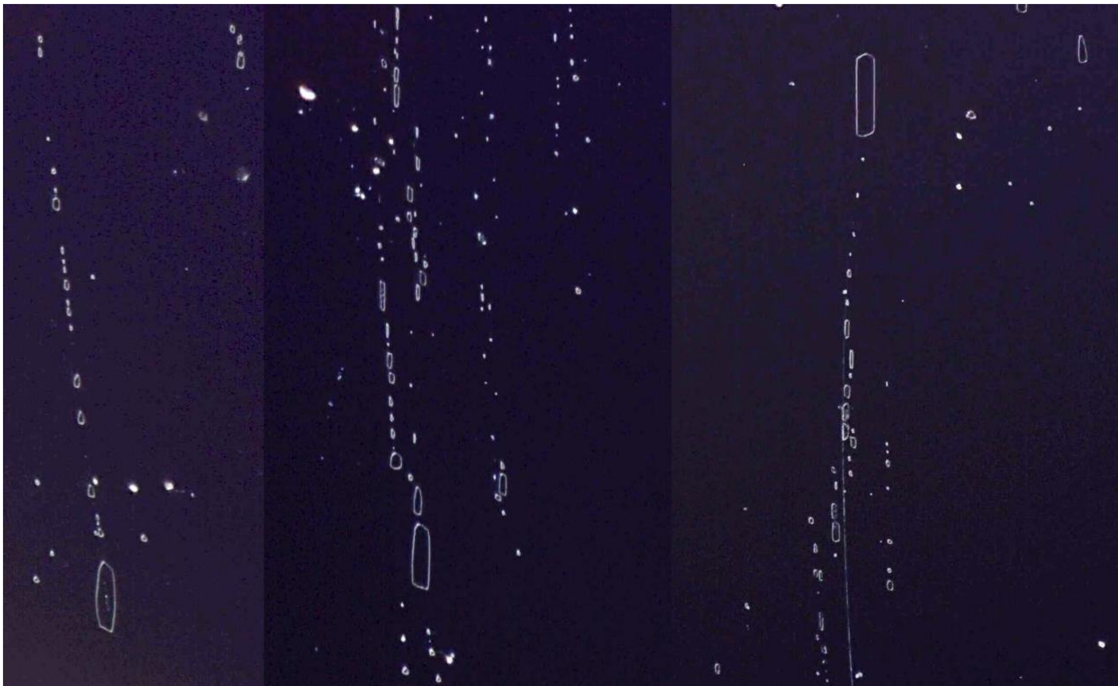

Figure 5.8. Three images of poled regions on an unprocessed, broken lithium niobate sample.

Another piece of evidence suggesting mechanical stress is the poling culprit is that the cleaved samples appear to have linear poling patterns that are roughly perpendicular to the cleaved edge. For example, the following two images all display poling trends on a lithium niobate sample cleaved into a triangle. In Figure 5.9, the majority of the lines are at about 45° off of the horizontal. There are, however, a few lines that are nearly vertical and some that are nearly horizontal. Interestingly enough, the linear poling trends are all approximately perpendicular to two of the three cleaved edges of the cleaved triangular sample. Figure 5.10 also shows an image of the linear poled patterns on this triangular piece of lithium niobate.

Another image, seen in Figure 5.11 shows a different lithium niobate sample. Here the linear poling patterns are mostly all vertical. These linear patterns are also perpendicular to the cleaved edges on that particular sample. Once again, these poling trends are essentially perpendicular to the cleaved edge of the sample.

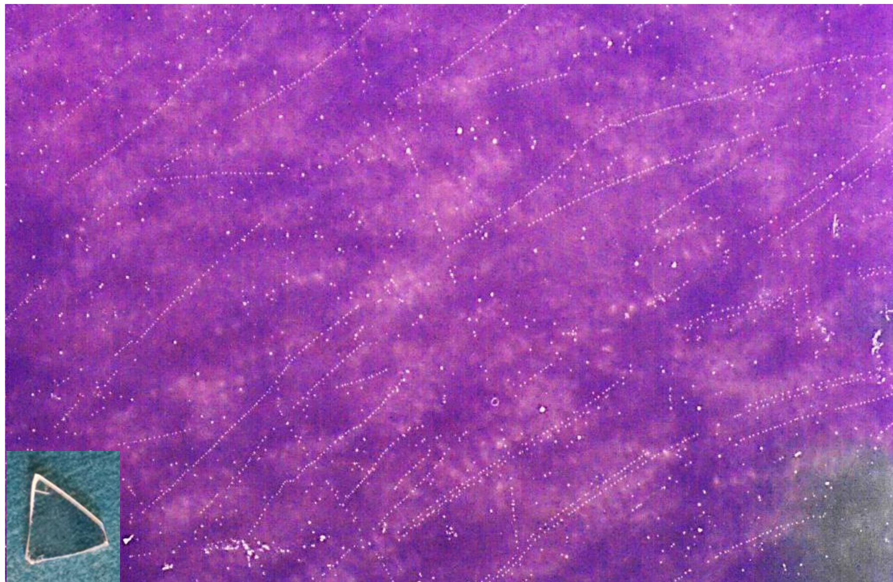

Figure 5.9. Optical microscope image of poling pattern seen on cleaved triangular piece of lithium niobate, etched in HF; inset showing image of cleaved LN chip.

Figure 5.10. Another image of the same triangular piece of lithium niobate.

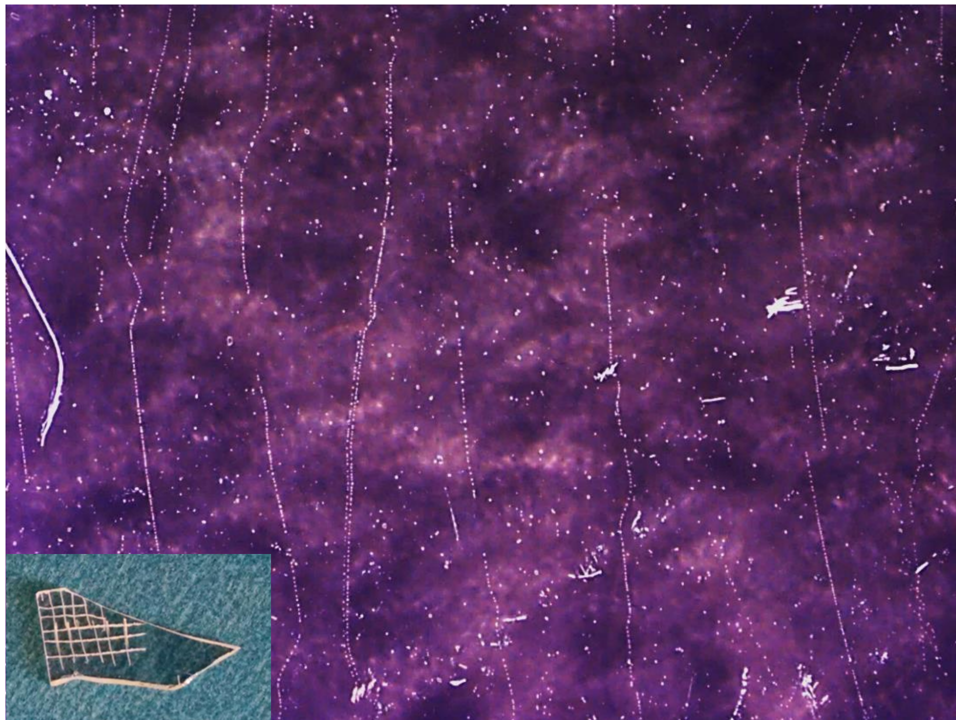

Figure 5.11. Linear poling patterns shown on a sample perpendicular to the cleaved edge; inset showing image of cleaved LN chip with grid scribed on surface.

Because of these two factors suggesting that mechanical stress is the cause of these seemingly random domain inversions (the dropped and broken sample being poled and the linear poling patterns perpendicular to cleaved edges), it can be speculated that this is what is actually happening. However, this cannot be said with absolute certainty. More research and testing is necessary in order to determine exactly what is the culprit for the poled regions on previously unpoled samples.

## 5.5 Sidewall Analysis

When examining these poled regions, it was seen that the edges of the etched structures had extremely smooth sidewalls, unlike the ICP-RIE etched structures that were seen in Chapter 4. Some comparison images are shown in Figure 5.12 and Figure 5.13. Figure 5.12 is of two SEM images taken at 40,000X magnification (40kX). On the left, an etched 400 nm period grating is shown and the right displays an etched poled region on lithium niobate. Figure 5.13 is of two SEM images taken to 150,000X magnification (150kX). The left image shows a grating edge and the right image shows the edge of a poled region. While sidewall smoothness is a concern when creating optical devices, as pointed out earlier in Chapter 4, it can be seen that these ICP-RIE structures had relatively high sidewall roughness (as can be seen in the left image in Figure 5.13). As mentioned previously, this roughness was measured to be on the scale of tens of nanometers.

However, poled areas that have been etched with HF reveal extremely smooth characteristics, as seen in the right image of Figure 5.13. The domain inversions tend to follow the crystalline structure of lithium niobate, which means any roughness in the

domain wall would be on the atomic scale. This causes etched walls to be extremely smooth, and much smoother than the sidewalls of ICP-RIE etched structures. If a poling / wet etch process can be developed and optimized, then these structures in lithium niobate can be easily made and have the potential to be significantly higher in quality than structures made via ICP-RIE.

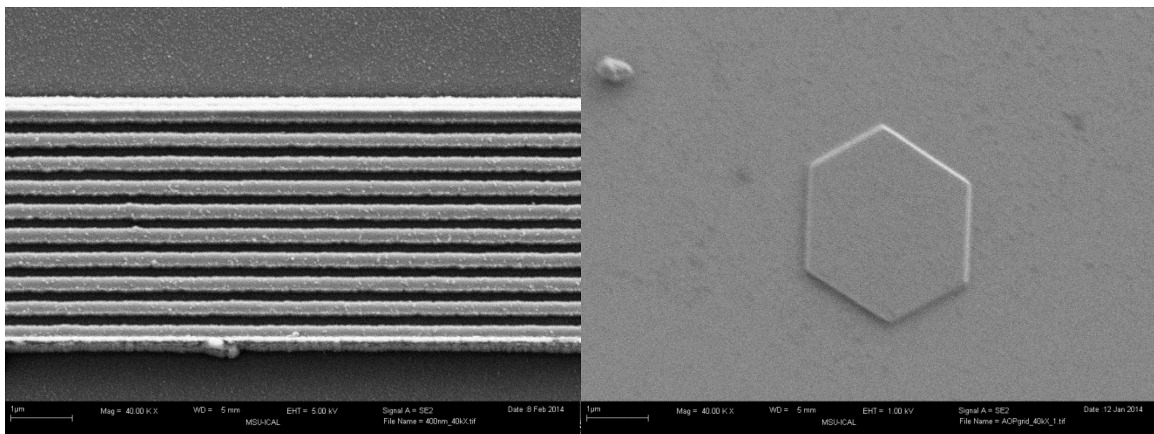

Figure 5.12. Left: SEM image of 400 nm period grating, magnification of 40kX; Right: SEM image of poled region, revealed during HF etch, magnification of 40kX.

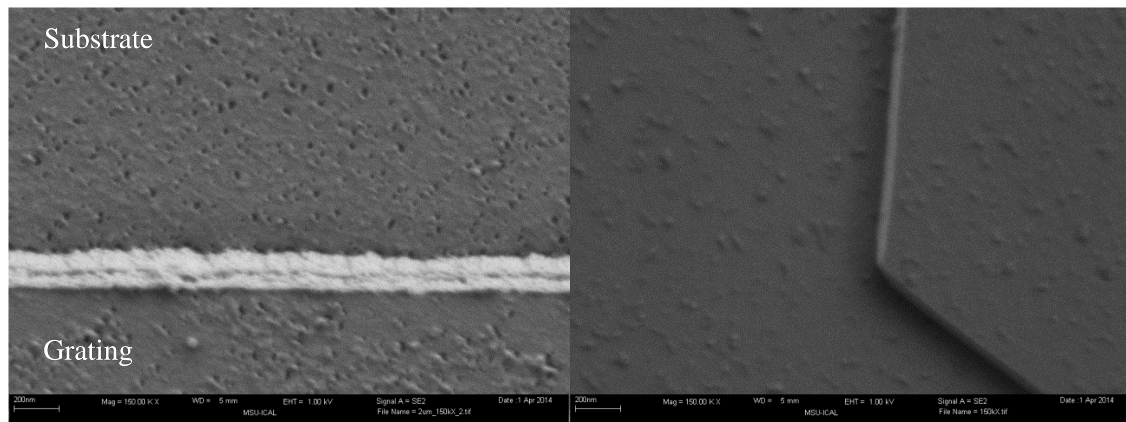


Figure 5.13. Left: SEM image of grating edge, magnification of 150kX; Right: SEM image of poled region, revealed during HF etch, magnification of 150kX.

Sidewall angles of structures made using a poling / wet etch technique have the potential to be nearly vertical, as seen by other groups [13, 36]. Therefore, this technique

will likely yield higher quality nanostructures in lithium niobate than the ICP-RIE. First, it will create structures with extremely smooth sidewalls. Second, it will create structures with sidewalls that are nearly vertical. Both of these factors will lead to structures better in quality than the structures resulting from the ICP-RIE technique, as seen in Chapter 4.

## 5.6 Conclusion

It was determined that the lithium niobate samples were not poled during the all optical poling trials. Most likely, there was simply not enough power at the surface of the samples to invert the domains. However, this testing resulted in better knowledge of fabrication processes during the ICP-RIE. It was discovered that samples being processed using standard fabrication procedures leading up to the ICP-RIE were inadvertently being poled. While it is uncertain as to exactly what step in the fabrication process is poling the samples, it is most likely mechanical stress induced on the sample causing it to become poled. The samples are all cleaved prior to spinning, which places significant stress on the samples. It was seen that the poling patterns are typically perpendicular to a cleaved edge of a sample, which implies that the act of cleaving induces stress large enough to pole the sample in particular areas. While this chapter was intended to illustrate how nanoscale domain inversions and nanostructures could be etched into lithium niobate, it turned out instead to be educating for the ICP-RIE fabrication process. Without this (failed) attempt at AOP, it is likely that it would have never been learned that something during standard fabrication procedures is poling the lithium niobate samples.

# CHAPTER 6

# CONCLUSION

## 6.1 Summary

The main goal of this thesis is to facilitate the making of more efficient and versatile second harmonic generation devices using nanoscale structures or features in LN. In order to achieve this, three methods are investigated. First, nanoscale domain inversions are explored for submicron periodic poling in quasi-phase matching. Currently, submicron poling is a difficult feat so quasi-phase matching devices are only useful for second harmonic devices in which microscale (or larger) periods are necessary. Nanoscale domain inversions will allow for quasi-phase matching to be achieved for a wide range of wavelengths.

The second method for improving current second harmonic generation devices is nanostructuring the surface of lithium niobate in order to achieve exact-phase matching. These structures can be made using standard fabrication procedures such as lithography, masking, and etching, or they can potentially be made by designing nanoscale domain inversion patterns in the crystal followed by a wet HF etch. Exact-phase matching will accommodate various frequencies as the structures will be scalable. The third method proposed to improve current second harmonic generation devices is to create microscale features on lithium niobate, which will act as ridge waveguides. Recall that SHG efficiency is improved when the interaction length is small and the intensity is high

(Section 1.3). Small microscale waveguides, which can confine high intensity EM waves over long distances, are ideal for this application.

These methods were investigated initially with a detailed literature review. In this review, the best methods for the Nano-Optics Group were identified and tested, as discussed in Chapters 3-5. First, an ICP-RIE technique was used to etch both micro- and nanoscale structures into lithium niobate. This resulted in promising structures, with the smallest features being around 150 nm (300 nm period) and the largest features being about 5 μm (10 μm period). However, parameters such as sidewall angle, sidewall roughness, and etch selectivities still need to be improved and optimized. Then, an AOP / wet etch method was attempted. This method was intended to result in both nanoscale domain inversions and nanoscale features (realized after the HF etch). However, the lithium niobate samples were not poled by the UV cw laser, so no structures were realized during this technique. During the AOP / wet etch trials it was discovered that samples being prepared for an ICP-RIE etch were somehow becoming poled. These samples are most likely being poled due to mechanical stress such as cleaving. Hence, although the AOP / wet etch did not result with the desired outcome, it did lead to some insight on handling and processing lithium niobate.

## 6.2 Recommendations for Future Trials

### 6.2.1 ICP-RIE

As mentioned previously, the results from the ICP-RIE trials in this thesis resulted in nano- and microstructured lithium niobate, albeit the structures require significant improvement. In order to improve the structures made by the ICP-RIE process, several

avenues must be pursued. First, the etch mask must be improved. A better quality etch mask will result in an improved etch selectivity and/or improved sidewall angles. For this thesis, a chromium etch mask is deposited with a thermal evaporator. In future trials, the chromium mask should be analyzed to determine if it is fairly porous or not. Porous etch masks will etch quickly, decreasing the etch selectivity and allowing for mask undercutting as the sides of the mask etch quicker during ICP-RIE than the center. If the etch masks are porous, it may be useful to deposit the chromium onto the sample at a faster deposition rate. The current deposition rate used is 3 Å/s, but faster deposition rates may yield denser etch masks. Another possibility is to consider other materials to be used as an etch mask. For instance, as seen in the literature survey, nickel is commonly used as an etch mask for lithium niobate.

The etch chemistry must also be optimized in order to attain better quality structures in lithium niobate. In this thesis, three different etch trials were performed. However, none of these trials resulted in stellar structured lithium niobate, making it necessary for further optimization. The only fluorine gas tested in this thesis is $CHF_3$, although various other fluorine based gases have been seen to etch lithium niobate using the ICP-RIE, such as $SF_6$, $C_4F_8$, and $CF_4$. While it was seen that $CHF_3$ resulted in better nanostructures than other fluorine gases in one study [61], it is possible that other gases would work better for the particular ICP-RIE in MMF. Therefore, other fluorine gases should be tested in order to see what works best for the Nano-Optics Group. Also, various etching parameters such as the DC bias and chamber pressure are often considered etch chemistry parameters. These factors may also be optimized to improve the quality of the structured lithium niobate. For example, the chamber temperature and

pressure were kept constant throughout all of the etch trials in this thesis, but in future trials these parameters could be adjusted in order to achieve the highest quality structures possible.

Last, the samples must be treated with caution so as to not inadvertently pole the lithium niobate substrates. While the research found in this thesis suggests that mechanical stress (specifically cleaving) causes the samples to be poled, it is not quite certain that this is the case. It is suggested that the exact cause of this issue be pinpointed to avoid inverting the domains on the lithium niobate samples in future trials.

#### 6.2.2 All Optical Poling / Wet Etch

During this experimental trial, the samples were not poled by the UV illumination. It is not known exactly why this did not work, as it could have been any of the following, among others:

1. The laser intensity was not high enough. This could be due to the fact that the focused spot size was much larger than anticipated (expected spot size was about 1-2 µm), or the power incident on the sample was much lower than the expected value of about 6 mW.
2. The beam was not properly focused. The light was focused onto the sample using visible light through a microscope objective. It was expected that the UV light would be focused when the sample was about 60 µm closer to the MO. Therefore, the UV light was never verified to be focused on the sample, so it is possible that the UV light was not properly focused.

3. Research groups who had performed cw AOP on lithium niobate had used pure LN and doped LN with iron and titanium. It had not been seen in the literature that AOP would work on MgO doped lithium niobate, which was the material used in this thesis. Therefore, it is possible that this process does not work on MgO doped lithium niobate.

However, it might be beneficial to try this experiment one more time using the pulsed Ti:Sapphire laser available in the Department of Chemistry and Biochemistry. Pulsed lasers have proved to result in better quality domain inversions, as mentioned in Section 2.4.2, and they can achieve higher peak intensities. If the cw laser used in this thesis simply could not supply a high enough intensity to pole the lithium niobate samples, it is possible that a pulsed laser could.

## 6.3 Impact

The objective of the thesis is to look into various methods for improving current SHG devices. In particular, the thesis investigates nanostructuring lithium niobate via poling and etching lithium niobate in order to pursue different avenues for improving SHG devices. Current devices are typically made using quasi-phase matching in lithium niobate. This quasi-phase matching technique can be extremely efficient, with nearly 100% wavelength conversion efficiency at fundamental wavelengths such as 1064 nm. However, these devices can be improved in one of two ways. First, they can be made more adaptable to a wide range of wavelengths while retaining high wavelength conversion efficiency. For many wavelengths, the coherence length required for quasi-phase matching is much smaller than the coherence length used for devices converting

1064 nm to 532 nm, which means nanoscale domain inversions are necessary. Second, the devices could be made to be more efficient which would specifically help in low-light applications.

More versatile SHG devices that could efficiently cover an extensive variety of wavelengths could provide nonlinear optical devices for various lasers of different frequencies. Currently, SHG devices perform extremely well converting IR light to green light. However, there is not yet an efficient method of converting visible light into UV light. Currently, there are not many economical, compact high power UV lasers, but there are a number of inexpensive high power visible lasers. Efficient SHG devices scaled to convert visible to UV light would be able to essentially create high powered, coherent UV light fairly inexpensively.

In low-light applications, specifically when using IR light, it may be necessary to have 100% wavelength conversion efficient SHG devices. As mentioned in Chapter 1, there are few high quality IR detectors, suggesting applications such as photon-counting in the IR spectrum are not ideal. However, a 100% efficient wavelength conversion device could shift all the IR light into visible light, where there are numerous high quality detectors that can be used for photon-counting. By nanostructuring lithium niobate, exact-phase matching can be achieved to potentially increase the wavelength conversion efficiency. This process of exact-phase matching not only increases wavelength conversion efficiency, but it is comprised of nanostructures that are scalable so that it can adapted to accommodate various frequencies. Also, by structuring microscale ridge waveguides onto lithium niobate, to be used for quasi-phase matching, the second harmonic signal can be increased.

While nanoscale poling was not achieved in this thesis, both nano- and microscale features were realized on lithium niobate using standard fabrication techniques. This means that this fabrication process can potentially be used to make both microscale ridge waveguides in lithium niobate for improved quasi-phase matching and nanoengineered structures to achieve exact-phase matching. The long-term goal is to use these structures in order to create efficient SHG devices. The process of creating nanoscale features on lithium niobate will need to be developed so that eventually, a reproducible grating will be able to be formed on the surface of LN that is accurately and precisely scaled to achieve exact-phase matching. The microstructuring process will also need to be improved so that low-loss waveguides can readily be made on lithium niobate. However, the groundwork research that has been done in this thesis supports these long-term goals. Further optimization is needed in order to realize the final product, but this thesis provides the foundation research so that in the future, these structures can be used and implemented into efficient second harmonic generation devices.

# REFERENCES

[1] A. Busacca, C. Sones, V. Apostolopoulos, R. Eason and S. Mailis, "Surface domain engineering in congruent lithium niobate single crystals: A route to submicron periodic poling," *Applied Physics Letters,* vol. 81, pp. 4946-4948, 2002.

[2] R. Weis and T. Gaylord, "Lithium niobate: Summary of physical properties and crystal structures," *Applied Physics A,* vol. 37, pp. 191-203, 1985.

[3] R. Boyd, Nonlinear Optics, Academic Press, 2008.

[4] R. Munn and C. Ironside, Principles and Applications of Nonlinear Optical Materials, Glasgow: Blackie Academic & Professional, 1993.

[5] B. Saleh and M. Teich, Fundamentals of Photonics, Wiley, 2007.

[6] N. Bloembergen, Nonlinear Optics, World Scientific Publishing Company, 1965.

[7] Y. Svirko and N. Zheludev, Polarization of Light in Nonlinear Optics, West Sussex: John Wiley & Sons, 1998.

[8] A. Rogalski, "Infrared detectors: an overview," *Infrared Physics & Technology,* vol. 43, pp. 187-210, 2002.

[9] M. Fejer, G. Magel, D. Jundt and R. Byer, "Quasi-phase-matched second harmonic generation: tuning and tolerances," *IEEE Journal of Quantum Electronics,* vol. 28, pp. 2631-2654, 1992.

[10] V. Gopalan, T. Mitchell, Y. Furukawa and K. Kitamura, "The role of nonstoichiometry in 180 domain switching of LiNbO3 crystals," *Applied Physics Letters,* vol. 72, pp. 1981-1983, 1998.

[11] D. Jundt, "Temperature-dependent Sellmeier equation for the index of refraction, ne, in congruent lithium niobate," *Optics Letters,* vol. 22, pp. 1553-1555, 1997.

[12] Y. Chen, W. Yan, D. Wang, S. Chen, G. Zhang, J. Zhu and Z. Wei, "Submicron domain inversion in Mg-doped LiNbO3 using backswitched poling with short voltage pulses," *Applied Physics Letters,* vol. 90, pp. 062908-1 - 062908-3, 2007.

[13] S. Grilli, P. Ferraro, P. D. Natale, B. Tiribilli and M. Vassalli, "Surface nanoscale periodic structures in congruent lithium niobate by domain reversal patterning and differential etching," *Applied Physics Letters,* vol. 87, pp. 233106-1 - 233106-3, 2005.

[14] D. Kuznetsov, V. Shur, S. Negashev, A. Lobov, D. Pelegov, E. Shishkin, P. Zelenovskiy, V. Platonov, M. Ivanov and V. Osipov, "Formation of nano-scale domain structures in lithium nioabte using high-intensity laser irradiation," *Ferrolectrics,* vol. 373, pp. 133-138, 2008.

[15] C. Sones, A. Muir, Y. Ying, S. Mailis and R. W. Eason, "Precision nanoscale domain engineering of lithium niobate via UV laser induced inhibition of poling," *Applied Physics Letters,* vol. 92, pp. 072905-1 - 0725905-3, 2008.

[16] S. Chiow, T. Kovachy, J. Hogan and M. Kasevich, "Generation of 43 W of quasi-continuous 780 nm laser light via high-efficiency, single-pass frequency doubling in periodically poled lithium niobate crystals," *Optics Letters,* vol. 37, pp. 3861-3863, 2012.

[17] J. Park, T. Kang, H. Jeon, B. Yim and H. Lee, "Highly efficient green light generation in compact second-harmonic module with a periodically poled MgO-doped lithium niobate planar waveguide," in *OptoElectronic and Communications Conference*, Kyoto, 2013.

[18] S. Kumar, G. Samanta, K. Devi and M. Ebrahim-Zadeh, "High-efficiency, multicrystal, single-pass, continuous-wave second harmonic generation," *Optics Express,* vol. 19, pp. 11152-11169, 2011.

[19] L. Novotny and B. Hecht, Principles of Nano-Optics, Cambridge: University Press, 2006.

[20] M. Ohtsu, Handbook of Nano-Optics and Nanophotonics, Springer, 2013.

[21] M. Ohtsu, Progress in Nanophotonics 1, Springer, 2011.

[22] A. Luo, Discontinuous Dynamical Systems, Springer, 2012.

[23] W. Nakagawa, R. Tyan and Y. Fainman, "Analysis of enhanced second-harmonic generation in periodic nanostructures using modified rigorous coupled-wave analysis in the undepleted-pump approximation," *Journal of the Optical Society of America A,* vol. 19, pp. 1919-1928, 2002.

[24] R. Jaeger, Introduction to Microelectronic Fabrication, Prentice Hall, 2002.

[25] C. Sones, M. Wengler, C. Valdivia, S. Mailis and R. Eason, "Light-induced order-of-magnitude decrease in the electric field for domain nucleation in MgO-doped lithium niobate crystals," *Applied Physics Letters,* vol. 86, pp. 212901-1 - 212901-3, 2005.

[26] H. Eggert, F. Kalkum, M. Wengler, U. Heinemeyer and K. Buse, "Light-assisted generation of tailored ferroelectric domain structures," *Ferroelectrics,* vol. 340, pp. 63-67, 2006.

[27] Y. Kong, J. Wen and H. Wang, "New doped lithium niobate crystal with high resistance to photorefraction - LiNbO3:In," *Applied Physics Letters,* vol. 66, pp. 280-281, 1995.

[28] M. Wengler, U. Heinemeyer, E. Soergel and K. Buse, "Ultraviolet light-assisted domain inversion in magnesium-doped lithium niobate crystals," *Journal of Applied Physics,* vol. 98, pp. 064104-1 - 064104-7, 2005.

[29] C. Sones, S. Mailis, W. Brocklesby, R. Eason and J. Owen, "Differential etch rates in z-cut LiNbO3 for variable HF/HNO3 concentrations," *Journal of Materials Chemistry,* vol. 12, pp. 295-298, 2001.

[30] H. Hu, R. Ricken, W. Sohler and R. Wehrspohn, "Lithium niobate ridge waveguides fabricated by wet etching," *IEEE Photonics Technology Letters,* vol. 19, pp. 417-419, 2007.

[31] F. Laurell, J. Webjorn, G. Arvidsson and J. Holmberg, "Wet Etching of Proton-exchanged Lithium Niobate - A Novel Processing Technique," *IEEE,* vol. 10, pp. 1606-1609, 1992.

[32] H. Lee and S. Shin, "Lithium niobate ridge waveguides fabricated by wet etching," *Electronics Letters,* vol. 31, pp. 268-269, 1995.

[33] I. Barry, G. Ross, P. Smith, R. Eason and G. Cook, "Microstructuring of lithium niobate using differential etch-rate between inverted and non-inverted ferroelectric domains," *Materials Letters,* vol. 37, pp. 246-254, 1998.

[34] I. Barry, G. Ross, P. Smith and R. Eason, "Ridge waveguides in lithium niobate fabricated by differential etching following spatially selective domain inversion," *Applied Physics Letters,* vol. 74, pp. 1487-1488, 1999.

[35] S. Mailis, C. Sones, J. Scott and R. Eason, "UV laser-induced ordered surface nanostructures in congruent lithium niobate single crystals," *Applied Surface Science,* vol. 247, pp. 497-503, 2005.

[36] S. Mailis, "UV laser induced ferroelectric domain ivnersion in lithium niobate single crystals," *Journal of Optics,* vol. 12, pp. 1-7, 2010.

[37] L. Wang, K. Wang, X. Wang, F. Chen, Y. Jiang, C. Jia, Y. Jiao, F. Lu, D. shen, H. Ma and R. Nie, "Selective etching in LiNbO3 combined of MeV O and Si ion implantation with wet-etch technique," *Surface and Coatings Technology,* vol. 201, pp. 5081-5084, 2006.

[38] T. Gischkat, H. Hartung, F. Schrempel, E. Kley, A. Tunnermann and W. Wesch, "Patterning of LiNbO3 by means of ion irradiation using electronic energy deposition and wet etching," *Microelectronic Engineering,* vol. 86, pp. 910-912, 2008.

[39] P. D. Nicola, S. Sugliani, G. Montanari, A. Menin, P. Vergani, A. Meroni, M. Astolfi, M. Borsetto, G. Consonni, R. Longone, A. Nubile, M. Chiarini, M. Bianconi and G. Bentini, "Fabrication of smooth ridge optical waveguides in LiNbO3 by Ion Implantation-Assisted Wet Etching," *Journal of Lightwave Technology,* vol. 31, pp. 1482-1487, 2013.

[40] F. Schrempel, T. Gischkat, H. Hartung, E. Kley and W. Wesch, "Ion beam enhanced etching of LiNbO3," *Nuclear Instruments and Methods in Physics Research B,* vol. 250, pp. 164-168, 2006.

[41] D. Gill, D. Jacobson, C. White, C. Jones, Y. Shi, W. Minford and A. Harris, "Ridged LiNbO3 modulators fabricated by a novel oxygen-ion implant/wet-etch technique," *Journal of Lightwave Technology,* vol. 22, pp. 887-894, 2004.

[42] V. Shur, "Domain Nanotechnology in Ferroelectric Single Crystals: Lithium Niobate and Lithium Tantalate Family," *Ferroelectrics,* vol. 443, pp. 71-82, 2013.

[43] R. Batchko, V. Shur, M. Fejer and R. Byer, "Backswitch poling in lithium niobate for high-fidelity domain patterning and efficient blue light generation," *Applied Physics Letters,* vol. 75, pp. 1673-1675, 1999.

[44] V. Shur, E. Rumyantsev, E. Nikolaeva, E. Shishkin and D. Fursov, "Nanoscale backswitched domain patterning in lithium niobate," *Applied Physics Letters,* vol. 76, pp. 143-145, 2000.

[45] A. Busacca, M. Cherchi, S. R. Sanseverino, A. Cino, A. Parisi, G. Assanto, M. Cichocki, F. Caccavale, D. Calleyo and A. Morbiato, "Surface periodic poling in ltihium niobate and lithium tantalate," *Fibres and Optical Passiv Components,* pp. 126-130, 2005.

[46] A. Busacca, A. Cino, S. R. Sanseverino, M. Ravaro and G. Assanto, "Silica masks for improved surface poling of lithium niobate," *Electronics Letters,* vol. 2, 2005.

[47] A. Busacca, C. Santini, S. R. Sanseverino, A. Parisi, A. Cino, R. Oliveri and G. Assanto, "Surface periodic poling in congruent lithium tantalite," *Electronics Letters,* vol. 42, 2006.

[48] S. Grilli, P. Ferraro, S. D. Nicola, A. Finizio, G. Pierattini, P. D. Natale and M. Chiarini, "Investigation on reversed domain structures in lithium niobate crystals patterned by interference lithography," *Optics Express,* vol. 11, pp. 392-405, 2003.

[49] S. Grilli, P. Ferraro, L. Sansone, M. Paturzo, S. D. Nicola, G. Pierattini and P. D. Natale, "Double-face and submicron two-dimensional domain patterning in congruent lithium nioabte," *IEEE Photonics Technology Letters,* vol. 18, pp. 541-543, 2006.

[50] Y. Ying, C. Valdivia, C. Sones, R. Eason and S. Mailis, "Latent light-assisted poling of LiNbO3," *Optics Express,* vol. 17, pp. 18681-18692, 2009.

[51] C. Sandmann and V. Dierolf, "The role of defects in light induced domain inversion in lithium niobate," *Physica Status Solidi,* vol. 2, pp. 136-140, 2005.

[52] M. Muller, E. Soergel and K. Buse, "Influence of ultraviolet illumination on the poling characteristics of lithium niobate crystals," *Applied Physics Letters,* vol. 83, pp. 1824-1826, 2003.

[53] C. Valdivia, C. Sones, S. Mailis, J. Mills and R. Eason, "Ultrashort-pulse optically-assisted domain engineering in lithium niobate," *Ferroelectrics,* vol. 340, pp. 75-82, 2006.

[54] V. Dierolf and C. Sandmann, "Direct-write method for domain inversion patterns in LiNbO3," *Applied Physics Letters,* vol. 84, pp. 3987-3989, 2004.

[55] I. Wellington, C. Valdivia, T. Sono, C. Sones, S. Mailis and R. Eason, "Ordered nano-scale domains in lithium niobate single crystals via phase-mask assisted all-optical poling," *Applied Surface Science,* vol. 253, pp. 4215-4219, 2006.

[56] C. Valdivia, C. Sones, J. Scott, S. Mailis and R. W. Eason, "Nanoscale surface domain formation fo the +z face of lithium niobate by pulsed ultraviolet laser illumination," *Applied Physics Letters,* vol. 86, pp. 022906-1 - 022906-3, 2005.

[57] A. Muir, C. Sones, S. Mailis, R. Eason, T. Jungk, A. Hoffmann and E. Soergel, "Direct-writing of inverted domains in lithium niobate using a continuous wave ultra violet laser," *Optics Express,* vol. 16, pp. 2336-2350, 2008.

[58] E. Palik, Handbook of Optical Constants of Solids, New York, NY: Academic, 1985.

[59] D. Deshpande, A. Palshe, E. Stach, V. Radmilovic and D. Alexander, "Investigation of femtosecond laser assisted nano and microscale modifications in lithium niobate," *Journal of Applied Physics,* vol. 97, pp. 074316-1 - 074316-9, 2005.

[60] H. Hu, R. Ricken and W. Sohler, "Etching of lithium niobate: micro- and nanometer structures for integrated optics," in *Photorefractive Materials, Effects, and Devices*, Bad Honnef, Germany, 2009.

[61] H. Hu, A. Milenin, R. Wehrspohn, H. Hermann and W. Sohler, "Plasma etching of proton-exchanged lithium niobate," *Journal of Vacuum Science and Technologies,* vol. 24, pp. 1012-1015, 2006.

[62] G. Ulliac, B. Guidchardaz, J. Rauch, S. Queste, S. Benchabane and N. Courjal, "Ultra-smooth LiNbO3 micro and nano structures for photonic applications," *Microelectronic Engineering,* vol. 88, pp. 2417-2419, 2011.

[63] S. Benchabane, L. Robert, J. Rauch, A. Khelif and V. Laude, "Highly selective electroplated nickel mask for lithium niobate dry etching," *Journal of Applied Physics,* vol. 105, pp. 094109-1 - 094109-6, 2009.

[64] S. Queste, "Deep reactive ion etching of quartz, lithium niobate, and lead titanate," in *Journees Nationales sur les Technologies Emergentes en Micronanofabrication*, Les Diablerets, 2008.

[65] S. Queste, G. Ulliac, J. Jeannot and C. K. Malek, "DRIE of non-conventional materials: first results," *Multi-material micro manufacture,* pp. 171-174, 2008.

[66] Z. Ren, P. Heard, J. Marshall, P. Thomas and S. Yu, "Etching characteristics of LiNbO3 in reactive ion etching and inductively coupled plasma," *Journal of Applied Physics,* vol. 103, pp. 034109-1 - 034109-8, 2008.

[67] G. Ulliac, N. Courjal, H. Chong and R. D. L. Rue, "Batch process for the fabrication of LiNbO3 photonic crystals using proton exchange followed by CHF3," *Optical Materials,* vol. 31, pp. 196-200, 2008.

[68] F. Lacour, M. B. N. Courjal, A. Sabac, C. Bainier and M. Spajer, "Nanostructuring

lithium niobate substrates by focused ion beam milling," *Optical Materials,* vol. 27, pp. 1421-1425, 2004.

[69] M. Roussey, M. Bernal, N. Courjal and F. Baida, "Experimental and theoretical characterization of a lithium niobate photonic crystal," *Applied Physics Letters,* vol. 87, pp. 241101-1 - 241101-3, 2005.

[70] Y. Chen, W. Yan, D. Wang, S. Chen and G. Zhang, "Submicron domain inversion in Mg-doped LiNbO3 using backswitched poling with short voltage pulses," *Applied Physics Letters,* vol. 106, pp. 081101-1 - 081101-29, 2009.

[71] H. Hartung, E. Kley, T. Gischkat, F. Schrempel, W. Wesch and A. Tunnermann, "Ultra Thin high index contrast photonic crystal slabs in lithium niobate," *Optical Materials,* vol. 33, pp. 19-21, 2010.

# APPENDIX A

## DETAILED FABRICATION PROCESS

A detailed outline of the two ICP-RIE fabrication processes, Method A and B, is discussed in this section. Figure A.1, on page 120, illustrates the numbered step in the fabrication sequence, and Sections A.1 and A.2 (Method A and Method B, respectively) detail out the necessary steps needed to fabricate structures on lithium niobate using an ICP-RIE process. The numbered step listed out correlate with the numbered sequence on the flowchart.

A.1. Fabrication Procedure: Method A

1. Clean samples off using a three solvent cleanse, dry
2. Spin on resist
    a. PMGI
        i. 4.5% PMGI (bottom layer, approximately 150 nm thick)
        ii. Brewer Spinner Program 5
            1. 300 RPM
            2. 10,000 R/S
            3. 10 sec.
            4. 4500 RPM
            5. 10,000 R/S
            6. 45 sec.
        iii. Dispense resist while chip is slowly rotating (built in to program)
        iv. 1-3 drops, enough to cover most of chip
        v. Spin at 4000 RPM for 45 seconds
        vi. Bake for 10 minutes at 250 °C (use portable hotplate)

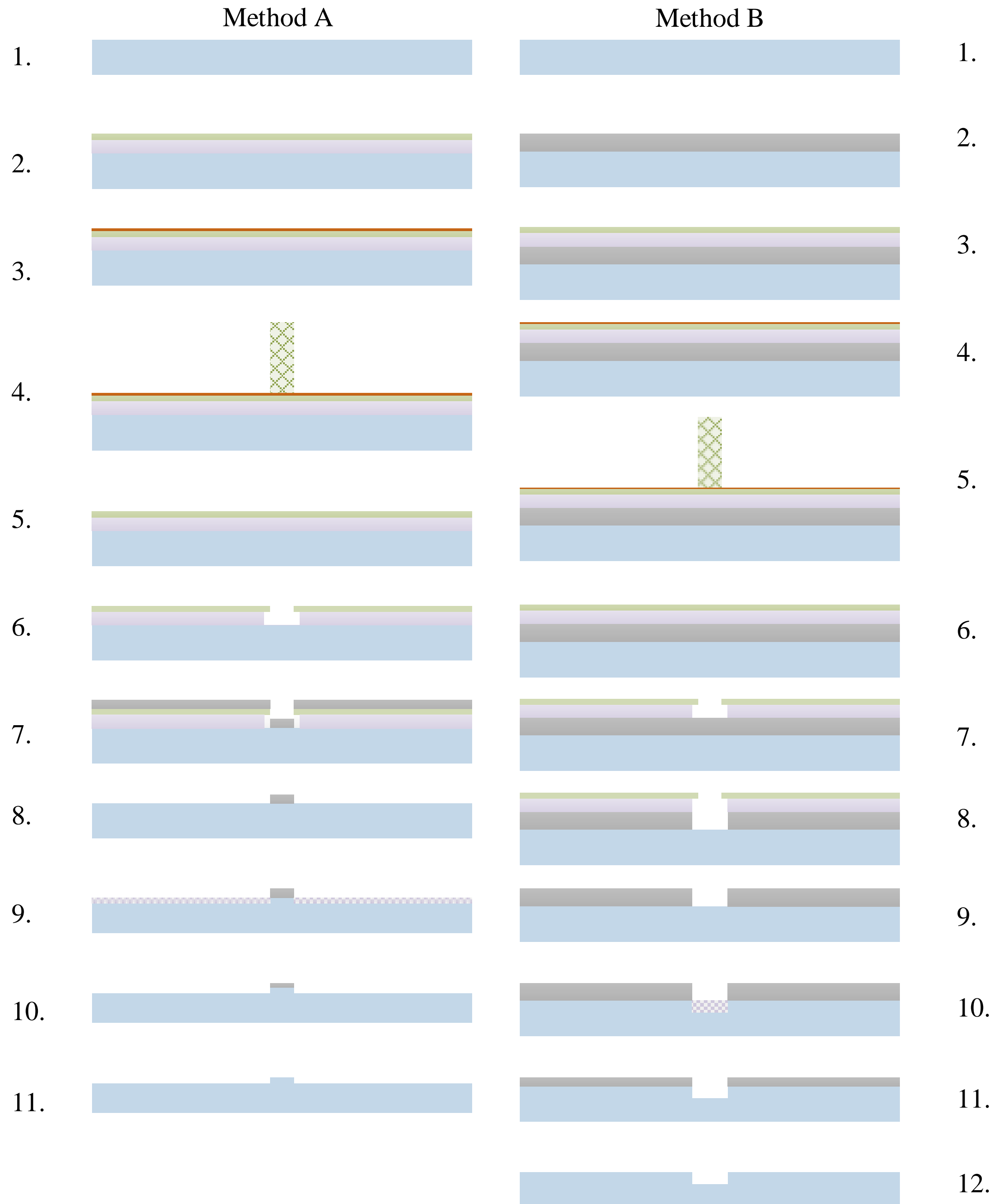


Figure A.1. Flowchart sequencing out the steps taken for the Method A (left) and Method B (right) processes used to etch lithium niobate using an ICP-RIE etch.

a. PMMA

vii. 1.5% PMMA 950 (top layer, approximately 50 nm thick)

viii. Brewer Spinner Program 7

1. 3500 RPM
2. 5000 R/S
3. 40 sec.

ix. Dispense resist while chip is stationary

x. Spin at 3500 RPM for 40 seconds

xi. Bake for 10 minutes at 180 °C (use portable hotplate)

3. Coat with gold film
   a. Sputter using EMITECH K575X in ICAL for 25 seconds at 35 mA
4. EBL
5. Etch gold off sample
   a. Place chip in Transene gold etchant for 30 seconds at room temperature
6. Develop
   a. PMMA
      i. Place in 3:1 isopropyl (IPA) : methyl isobutl ketone (MIBK) solution for 40 seconds, room temperature
   b. PMGI
      i. Place in 1:1 AZ726 developer : de-ionized water (DI) for 90 seconds at room temperature
7. Chromium deposition
   a. Use AMOD electron-beam evaporator to thermally evaporate chromium off of a chromium rod at a rate of 3 Å/s
8. Lift-off
   a. Place samples in beaker of Remover PG, heated to 80 °C on a hotplate

   b. Leave samples in beaker until lift-off complete (30-60 minutes)

9. Proton exchange
   a. Place samples in a heated benzoic bath solution, temperature and time will vary depending on desired depth
   b. Assisted by AdvR, Inc.
10. ICP-RIE
    a. Etch samples with Oxford Plasma Lab ICP-RIE
    b. Parameters discussed in detail in Chapter 4
11. Chromium etch
    a. Etch residual chromium mask away using Transene chromium etchant for 10 minutes at room temperature

A.2. Fabrication Procedure: Method B

1. Clean samples off using a three solvent cleanse, dry
2. Chromium deposition
   a. Use AMOD electron-beam evaporator to thermally evaporate chromium off of a chromium rod at a rate of 3 Å/s
3. Spin on resist
   a. PMGI
      i. 4.5% PMGI (bottom layer, approximately 150 nm thick)
      ii. Brewer Spinner Program 5
         1. 300 RPM
         2. 10,000 R/S

3. 10 sec.
4. 4500 RPM
5. 10,000 R/S
6. 45 sec.

iii. Dispense resist while chip is slowly rotating (built in to program)

iv. 1-3 drops, enough to cover most of chip

v. Spin at 4000 RPM for 45 seconds

vi. Bake for 10 minutes at 250 °C (use portable hotplate)

b. PMMA

i. 1.5% PMMA 950 (top layer, approximately 50 nm thick)

ii. Brewer Spinner Program 7

1. 3500 RPM
2. 5000 R/S
3. 40 sec.

iii. Dispense resist while chip is stationary

iv. Spin at 3500 RPM for 40 seconds

v. Bake for 10 minutes at 180 °C (use portable hotplate)

4. Coat with gold film

a. Sputter using EMITECH K575X in ICAL for 12 seconds at 35 mA

5. EBL

6. Etch gold off sample

a. Place chip in Transene gold etchant for 30 seconds at room temperature

7. Develop

  a. PMMA
     i. Place in 3:1 isopropyl (IPA) : methyl isobutl ketone (MIBK) solution for 40 sec., room temperature
  b. PMGI
     i. Place in 1:1 AZ726 developer : de-ionized water (DI) for 90 sec. at room temperature

8. Chromium etch
   a. Etch chromium where patterned windows are located using Transene chromium etchant at room temperature (time will vary depending on chromium thickness)
9. Proton exchange
   a. Place samples in a heated benzoic bath solution, temperature and time will vary depending on desired depth
   b. Assisted by AdvR, Inc.
10. ICP-RIE
    a. Etch samples with Oxford Plasma Lab ICP-RIE
    b. Parameters discussed in detail in Chapter 4
11. Chromium etch
12. Etch residual chromium mask away using Transene chromium etchant for 10 minutes at room temperature